AN ELECTROCHEMICAL INVESTIGATION OF MASS TRANSFER AND SHEAR STRESS IN PULSATILE LAMINAR FLOW: IMPLICATIONS FOR ATHEROGENESIS

by

STEVEN S. EMMER

B.S., Massachusetts Institute of Technology
(1973)

SUBMITTED IN PARTIAL FULFILLMENT
OF THE REQUIREMENTS FOR THE
DEGREE OF MASTER OF SCIENCE
at the
MASSACHUSETTS INSTITUTE OF TECHNOLOGY
August 1973

Signature of Author: . . . . . .
Department of Chemical Engineering

Certified by: . . . . . .
Kenneth A. Smith, Thesis Supervisor

. . . . . .
Clark K. Colton, Thesis Supervisor

Accepted by: . . . . . .
Glenn C. Williams, Chairman
Departmental Committee on Graduate Theses

Department of Chemical Engineering
Massachusetts Institute of Technology
Cambridge, Massachusetts 02139
August 13, 1973

Professor David B. Ralston
Secretary of the Faculty
Massachusetts Institute of Technology
Cambridge, Massachusetts 02139

Dear Professor Ralston:

In accordance with the regulation of the Faculty, I herewith submit a thesis entitled, "An Electrochemical Investigation of Mass Transfer and Shear Stress in Pulsatile Laminar Flow: Implications for Atherogenesis", in partial fulfillment of the requirements for the degree of Master of Science in Chemical Engineering at the Massachusetts Institute of Technology.

Respectfully submitted,

Steven S. Emmer

ABSTRACT

AN ELECTROCHEMICAL INVESTIGATION OF MASS TRANSFER AND SHEAR STRESS IN PULSATILE LAMINAR FLOW: IMPLICATIONS FOR ATHEROGENESIS

by

STEVEN S. EMMER

Submitted to the Department of Chemical Engineering on August 13, 1973, in partial fulfillment of the requirements for the degree of MASTER OF SCIENCE at the Massachusetts Institute of Technology.

.....

A theoretical and experimental program was undertaken to examine the applicability of diffusion controlled electrodes to the measurement of the fluctuating shear stress on the wall of a tube under conditions of pulsatile laminar flow. The objective of this investigation was to experimentally obtain the same description of the time-varying wall shear stress as given by analytical expressions available for the tubuler geometry. Agreement between the two descriptions was a prerequisite for further shear stress studies in models of the human arterial system for which no analytical comparisons are available.

The experimental technique involves monitoring a diffusion controlled electrochemical reaction that takes place on the surfaces of nickel electrodes mounted flush with the wall of a pipe. The use of small area electrodes together with the large Schmidt number of the fluid assures the validity of mathematical assumptions which allow one to relate shear stress at the wall to the measured mass transfer coefficient.

Theoretical models are presented which characterize the effects of the amplitude and frequency of pulsation upon the measurable mass transfer coefficient, and which relate this quantity to the instantaneous wall shear stress. The resulting expressions are valid over all frequencies and for all oscillatory pressure ratios which do not cause boundary layer reversal.

Experimental results are in excellent agreement with the theoretical model relating the frequency and amplitude of the fluctuating pressure gradient to the interphase mass transfer coefficient, particularly for values of the dimensionless frequency parameter, Ω, $(R\sqrt{\frac{n\omega}{\nu}})$, exceeding 16. This conformity with theory provided the basis for deriving a transfer function between the experimental mass transfer coefficient and the wall shear rate. This transfer function eliminates the need to measure the pressure gradient and is universal in that it can be applied to arbitrary geometries with arbitrary flow fields.

Thesis Supervisors: Kenneth A Smith
Professor of Chemical Engineering

Clark K Colton
Associate Professor of Chemical Engineering

ACKNOWLEDGEMENTS

Without the assistance of several individuals this project could never have succeeded. For their aid in my efforts to complete this thesis I would sincerely like to thank:

First and foremost, Richard Freedman, whose invaluable collaboration in this research was an integral part of its successful completion;

Professor Kenneth A. Smith, my advisor, for his constructive criticisms and suggestions regarding theoretical aspects of this work, and for his continued interest and encouragement, especially through times of difficulty;

Professor Clark K. Colton, my advisor, for introducing me to the field of biomedical engineering. His contributions in focusing on experimental problems are appreciated;

Dave Gossard, coordinator of the Engineering Projects Laboratory, who facilitated the data analysis by developing the software for the analog-digital computer hybrid;

Paul Bletzer and Jack Russell for their assistance with the construction of the mechanical equipment;

Rita Albee for her assistance in preparing the final draft of this thesis;

With special appreciation, my parents, Sol and Millicent Emmer, for their inspiration, encouragement, and moral support.

TABLE OF CONTENTS

LIST OF FIGURES

LIST OF TABLES

SUMMARY

The focal nature of atherosclerosis suggests that atherogenesis is associated with interactions between the bloodstream and the intimal endothelium via either the shear stress or the fluid-phase resistence to mass transfer. A number of hypotheses have been proferred to account for the effects of shear stress and mass transfer upon the atherosclerotic process, but it has not been possible to evaluate these theories in a meaningful way because of the lack of quantitative data regarding the magnitude of these influences. Even the question of whether a given region is one of high or low shear rate has not been adequately resolved.

The objectives of this work were to test the applicability of diffusion controlled electrodes and associated mathematical analyses to determining the magnitude of the instantaneous shear stress on the wall of a tubular conduit under conditions of pulsatile laminar flow, and to investigate the feasibility of applying these techniques to more complex geometries. The oscillations were superimposed on the steady flow by applying a periodically varying pressure driving force.

Measurement of the shearing stress was accomplished by following a diffusion-controlled electrochemical reaction that takes place on the surface of nickel electrodes mounted flush with the wall of the pipe. A voltage potential difference applied across the test electrode and a downstream anode causes the following reactions to occur between

the electrolytic fluid and the electrode surfaces:

$$\text{Test Cathode:} \quad Fe(CN)_6^{-3} + e^- \rightarrow Fe(CN)_6^{-4}$$

$$\text{Anode:} \quad Fe(CN)_6^{-4} \rightarrow Fe(CN)_6^{-3} + e^-$$

The kinetics of these reactions are fast, thus ensuring that the rate of the cathodic reaction is limited by the rate of transfer of the ferricyanide ion from the bulk of the fluid to the electrode surface. The rate of the reaction is directly proportional to the measured electrode current, thereby permitting calculation of the mass transfer coefficient. The use of small area circular electrodes together with the large Schmidt number (≈1500) of the fluid assured the validity of mathematical assumptions which allow one to relate shear stress at the wall to the measured mass transfer coefficient. The shear thus determined was compared to the known exact expression for the wall shear rate in a cylindrical tube. Hence, a rigorous test of the accuracy of the measurement of wall shear from mass transfer data was obtained.

The results demonstrated that the electrochemical technique can be applied to geometrical models of arterial branches where the description of the flow field is too complex to provide an analytical expression for the pulsatile wall shear stress.

The theoretical analysis required the solutions to both the Navier Stokes momentum equation and the conservation of mass equation

for a time-varying flow field. To provide an expression for the instantaneous velocity within the fully developed flow regions of the pipe, including the electrode test section, the exact solution to the Navier Stokes equation for this system,

$$\frac{\partial u}{\partial t} = -\frac{1}{\rho} \cdot \frac{\partial p}{\partial x} + \frac{\nu}{r} \frac{\partial}{\partial r}\left(r \frac{\partial u}{\partial r}\right) \tag{S-1}$$

$$u(r = R) = 0$$

$$\left(\frac{\partial u}{\partial r}\right)_{r=0} = 0$$

was given as

$$u(r,t) = 2U_o\left(1 - \frac{r^2}{R^2}\right) - 8iU_o \sum_{n=1}^{N} \left\{ \frac{\lambda_{p(n)}}{\Omega_n^2} \left[1 - \frac{J_o\left(i^{3/2}\, \Omega_n \frac{r}{R}\right)}{J_o\left(i^{3/2}\, \Omega_n\right)} \right] e^{in\omega t} \right\} \tag{S-2}$$

where U_o is the mean velocity; λ_p is the ratio of the amplitude of the oscillatory pressure gradient to the steady flow value; and Ω is the dimensionless frequency parameter, $R\sqrt{\frac{n\omega}{\nu}}$. Only the real part of the expression for velocity has physical significance.

Since the Schmidt number for the fluid is large, the concentration boundary layer is very much thinner than the momentum boundary layer; the velocity in the concentration boundary layer above the electrode surface can then be expressed as

$$u(y,t) = y\left(\frac{\partial u}{\partial y}\right)_{y=0} \tag{S-3}$$

which, when coupled with equation (S-2) becomes

$$u(y,t) = \frac{U_o y}{R}\left[4 + \sum_{n=1}^{N} \lambda_{p(n)}\, \gamma_n e^{in\omega t}\right] \tag{S-4}$$

where

$$\gamma_n = \frac{-8i^{1/2}}{\Omega} \cdot \frac{J_1(\Omega i^{3/2})}{J_o(\Omega i^{3/2})} \tag{S-5}$$

With u, equation (S-4), inserted into the conservation of mass equation,

$$\frac{\partial C}{\partial t} + u\,\frac{\partial C}{\partial x} = \mathcal{D}\,\frac{\partial^2 C}{\partial y^2} \tag{S-6}$$

$$C(x,y = o,t) = C_W = 0$$

$$C(x,y = \infty,t) = C_B$$

$$C(x = o,y,t) = C_B$$

the solution for the time-varying concentration field is obtained as a first-order series expansion about the steady flow condition, with λ_p as the perturbation parameter. The result characterizes the response of the measurable mass transfer coefficient to the amplitude and frequency of pulsation and is given as,

$$\frac{\lambda_m}{\lambda_p} = \frac{2M_1}{3\Omega M_o} \cdot \frac{1}{(1 + \tau^2\alpha^4 Gz^{4/3})^{1/2}} \qquad \text{(S-7)}$$

where λ_m is the ratio of the amplitude of the fluctuating mass transfer coefficient to the time-averaged value; M_o and M_1 are the moduli of J_o and J_1 respectively; τ is a constant of integration; Gz is the Graetz number; $\alpha = \Omega Sc^{1/2}$; and Sc is the Schmidt number.

The ratio $\frac{\lambda m}{\lambda_p}$ $(=A_{mp})$, can be related to the analogous expression for the wall shear rate, $\frac{\lambda_s}{\lambda_p}$ $(=A_{sp})$, by correcting equation (S-7) for the frequency response of the concentration boundary layer to changes in the shear rate. The correction takes the form

$$A_{sp} = \frac{3}{\hat{A}} A_{mp} \qquad \text{(S-8)}$$

where $\hat{A}$, the correction factor, is a function of the Graetz number, Schmidt number, and Ω.

Experimental results for A_{mp} were in excellent agreement with the theoretical model, equation (S-7), for values of Ω greater than 16. Slight departures from the predictions of (S-7) occurred in the dimensionless frequency range ($6<\Omega<16$). A possible explanation for these deviations is that equation (S-7) is restricted to low and high values of Ω, and is not applicable in the intermediate dimensionless frequency region.

Corrections for the frequency response of the concentration boundary layer were made with the use of a numerical solution for $\hat{A}$

available in the literature. Resulting values for the wall shear rate (A_{sp}) failed to agree with the known exact solution for pulsatile wall shear. An alternate correction which yielded agreement of A_{sp} with theory was therefore derived which acquired the form,

$$A_{sp} = 3(1 + \tau^2\alpha^4 Gz^{4/3})^{1/2} A_{mp} \qquad (S\text{-}9)$$

This expression is no longer restricted to the tubular geometry since by rearrangement there results

$$\frac{A_{sp}}{A_{mp}} = \frac{\lambda_s}{\lambda_m} = 3(1 + \tau^2\alpha^4 Gz^{4/3})^{1/2} \qquad (S\text{-}10)$$

Thus it is necessary only to measure the mass transfer ratio, λ_m, to determine the desired result, λ_s. The need to determine the oscillatory pressure gradient has been eliminated, and the diffusion controlled electrode becomes a very effective devise for measuring the wall shear stress in arbitrary geometries with arbitrary laminar flow fields.

I. INTRODUCTION

One hundred years of countless investigations aimed at illuminating the causative mechanism of atherosclerosis have produced a plethora of mechanistic theories, some partially substantiated, others purely conjectural, and most tentatively acceptable as bearing on the truth of atherogenesis. Unfortunately there is as yet insufficient evidence to support the acceptance of one or more unifying theories to the exclusion of all others.

A considerable amount of influence has been exerted upon atherosclerotic research by the filtration hypothesis of atherogenesis which attributes the formation of atherosclerotic lesions to the deposition of cholesterol within the arterial wall. This accumulation arises from the precipitation of lipoid material contained within a nutrient stream of plasma filtering through the arterial wall. The passage of fluid supplies part of the artery with nutrition to meet the metabolic requirements of several layers of cells, and forms a closed loop between the blood on the lumen side and the lymphatic system exterior to the vessel wall. One observation unaccountable by this theory is the preferential localization of atherosclerotic lesions. (Texon et al 1960, Sandler and Bourne 1963, Mitchell and Schwartz 1965, Wesolowski 1965, Fox 1966, Caro 1971). Additionally, it is questionable whether the magnitude of the filtration flux is sufficient to convey more lipoid material than the arterial cells can safely accomodate (Bratzler 1972). There are other factors whose importance must be emphasized and these have generated alternate theories whose premises fall under the

consideration of hemodynamic stress (Texon 1963, Sako 1962, Fry 1968 and 1969, Gutstein 1970, Duncan 1965); encrustation of micro-thrombi and platelets (Duguid 1960, Fox 1966, Murphy 1962, Mustard 1964), and alterations in local metabolism (Getz 1969, Lazzarini-Robertson 1962, 1968).

This thesis is motivated by the viewpoint that the initiation of atherosclerosis is intimately associated with the natural function of the cardiovascular system - namely that the time varying shear stress, produced by the pulsating flow of blood past sections of the arterial wall located in regions of geometrical irregularity (such as the entrances of branching vessels and bifurcations where the atherosclerotic process is seen to dominate), can reach magnitudes sufficiently high enough to induce a microtrauma in the cellular lining of the vessel. Subsequent events at the point of insult to the integrity of this monolayer of endothelial cells lead toward and contribute to the development of an atheromatous plaque. These processes are discussed in detail in Section II.

The immediate intention of this work is to utilize existing flow study techniques, combined with appropriate mathematical analyses, to determine the instantaneous shear stress imparted to the wall of a rigid cylindrical conduit transporting laminar pulsatile flow of a Newtonian fluid. The oscillations are superimposed on the steady flow by applying a periodically varying pressure driving force.

The investigation consists of generating a known periodic laminar velocity field composed of several sinusoidal harmonics. Profiles of

the changing velocity are obtained from measurements of the periodic exciting force, the oscillating pressure gradient. The fluid contains a dissolved electrolyte which reacts at the surface of a nickel electrode implanted in the tube and smoothed flush with the wall. Mass transfer rates are measured from the resultant current and shear stress is then determined by the superposition of contributions from each harmonic. The shear thus determined is compared to the known exact expression for the wall shear rate in a cylindrical tube. Hence, an excellent test of the accuracy of mass transfer measurements of wall shear is obtained.

Ultimately the use of these techniques will be applied to geometrical models of arterial branches, particularly a Y bifurcation where the description of the flow field is too complex to serve as a guide in evaluating unknown mass transfer and shear stress phenomena occurring along the wall of the branching conduit. In such regions, experimental data containing information about these events will have to be totally and confidently relied upon for their informational content. Thus it is the additional purpose of this investigation to insure the validity of the analytical techniques in order to permit the extension of shear stress determination into regions not describable by closed form tractable mathematical expressions.

The electrochemical technique, used in this investigation to determine instantaneous pulsatile wall shear stress, was developed by Reiss (1962), refined by Mitchell (1965), and used by them to measure turbulent velocity and mass transfer intensities at the wall of a pipe. It involves the use of a tiny circular nickel wire electrode imbedded into

the wall of the tubular conduit and smoothed flush with the inside surface of the pipe. This method of measurement consists in the diffusion controlled electrochemical reduction of ferricyanide ions to ferrocyanide ions. The rate of this reaction is limited (and therefore controlled) by the rate of diffusional mass transfer from the fluid bulk, through a concentration boundary layer initiated at the leading edge of the nickel wire, to the electrode surface. It is measured by a flow of current through an external circuit. For each ferricyanide ion reduced at this circular electrode a ferrocyanide ion is oxidized to a ferricyanide ion at a large downstream anode which forms the other half of the electrolytic cell. Conveniently, no plating of material occurs and the equimolar concentrations of reacting species are conserved. The fluid vehicle containing these ions is 2M sodium hydroxide which acts both as an electrolytic buffer, reducing the migration of ferricyanide ions within the electric field of the electrode to negligible proportions, and as a low resistance electrolyte connecting the test cathode to the anode.

The distinct utility of using this pair of ions is that as a result of the redox reaction, the current generated at the cathode is directly proportional to the mass flux of ferricyanide ion to its surface. This proportionality factor, the mass transfer coefficient, is in turn a function of the velocity gradient, and therefore the current is an indirect measure of the wall shear stress. Two added advantages of determining flow characteristics with this <u>in vitro</u> technique, over that of a hot wire anemometer for example, are that the flow conditions are not

disturbed by the presence of the measuring device, and the properties of the fluid are not affected by the process.

The concentration boundary layer is the region of the flow field within which the concentration of the reacting ion changes from its value at the electrode surface to the value of the bulk concentration. The thickness of this layer is commonly given as

$$\delta_c = \frac{\mathcal{D}(C_B - C_W)}{J}$$

with J representing the amount of mass transferred to the electrode. The value of δ_c is zero at the leading edge of the reacting section (x=0) and increases to some final finite thickness at the trailing edge of the electrode. Attendant to this enlargement is a decrease in the concentration gradient within the concentration boundary layer, with an associated decrease in the rate of mass transfer to the nickel surface.

The flux of ferricyanide to the reacting surface procedes along the concentration profile established within the developing concentration boundary layer. This profile is intimately associated with the velocity distribution since the two are coupled via the equation describing the conservation of mass. For the particular combination of species used in this investigation the Schmidt Number

$$Sc = \frac{\nu}{\mathcal{D}}$$

for the diffusing ion is very large ($\simeq$ 1500). The thickness of the concentration boundary layer over the small electrode is therefore much

smaller than that of the fully developed momentum boundary layer, which validates a very powerful simplifying assumption for the form of the velocity profile in this thin mass transfer resistance layer adjacent to the wall. The conservation of mass equation can be linearized by introducing into this differential equation a linear relation for the velocity profile in this region, equal to the velocity gradient (or shear rate) at the wall times the radial distance from the wall. With an appropriate solution to the resulting simplified equation the shear rate can be related to the mass transfer coefficient which is directly obtainable.

Three mathematical models are presented, each representing a transfer function between fluctuating parameters as the following diagram depicts:

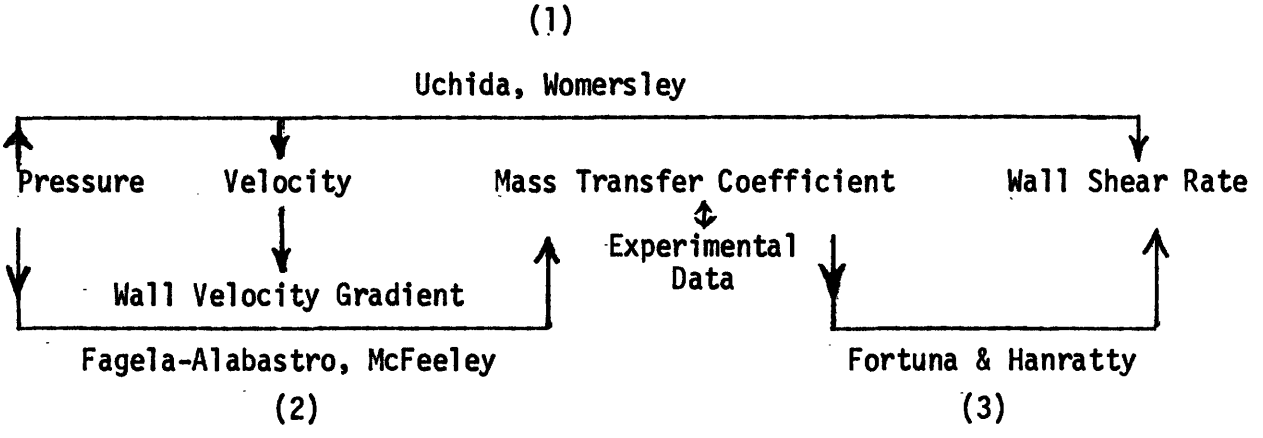

(1) The exact analytical solution to the Navier Stokes equations for a time varying pressure gradient superimposed upon a steady flow was derived by Uchida (1956), (and equivalently by Womersley (1957) for the

oscillatory component only), and is used here as an incontrovertible theoretical model for the amplitude and periodic variation of the wall shear rate as a function of the amplitude and frequency of the pulsating pressure gradient.

(2) Since the wall shear is calculated from mass transfer data, a mathematical model is presented which characterizes the mass transfer coefficient in terms of the pulsating flow field parameters.

The solution given in the form of Womersley (1957) to the oscillatory motion of the fluid velocity, linearly separate from the steady flow, is used to determine the velocity gradient at the wall which inserted into the equation for the concentration distribution serves to couple the known velocity field with the unknown concentration field. The resulting solution, based upon the known wall shear rate (previously inserted), relates the amplitudes of pulsation to the responding amplitudes of mass transfer. Model (2), then, is a transfer function between pressure oscillation (known) and the magnitude of the fluctuating mass transfer coefficient (which can be measured). This solution was first obtained by Fagela-Alabastro (1967, 1969) through a perturbation technique around the steady flow solution, but the analysis of McFeeley (1972), a slight modification of the approach, is borrowed for use here because of its more convenient form.

(3) Fortuna and Hanratty (1971) solved numerically the conservation of mass equation to yield the frequency dependent relations between the amplitude and phase of the measured mass transfer and that of the entity desired in this work - the shear rate at the wall. Their results were

applied to turbulence; this investigation is the first extension to pulsatile laminar flow. The formulation of the model for this transfer function is written in general terms and treats the shear rate as an unknown function for which it then solves; the model can therefore be applied to geometries other than the cylindrical conduit. This thesis tests its applicability and validity by applying the transfer function to a tube for which the solution is known a priori via model (1).

The results of model (1), described in Appendix 4, represents the goal of the experimental method. Because of the difficulty in measuring directly the shear rate at the wall for non-steady flow and arbitrary geometries, the objective here is to establish the technique (and test the method for a tubular geometry) of combining the experimental data with model (3), the theoretically derived transfer function which operates upon the experimentally measured fluctuating mass transfer coefficient to yield the desired fluctuating wall shear rate (considered as an unknown entity). The results show that the experimental route (model (3)) obtains the same description (within 5%) of the laminar periodic motion of the wall shear rate as is predicted directly from the pressure pulse by the theoretical model (1).

The results of the mass transfer studies of this work are presented in terms of a ratio of the mass transfer coefficient to the pulsating pressure amplitude, and are reported as a function of the dimensionless frequency parameter, Ω. The work of McFeeley provides data in this convenient form with which the results of this thesis are compared.

The shear rate determinations, derived from the mass transfer results via the analytical methodology of Fortuna and Hanratty are plotted in analogous fashion and are compared to the exact analytical solution of Uchida.

II. A CAUSAL RELATIONSHIP BETWEEN SHEAR STRESS AND ATHEROSCLEROSIS

The local accumulation of lipids (mostly cholesterol and its esters, phospholipids, and triglycerides) within the tunica intima and tunica media of the vascular wall is often described as the first phase of the pathogenesis of atherosclerosis. This accumulation leads to cell damage and frequently to the stimulation of intima cell proliferation resulting in intimal thickening.

It has been suggested (Adams 1963) that the accumulation and thickening causes ischemia of the tunica media and interferes with the lipid transport mechanism across the cell membrane, thus preventing the extracellular lipid from being utilized and perpetuating the process of accumulation. In response to the abundance of lipid, the cells become disrupted or necrosis ensues resulting in an inflammatory and reparative reaction that leads to the formation of a fibrous placque. Calcification and local intramural hemorrage may follow.

This placque may grow outwards into the arterial lumen leading ultimately to complete occlusion of the lumen, or it may set the stage for the formation of an occlusive thrombus by impeding blood flow and distorting the endothelial surface. As the placque or thrombus grows outward, the blood velocity in the lumen must increase in order to conserve mass flow, and the accompanying increased shear will tend to dislodge the growth from the arterial wall, carrying it downstream where the embolism may lodge in a vital pathway causing death or loss of function of an important body system or limb. A fatal heart attack is

often the result.

One of the distinctive features of early atherosclerosis is its characteristic topography. Lesions occur at certain sites of predilection with remarkable regularity. These sites are at vessel orifices, and their associated entrance regions, at bifurcations, and on regions of the large arteries possessing curvature. (Fox 1966, Texon et al. 1960, Mitchell and Schwartz 1965, Sandler and Bourne 1963, Wesolowski 1965, Caro 1970). Atheromatous lesions are commonly found at the mouths of junctions of arteries in the aortic arch - the carotid, innominate and subclavian vessels, and especially at the orifices of the visceral branches of the aorta - the superior mesenteric, coeliac, renal, and intercostal arteries. The carotid sinus is also commonly stricken. In the case of iliac bifurcation, the initial disease occurs at the outside wall and extends down the lateral side of the iliac vessels; the inner wall is relatively spared. These investigators have all observed well-developed atheromatous placques in the aortic arch. It is interesting to note that the lesions on the inner wall of curvature are far more pronounced than those of the outer wall. Caro (1970) in particular has found concentric lesions in the straight sections of the coronary arteries whereas the curving portions of these and the splenic artery contain eccentric lesions. Indeed, a correlation exists between the incidence of placque formation and the angle of bending in the coronary system (Tjotta 1963). The abdominal aorta too is a frequent site of atheromatous placques; particularly in areas around branch vessel points; in fact, lesions here are usually more abundant than in

the aortic arch.

Such consistent observations of the focal nature of the disease demands attention from a fluid mechanical viewpoint since it is these very regions of atherosclerotic predilection which witness changes in the nature of the interfacial contact between the pulsing blood and the surface of the arterial wall. These changes are in part characterized by a local elevation of the wall shearing force imparted by alterations in the structure of the flow.

The interfacial boundary between the blood and the arterial wall is formed by a single continuous layer of endothelial cells firmly attached to each other by adhesion of their cell membranes. Thus, all substances which enter the arterial tissue from the lumen must pass through this endothelial matrix. Acting in the capacity of a protective barrier preventing direct endothelial sublayer-blood contact and excessive deposition of cholesterol in arterial tissue, it is the first structure to be influenced by hemodynamic forces. Much evidence has been presented to support the view that hemodynamic trauma is an important factor in atherogenesis.

For instance, Fry (1968, 1969a, 1969b) has observed that experimentally increased hemodynamic stress can cause endothelial injury and cellular death in the aorta of dogs. By introducing a specially designed non-traumatic plug into the aorta of a dog, a rapid convergence of blood flow through a channel machined into the device was obtained. This accelerating flow imparted a spatially varying shearing force against the endothelial lining of a longitudinal segment of the arterial wall.

Increased shear stress levels were accompanied by cellular swelling and architectural changes in the blood wall interface, cytoplasmic deformation, and with higher magnitudes of shear, progressive disintegration. Very high shearing force levels (380 dynes/cm^2) were accompanied by the fragmentation of the underlying fibrillar structure. This value was referred to as the endothelial critical yield stress.* It was found additionally that there was an increase in the protein permeability of the intima at stress levels below fragmentation and that this change in permeability, as manifested by enhanced Evans Blue uptake, increased with increasing shear. The shear induced enhancement of permeability was prevalent even when superficial histological changes could not be discerned.

Other observers have reported an increased evidence of intimal thickening and atherosclerosis in man (Texon 1957, 1960, Sandler and Bourne 1963, Mitchell and Schwartz 1965) and dietarily induced atherosclerotic lesions in animals (Lazzarini-Robertson 1968) in regions commonly associated with localized critical hemodynamic stress. Together with the discovery of injured endothelium and media in branch entrances of rabbits (Bjorkerud and Bondjers 1972) as revealed by dramatically

---

* The limitation of an approximate theory to predict the shear stress *in vivo* due to the complexity of the flow field through the channel introduced an uncertain error in the estimation of critical stress. Further investigations were undertaken by Carew (1971) who performed controlled shear stress and permeability experiments on aortic tissue *in vitro* to determine the effects of several uncontrolled variables in the *in vivo* situation. His results for the critical stress, obtained for the non-physiological temperature of 18^{o}C, were that cells exposed to shear stresses above 590 dynes/cm^2 underwent progressive deterioration and suffered morphological transformations.

altered tissue morphology and tremendously increased dye staining characteristics, these findings point to the fundamental importance of the mechanical interactions at the vascular interface in the normal function of the endothelium as an interfacial barrier between blood and the vessel wall, and the probable degeneration of this function during the initiation of the disease process. The observations highly suggest that cell injury due to locally augmented hemodynamic shearing stress, and the tissue reaction to such injury, are extremely important factors in the development of atherosclerotic lesions.

The artery responds to imparted stress loads very rapidly, increasing tremendously the amount of connective tissue within one hour of stress inducement. This dynamic proliferative response implies that the arterial wall is a structure continuously under load, normally capable of meeting the need to provide constant repair. Arterial metabolism, then, can respond continuously to changes in the physical forces experienced by the wall.

Such a condition requires that a supply of nutrients be readily available and presumably this is accomplished by the filtration (Anitschkow 1933) or diffusion (Bratzler 1972) of minute amounts of glucose and lipid in the form of fatty acids and cholesterol through the endothelial membrane to the underlying intima.

When an insult or injury occurs to the vessel wall this delicate equilibrium situation changes. Subsequent to the trauma there is an excessive influx of plasma-borne material. A reparative response is elicited and intimal cells begin to proliferate in order to accomodate

(ingest) the overload of nutrient. If successful repair occurs, and this may take some time, the process can stop and no atheromatous lesion will appear. But if the tissue response is ineffective and successful repair is not readily accomplished, (such as in the case of a continuous trauma), then the proliferative activity may compromise the filtration of nutrients to the underlying layers (by increasing resistence to permeation), causing localized anoxia with concomitant inability to handle the influx of lipid.

An increased accumulation of lipoprotein may interfere with the lipid transport mechanism across the cell membrane, preventing the extracellular lipid from being utilized and perpetuating the process of accumulation, or it may increase the metabolic requirements of the cell and hence aggravate the hypoxia leading to further increase in endothelial permeability. Thus, the hypoxia might result in the self-perpetuating growth of the atherosclerotic placque. The reparative reaction serves to propagate the formation of an early lesion. The progression of an atheroma can thus be considered as an unsuccessful repair response to an injury of the arterial wall.

To imitate the effect of fluid mechanical injury to the endothelial layer, Bjorkerud (1969) devised a microsurgical instrument to induce defined mechanical injuries to the aorta of rabbits. He showed that a superficial small injury induces progressive intimal thickening and that a larger superficial injury induces changes morphologically similar to those in early human atherosclerosis (Bjorkerud 1969) - a proliferation of smooth cells which are the predominant nutrient of

atheromatic lesions (Getz 1969). Gutstein et al (1962) found that a microtrauma in the abdominal aorta of a rabbit produced in time extensive fibroelastic placques. They commented that blood constituents gained access to the intima as a result of the extension of the opening on the endothelial surface due to elastic forces and hemodynamic stresses. (Endothelium with small traumatic discontinuities develop greater stresses than intact membranes; an initial loss of integrity would be expected to enlarge if the repair response is unsuccessful). Other observers have also detected vastly increased deposition of blood-borne lipoprotein particles in regions of mechanically induced trauma. (Constanides 1968, 1969; Packham 1967; Fry 1969a). Since the flux of macromolecular species from the blood to the arterial wall is intimately linked to the nature of the shearing force on the endothelial surface, in regions where shear damage might occur there is sufficient driving force to deliver an unaccustomed overload to the arterial cells newly exposed to the constituents of the blood stream.

The progressive effects of shear and surgically induced injury to the endothelium are congruent with the pathological processes associated with the development of atherosclerosis; the pathological histology of the region immediately surrounding the point of mechanical injury in all of these experiments is indistinguishable from a naturally occurring atheromatous lesion. Combining these consistent observations with the normal hemodynamically induced mechanical events at the endothelium-blood interface, together with the focal nature of the

disease, it is reasonable to assign a disease initiating role to the wall shear stress which, at some moment in its periodic fluctuation in the regions of atherosclerotic predilection, might reach magnitudes adequate to induce a superficial microtrauma in the endothelial matrix. One pulsation may well be ineffective, but cyclic repetition over a long period of time could progressively weaken the resistance of the endothelium to withstand an instantaneously elevated shear force. Subsequent events including lipoprotein influx, blood elements deposition and tissue repair response would then lead to intimal thickening, anoxia, necrosis, and the establishment of an atheromatous lesion.

There is further evidence to support the shear stress mechanism of disease causation, even in the absence of instantaneous shear levels sufficient to cause micro-injury. Associated with the above observations and the aforementioned process of enhanced convective transport in regions of high shear is the effect of shear stress and discontinuities in the aortic endothelium on endothelial permeability to the passage of lipoproteins and cholesterol.

Unfortunately, most investigations on endothelial permeability have been restricted to capillaries. The characteristic high permeability of these vessels to blood plasma and macromolecules has been attributed to discontinuities in the endothelial lining (French 1966), but no evidence has been presented for the existence of these discontinuities in the normal intact aortic endothelium. The passage of macromolecules across the aortic wall is restricted (Duncan 1965) and the existence of a barrier against the influx and deposition of

cholesterol and lipoproteins in arterial tissue has been postulated to account for the restricted movement of blood components (Zilversmit 1968). The observations of Zilversmit (1964, 1966) are consistent with the suggestion that it is the breakdown of this barrier (or the loss of endothelial integrity) which allows the passage of plasma constituents and the accumulation (deposition) of cholesterol within the arterial wall. There is evidence that stretching (Baumgartner 1963; Fry 1969b) or deforming (Fry 1968) the endothelial membrane decreases its integrity, causing changes in permeability, rendering the cell more susceptible to the influx of matter being convected from the blood to the blood-wall interface. Fry (1969a) and Carew (1971) found that cellular permeability increased at stress exposures below those associated with detectable histological change.

These investigations support the concept that plasma protein filtration is restricted by the intact arterial endothelium and that endothelial integrity is of primary importance for the regulation of permeability through the arterial wall. The significance of endothelial permeability is further attested by the findings that the deposition of blood-borne particles is almost exclusively confined to tissue with decreased endothelial integrity (Bondjers 1972).

Thus the wall shear stress, at all levels of exposure, acts to reduce the integrity of the endothelium by increasing its permeability to the passage of macromolecules. At critical magnitudes (for dog aorta - 380 dynes/cm^2) the shearing force can impart a discontinuity or microtrauma to the cellular membrance, an insult which, if repair

is ineffective, can lead to further invasion by macromolecules and progressive deterioration.

In an attempt to determine the levels of shear within the circulatory system the magnitudes of shear stress within the thoracic aorta of dogs was measured by Ling et al (1968) with the use of a specially adapted heated film anemometer system. Preliminary measurements indicated that peak wall shear stresses reach values approximately one-third (160 dynes/cm^2) of the endothelial critical yield stress reported by Fry (1968). Subsequent measurements were made by Ling and Atabek (1972). Using a model system designed to simulate the systemic circulation of a medium sized dog they obtained for the peak wall shear stress levels in the descending aorta a value of approximately 60 dynes/cm^2, half the value previously reported.

Regions of the arterial tree experience local shear stress forces elevated above the values in the descending aorta. Accordingly, it is reasonable to presume that the endothelial layer in these areas (entrances of branching vessels and bifurcations) will be subjected to shearing forces more closely approaching the critical yield stress. With the attendant effects of altered protein permeability through the endothelium and its associated proliferating response, it is no surprise that the zones experiencing elevated shear forces are identical to the regions of the circulation that witness a predilection for atherosclerosis.

III. PHYSICS OF PULSATILE FLOW: EFFECTS UPON ELECTRODE RESPONSE

A non-steady, but periodic exciting force is exerted upon the fluid by varying the height of a pressure head driving the steady incompressible flow. The fluid motion that results is incompressible pulsatile laminar flow whose streamline character has been verified by (Linford 1965, Krasuk 1963, and Hershey 1967). The unsteady nature produces velocity profiles, differing markedly from the accustomed parabolic shape for steady laminar flow, which are governed by the relationship of two parameters, the non-dimensional frequency Ω, and the dimensionless amplitude of pulsation, λ_p, which is a ratio of the amplitude of the oscillatory pressure gradient to that which drives the steady flow.

The frequency parameter, Ω, defined as $R\sqrt{\frac{\omega n}{\nu}}$, is an oscillatory Reynold's Number since it is a ratio of inertial to viscous forces. It is also a measure of the ratio of the radius of the tube to the distance the velocity gradient diffuses from the wall in one period of oscillation. Since conditions are constantly changing this vorticity may not have sufficient time to diffuse to the center of the tube before being convected away and the cycle repeated. Thus for oscillatory motion without a steady flow, at high frequency, when Ω is large ($\Omega > 10$), the fluid near the center moves in a plug like manner without velocity gradients.*

---

* Inertial resistance of the fluid in this region causes the flow in the core of the tube to translate out of phase with respect to the driving force. This phase lag approaches 90^0 as the frequency of oscillation increases.

If a steady stream is added, the velocity profile in a region beyond the flow development length will once again acquire a parabolic profile near the center of the conduit. Once past the development zone the non-linear terms in the equations of motion describing parallel laminar flow vanish. The resulting linear expression implies that the steady and oscillatory motions are decoupled and behave independently of one another. Thus the effect of the oscillatory piston-like center moving with zero net velocity disappears. For motion at low frequency ($\Omega < 1$), the velocity profile is that of steady flow with a parabolic velocity profile corresponding to the instantaneous value of the exciting pressure gradient. The fluid motion is now in phase with the time varying pressure gradient. This is the quasi-steady state.

The fluid motion within the momentum boundary layer, especially very close to the wall, behaves quite differently. In contradistinction to the center region of the pipe, where inertial effects are dominating, the boundary layer is a zone where velocities are small and frictional forces prevail. Fluid particles here are more sensitive and responsive to the fluctuation in the pressure gradient, characterized in amplitude by λ_p and in frequency by Ω. The motion in this layer can be described as being oscillatory in nature, with the thickness of the boundary layer decreasing as Ω increases. The small kinetic energy of the fluid near the wall allows for an acceleration in phase with the periodicity of the pressure gradient. Thus a change in this gradient, transmitted with an infinite celerity because of the fluid incompressibility, will first affect the boundary layer and therefore change the shear stress at the

wall before the mean velocity (averaged over the cross section of the pipe) is altered. If the pressure fluctuation is of sufficient magnitude, the motion of fluid in the boundary layer can, if the period of oscillation is long enough, completely halt and even reverse in direction.

These phenomena must be well characterized in order to understand the state of conditions at and near the surface of the test cathode. This electrode exhibits an effect similar to that associated with the heat capacity of a hot wire anemometer in that the concentration boundary layer over the electrode surface causes a response which is not in phase with the velocity fluctuations or transient shear stress. The mass boundary layer acts as a capacitor imparting a delayed electrode response to the accelerations and decelerations occurring above its surface. The resulting current as a measure of these changing gradients is damped in amplitude as well. This is not to imply that the electro-chemical technique is therefore defective, but rather that changes in mass transfer arising from variations in the pressure gradient are effected, not by a direct response to this force, but through an intermediate - the velocity gradient whose fluctuations are imparted to the concentration gradient in a manner described by the solution to the conservation of mass equation.

IV. DESCRIPTION OF THE ELECTROCHEMICAL METHOD OF DETERMINING TRANSIENT MASS TRANSFER COEFFICIENTS

The circular diffusion-controlled electrode mounted flush with the inside wall of the test section is one part of an electrochemical cell consisting of an electrolyte and a downstream anode. The electrolyte consisted of equi-molar concentrations of potassium ferricyanide and potassium ferrocyanide at approximately 0.01 M, contained in a solution of 2M sodium hydroxide.

This combination has been used earlier to study the unsteady nature of the viscous sublayer in turbulent pipe flow (Reiss 1962, Reiss and Hanratty 1963), to measure the effect of turbulent fluctuations on the local rate of mass transfer to the wall (Van Shaw 1964), for studying the effects of electrode geometry on the measurement of turbulent property intensities (Mitchell 1965), and to determine the frequency response of the boundary layer on wall mass transfer elements (Fortuna 1971, Fortuna and Hanratty 1971). McFeeley (1972) has used the technique to investigate the amplitude of the sinusoidal variation of the mass transfer coefficient and gives a review of additional previous applications of the method. This investigation comprises an extension of his work.

The ferricyanide ions and ferrocyanide ions react at the electrode surfaces according to the following half cell reactions:

Cathode (test electrode): $Fe(CN)_6^{-3} + e^- \rightarrow Fe(CN)_6^{-4}$

Anode (downstream electrode): $Fe(CN)_6^{-4} \rightarrow Fe(CN)_6^{-3} + e^-$

An advantage of this pair of redox reactions is that only an electron is transferred and no plating occurs on the electrode surfaces. Since for every ion reduced, one is oxidized, the concentrations of all species remain constant in the bulk of the fluid which is recycled, thus maintaining a closed loop system.

A potential difference (measured between the test electrode and a proximal reference anode) is applied across the electrodes and the reaction begins as evidenced by a flow of current in an external current monitoring circuit. Because of the equimolarity of the electron transfer, the current produced is directly proportional to the number of moles reacting.

The magnitude of the current is controlled by the rate at which ferricyanide ions react at the cathode because the surface area of this test electrode is less than one ten-thousandth of the reacting area of the downstream anode. The rate of reduction is in turn controlled by two factors: the kinetics of the reaction itself and the rate of transfer of the ferricyanide ion from the bulk of the solution to the nickel surface. This transport is the result of migration due to the effects of the electric field produced by the cathode, and by a convective diffusion mechanism. Reiss (1962) has shown that the use of the large excess of sodium hydroxide reduces the effect of electric field migration to insignificance. Thus the rate of appearance of the ferricyanide ion at the electrode surface is solely limited by the rate of its diffusion from the bulk, through the developing concentration boundary layer, to the reacting surface.

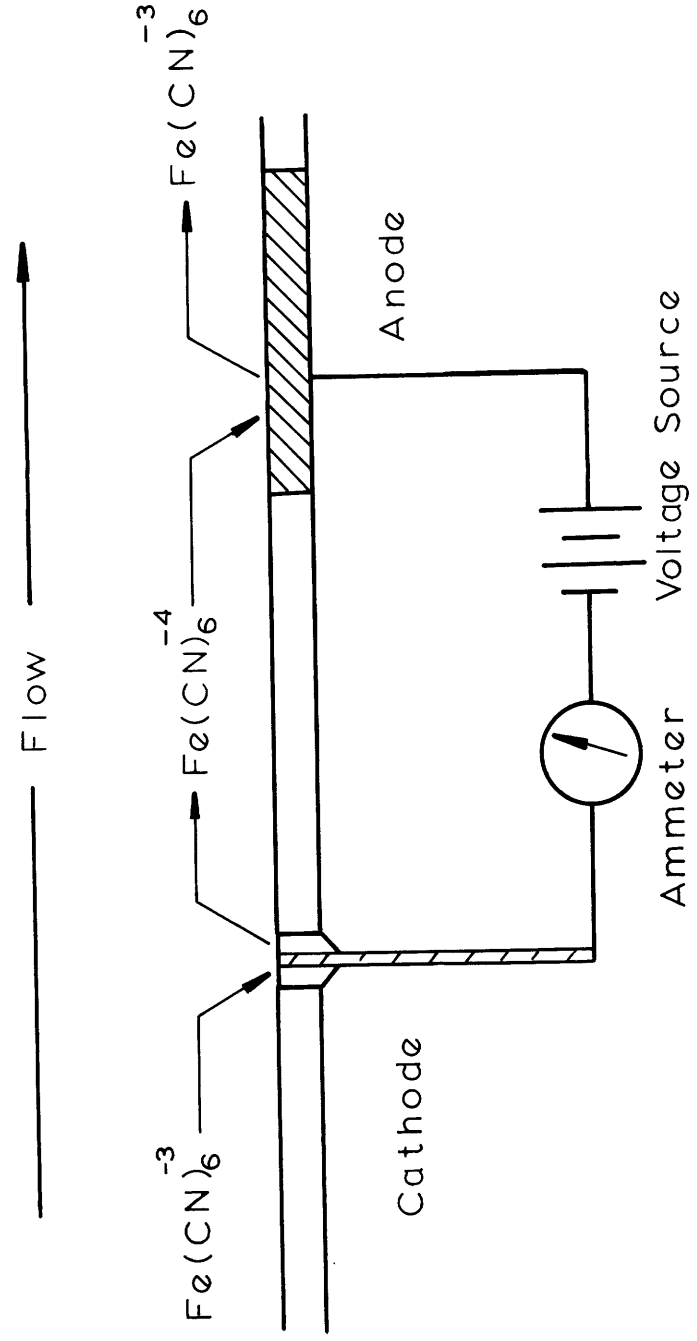

Reactions

Cathode: $Fe(CN)_6^{-3} + e^- \longrightarrow Fe(CN)_6^{-4}$

Anode: $Fe(CN)_6^{-4} \longrightarrow Fe(CN)_6^{-3} + e^-$

Figure 1. Electrochemical Technique

The electrochemical technique described here attains its usefulness from the high rate of electron transfer on the electrode. The surface concentration is virtually identical to zero. Reiss (1962) considered this reaction and concluded that even if the cathode were suddenly flooded with unreacted electrolyte the surface concentration would be restored to zero within 10^{-4} seconds. Ferricyanide reduction on the electrode surface then, is effectively instantaneous.

As the electrode potential difference is increased above zero the kinetics of the reaction also increase and the flow of current is augmented in a linear fashion (See Figure 2) demonstrating that the reaction rate is proportional to the potential difference.

As the voltage is increased still further the current reaches a plateau, leveling at a constant value insensitive to a continued increase in the potential difference. In this region all ions reaching the cathode surface are reduced instantly. The surface concentration of ferricyanide ion remains constant at zero. Since there is no change in the measured current as the voltage is increased one can conclude that in this plateau zone the rate of reaction is limited by the diffusion of ions to the electrode surface.

The rate of mass transfer to the cathode is related to the measured current by

$$N = \frac{I}{A_e n_e F} \qquad (1)$$

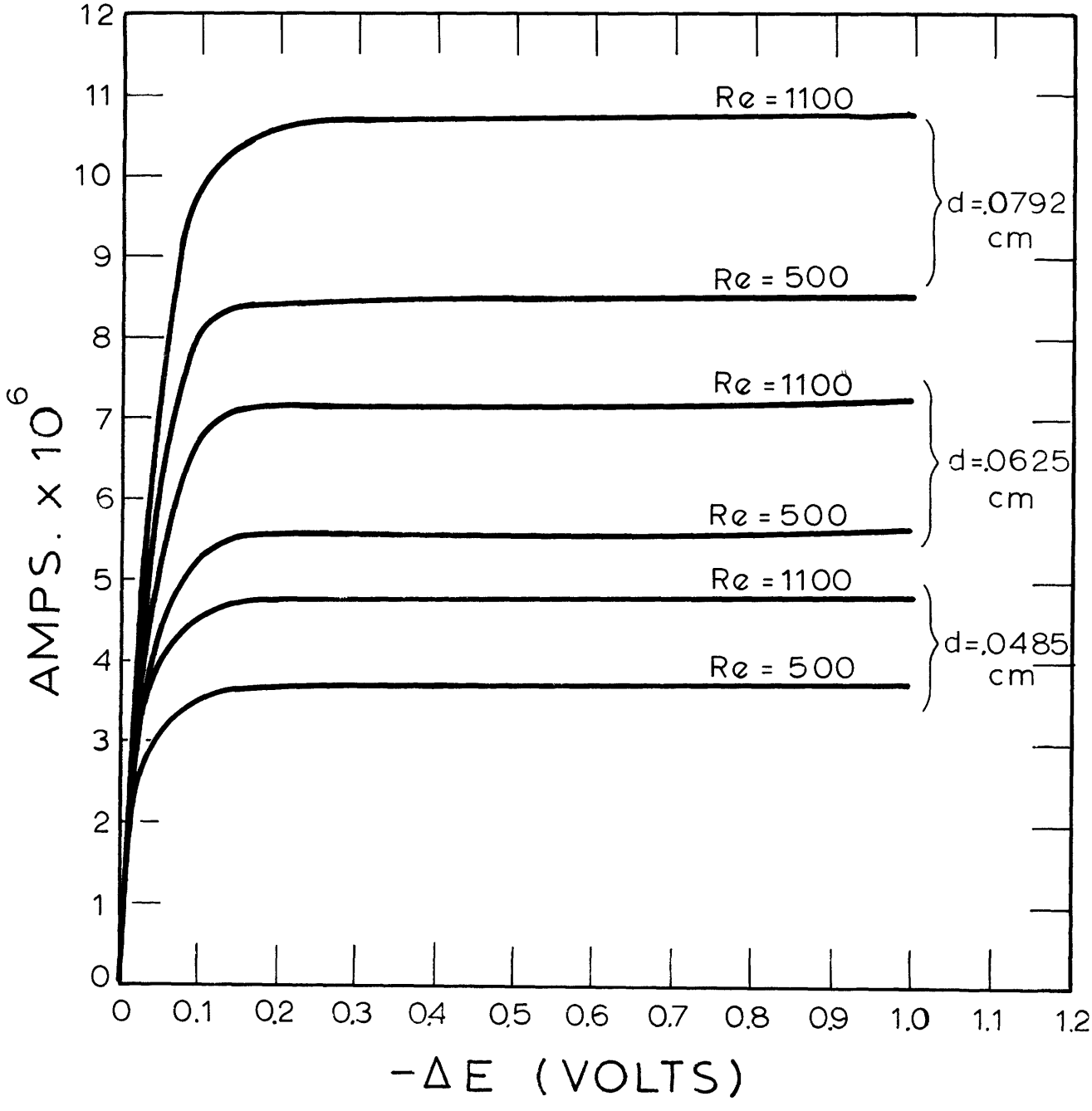

Figure 2. Current-Voltage Curves for Three Electrode Sizes

where N = mass flux of ferricyanide

A_e = electrode surface area

n_e = No. electrons transferred = 1

F = Faraday's constant

I = current measured in external circuit

Interphase mass transfer is more conveniently expressed in terms of a mass transfer coefficient. Then

$$N = K(C_B - C_W) \tag{2}$$

where C_B = bulk concentration of ion

C_W = concentration at electrode surface = 0

Combining (1) and (2),

$$K = \frac{I}{A_e F(C_B - C_W)} \tag{3}$$

Since $C_W = 0$ in the plateau region,

$$K = \frac{I}{A_e F C_B} \tag{4}$$

Thus the mass transfer coefficient is an entity directly obtainable by the electrochemical technique.

Since the flow under consideration in these experiments is non-steady, the mass transfer rate and therefore the measured current will vary in time. The current can be defined to consist of a time average component and a fluctuating component,

$$I = \bar{I} + I' \tag{5}$$

I' is a periodic function of time. The mass transfer coefficient can be expressed in a similar form,

$$K = \bar{K} + K' = \frac{(\bar{I} + I')}{A_e F C_B} \tag{6}$$

At the interface between the fluid and the electrode surface the mass flux is equal to the product of the diffusivity and the concentration gradient at the wall averaged over the electrode surface.

$$N = \langle -\mathcal{D}\left(\frac{\partial C}{\partial y}\right)_W \rangle \tag{7}$$

where the brackets <> signify a spatial average over the surface of the electrode. The time averaged and fluctuating mass transfer coefficients are therefore given by

$$\bar{K} = -\frac{\mathcal{D}}{C_B} \langle \left(\frac{\partial \bar{C}}{\partial y}\right)_W \rangle \tag{8}$$

$$K' = -\frac{\mathcal{D}}{C_B} \langle \left(\frac{\partial c'}{\partial y}\right)_W \rangle \tag{9}$$

V. HYDRODYNAMICS OF PULSATILE FLOW - VELOCITY DISTRIBUTION

The non-steady, fully developed laminar flow of incompressible fluid through a rigid walled cylindrical pipe is considered. The liquid is Newtonian with a constant density and viscosity, and is homogeneous in composition. The physical situation is axisymmetric. Since the flow is fully developed there are no radial velocities, nor is there azimuthal motion (no circumferential velocity). All external body forces are negligible.

The equation of continuity

$$\frac{\partial u}{\partial x} + \frac{\partial v}{\partial r} + \frac{v}{r} = 0 \tag{10}$$

reduces to

$$\frac{\partial u}{\partial x} = 0. \tag{11}$$

The equations of motion for this system then simplify to

$$\frac{\partial u}{\partial t} = -\frac{1}{\rho} \cdot \frac{\partial p}{\partial x} + \frac{\nu}{r} \frac{\partial}{\partial r} \left(r \frac{\partial u}{\partial r}\right) \tag{12}$$

$$u(r = R) = 0$$

$$\left(\frac{\partial u}{\partial r}\right)_{r=o} = 0$$

The non-linear terms are all equal to zero.

It can be shown that

$$\frac{\partial p}{\partial r} = 0 \tag{13}$$

which states that the pressure is constant across a section of pipe and is only a function of axial distance and time.

Pulsations can be regarded as being composed of a steady component and several oscillatory components of various frequencies, each some integral multiple of the fundamental frequency. The periodic function which represents the superimposition of a disturbance of arbitrary form upon a steady pressure gradient can be represented as the Fourier series

$$-\frac{1}{\rho} \cdot \frac{\partial p}{\partial x} = P_s \left[1 + \sum_{n=1}^{N} (a_n \cos n\omega t + b_n \sin n\omega t) \right] \tag{14}$$

where a_n and b_n are real coefficients, or alternately in phase amplitude form as

$$-\frac{1}{\rho} \cdot \frac{\partial p}{\partial x} = P_s \left[1 + \sum_{n=1}^{N} \lambda_{p(n)} \cos (n\omega t - \Theta_n) \right] \tag{15}$$

where

$$\lambda_{p(n)} = (a_n^2 + b_n^2)^{1/2} = \frac{\left(\frac{\partial p}{\partial x}\right)_{n_{osc}}}{\left(\frac{\partial p}{\partial x}\right)_s} \tag{16}$$

is the amplitude of the oscillatory pressure ratio for any particular frequency and

$$\Theta_n = \tan^{-1} \frac{b_n}{a_n} \tag{17}$$

is the phase angle of the n^{th} harmonic with respect to the fundamental frequency.

For the sake of simplicity in calculation it is more convenient to write (14) in the form (see Appendix 1)

$$-\frac{1}{\rho}\cdot\frac{\partial p}{\partial x} = P_s\left[1 + \sum_{n=1}^{N} \lambda_{p(n)}\, e^{in\omega t}\right] \tag{18}$$

The disturbance is seen to be comprised of n sinusoidal harmonics each of frequency $n\omega$ and amplitude $P_s\lambda_{p(n)}$. It is understood that only the real part of (18) has any physical significance.

It should be pointed out here that there are limitations placed upon the amplitude of the pressure perturbation λ_p in order to assure the validity of the linearized perturbation solution to the conservation of mass equation (which follows in the next section), but these restrictions are more lenient than the constraints for λ_p imposed upon the system by other considerations such as the incipience of boundary layer reversal. Details about the magnitude of allowable values for λ_p are in Appendix 2.

The periodic driving force will produce a periodic response in the fluid at the same frequency or integral multiples of the disturbance. This is because the rigidity of the conduit walls provide a linear system. It is reasonable to assume then, that the velocity will acquire the form

$$u(r,t) = u_s + \sum_{n=1}^{N} u_n(r)\, e^{in\omega t} \tag{19}$$

where $u_n(r)$ is a complex coefficient whose description is sought. Substituting (18) and (19) into the single equation of motion (12) and

collecting like terms, separate equations are obtained for the steady state velocity u_s and the fluctuating terms u_n.

$$\frac{\nu}{r}\frac{d}{dr}\left(r\frac{du_s}{dr}\right) + P_s = 0 \tag{20}$$

$$u_s(r = R) = 0$$

$$\left(\frac{du_s}{dr}\right)_{r=o} = 0$$

$$in\omega u_n = P_s\lambda_{p(n)} + \frac{\nu}{r}\frac{d}{dr}\left(r\frac{du_n}{dr}\right) \tag{21}$$

$$u_n(r = R) = 0$$

$$\left(\frac{du_n}{dr}\right)_{r=o} = 0$$

The solution to (20) is the familiar relation for Poiseuille flow

$$u_s(r) = \frac{P_s R^2}{4\nu}\left(1 - \frac{r^2}{R^2}\right) = 2U_o\left(1 - \frac{r^2}{R^2}\right) \tag{22}$$

where U_o is the area averaged mean velocity in the pipe.

For any $\lambda_{p(n)}$ the solution to (21) for the n^{th} harmonic fluctuation of the velocity u_n is obtained as described in Appendix 1. The results are given here.

The expression for u_n is in the form of Bessel functions,

$$u_n(r) = \frac{-8iU_o\lambda_{p(n)}}{\Omega^2}\left[1 - \frac{J_o\,(i^{3/2}\,\Omega\,\frac{r}{R})}{J_o\,(i^{3/2}\,\Omega)}\right] \qquad (23)$$

where the J_o terms are zero order Bessel functions, and Ω is the dimensionless frequency parameter defined as

$$\Omega = R\sqrt{\frac{n\omega}{\nu}}\;; \quad \omega \equiv \text{fundamental frequency}$$

It is effectively an oscillatory Reynold's number, a ratio of inertial to viscous forces.

For each $\lambda_{p(n)}$ there is but one response, u_1. All other harmonics are seen to vanish. The differences in amplitude between the individual frequency components are expressed in the single factor Ω.

Equation (19), the exact solution for the velocity profile, then becomes

$$u(r,t) = 2U_o(1 - \frac{r^2}{R^2}) - 8iU_o \sum_{n=1}^{N}\left\{\frac{\lambda_{p(n)}}{\Omega^2}\left[1 - \frac{J_o(i^{3/2}\,\Omega\,\frac{r}{R})}{J_o(i^{3/2}\,\Omega)}\right] e^{in\omega t}\right\} \qquad (24)$$

Equation (24) is the distribution of velocities as a function of time and radial position and has been verified experimentally by Müeller (1954), Atabek and Chang (1964), Linford and Ryan (1965), Florio and Mueller (1968), and Denison et al (1971). The velocity is written in complex form but only the real part has any physically meaningful significance. It is important to note that the fluctuating components do not contribute to the mean flow.

The foregoing expression for the velocity profile is equivalent to that derived by Womersley (1957). The transient analysis of shear

stress, however, required a more convenient form of the solution, one that was more suitable for computer computation. A description of the procedure is included in Appendix 4.

If the Bessel functions are separated into their real and imaginary components,

$$J_0(i^{3/2}\,\Omega) = \text{ber}\,(\Omega) + i\,\text{bei}\,(\Omega) \tag{25}$$

where ber (x) and bei (x) are Kelvin functions which refer to the real and imaginary parts respectively. These functions are well known for all values of the frequency parameter used in this investigation (Abromowitz 1965).

Uchida (1956) has employed this notation in his analysis of flow disturbed by a known time varying pressure gradient of arbitrary form. His solution is in the form

$$\frac{u(r,t)}{U_o} = \frac{u_s}{U_o} + \sum_{n=1}^{\infty} \frac{u'(n)}{U_o} \tag{26}$$

where $u'_n = u_n e^{in\omega t}$

and

$$\frac{u_s}{U_o} = 2\left(1 - \frac{r^2}{R^2}\right) \tag{27}$$

The expression for the fluctuating component of the velocity field is given by Uchida as

$$\frac{u'(n)}{U_o} = a_n \left\{ \frac{8B}{\Omega^2} \cos\,(n\omega t) + \frac{8(1-A)}{\Omega^2} \sin\,(n\omega t) \right\} + b_n \left\{ \frac{8B}{\Omega^2} \sin\,(n\omega t) - \frac{8(1-A)}{\Omega^2} \cos\,(n\omega t) \right\} \tag{28}$$

where

$$A = \frac{\text{ber}(\Omega)\cdot\text{ber}(\Omega\frac{r}{R}) + \text{bei}(\Omega)\cdot\text{bei}(\Omega\,\frac{r}{R})}{\text{ber}^2(\Omega) + \text{bei}^2(\Omega)};\quad B = \frac{\text{bei}(\Omega)\cdot\text{ber}(\Omega\,\frac{r}{R}) - \text{ber}\,(\Omega)\cdot\text{bei}(\Omega\,\frac{r}{R})}{\text{ber}^2(\Omega) + \text{bei}^2(\Omega)}$$

which, for a pressure gradient in the form of (15), becomes

$$\frac{u'_{(n)}}{U_o} = \lambda_{p(n)}\left\{\left[\frac{8B}{\Omega^2}\right]\cos\,(n\omega t-\Theta_n) + \left[\frac{8(1-A)}{\Omega^2}\right]\,\sin\,(n\omega t-\Theta_n)\right\} \qquad (29)$$

where $\Theta_n = \tan^{-1}\frac{b_n}{a_n}$.

Equation (29) is the basis for the theoretical determination of the time varying wall shear rate. (See Appendix 4).

VI. DEVELOPMENT OF THE THEORETICAL MODEL FOR MASS TRANSFER

The route to the experimental determination of the instantaneous shear stress is through the direct measurement of the fluctuating mass transfer coefficient. This quantity is directly obtainable whereas the frictional force is not, being related to it through the conservation of mass equation. It is therefore desirable to have a mathematical model which will both predict the effects of pulsatile parameters upon the transient behavior of the mass transfer process and characterize the response of the diffusion controlled electrode to changes in the flow near the wall of the tube where the velocity profile is virtually linear. The theory that constructs this mathematical model was initially developed by Fagela-Alabastro (1967, 1969) and more recently refined by McFeeley (1972) who conducted an extensive investigation into the response of the diffusion controlled nickel electrode to pulsed laminar flow. His results were reported as the dependence on various flow parameters of the ratio of the amplitude of the first harmonic fluctuating component of the mass transfer coefficient to the steady flow value. The results of this work echo this format. It was necessary to repeat these mass transfer studies to determine whether the results could be extended to the analysis of shear stress. The theory presented here follows closely the constructions outlined by McFeeley. The reader should bear in mind that the mass transfer analysis presumes a knowledge of the velocity profile at the wall in order to couple the conservation of mass equation to the momentum equation, whereas the subsequent

mathematical model, that which relates the shear rate to the measured mass transfer coefficient treats this quantity as an unknown variable. This seeming paradox is resolved when one realizes that the purpose of this investigation was to reconstruct indirectly, through experimentally derived, well characterized quantities, the wall velocity gradient whose exact value was known a priori via the hydrodynamic theory of axisymmetric cylinderical flow presented in the last section. An accurate conformity between experiment and the theory of Uchida was an essential prerequisite for similar studies in geometrical flow models where no analytical fluid mechanical model can be applied.

Concentration Distribution

The analysis is restricted to the region above the electrode surface where the concentration boundary layer, commencing at the leading edge of the cathode, is developing in thickness. Since the Schmidt Number $(\frac{\nu}{D})$ for this system is very large ($\simeq$ 1500), the concentration boundary layer is very much thinner than the momentum boundary layer. It therefore lies immediately adjacent to the wall.

In this region it is valid to consider the velocity profile to be a linear function of the distance from the wall with a slope equal to the actual slope at the wall. The velocity in the boundary layer is then expressed as

$$u(y,t) = y\left(\frac{\partial u}{\partial y}\right)_{y=o} \tag{30}$$

upon the introduction of the transformation $y = R - r$.

With this relation the differentiation of equation (24) becomes linearized and is substituted into the conservation of mass equation. The velocity in the boundary layer is given by

$$u(y,t) = \frac{U_o y}{R}\left[4 + \sum_{n=1}^{N} \lambda_{p(n)}\, \gamma_n e^{in\omega t}\right] \tag{31}$$

where $$\gamma_n = \left[\frac{-8i^{1/2}}{\Omega} \cdot \frac{J_1(\Omega i^{3/2})}{J_o(\Omega i^{3/2})}\right]$$

Neglecting curvature, the conservation of mass equation for the concentration boundary layer is expressed as

$$\frac{\partial C}{\partial t} + u\frac{\partial C}{\partial x} + v\frac{\partial C}{\partial y} = \frac{\partial}{\partial x}\left(\mathcal{D}\frac{\partial C}{\partial x}\right) + \frac{\partial}{\partial y}\left(\mathcal{D}\frac{\partial C}{\partial y}\right) \tag{32}$$

which simplifies to (see Appendix 3)

$$\frac{\partial C}{\partial t} + u\frac{\partial C}{\partial x} = \mathcal{D}\frac{\partial^2 C}{\partial y^2} \tag{33}$$

$$C(x, y = o, t) = C_W = 0$$

$$C(x, y = \infty, t) = C_B$$

$$C(x = o, y, t) = C_B$$

The last boundary condition requires that neither boundary layer separation nor reversal occur at the wall. The constraints upon the flow parameters which must be respected to maintain the validity of this boundary condition and ensure that flow reversal at the wall does

not take place are described in detail in Appendix 2. McFeeley in his investigation (1972), unnecessarily kept $\lambda_{p(n)}$ small at values not exceeding 0.2. The results of Appendix 2 demonstrate that the magnitude of $\lambda_{p(n)}$ can exceed unity under certain conditions without reversing the motion of the boundary layer.

The solution to (33) is obtained by a perturbation around the steady state solution with λ_p as the perturbation parameter. (Fagela-Alabastro 1967, McFeeley 1972). A different form of the equation is obtained by making the substitution

$$\phi = \frac{C - C_W}{C_B - C_W} = \frac{C}{C_B} \tag{34}$$

With the introduction of this dimensionless variable equation (33) becomes

$$\frac{\partial \phi}{\partial t} + u \frac{\partial \phi}{\partial x} = \mathcal{D} \frac{\partial^2 \phi}{\partial y^2} \tag{35}$$

$$\phi(x, y = o, t) = 0$$

$$\phi(x, y = \infty, t) = 1$$

$$\phi(x = o, y, t) = 1$$

Using $\lambda_{p(n)}$ as a perturbation parameter a solution is constructed for each harmonic $\lambda_{p(n)}$. The linearity of the system precludes harmonic-harmonic interaction; therefore a solution for n sinusoidal waves is constructed by the superposition of solutions for each value of n. The first harmonic only of the pressure ratio will be considered here to simplify notation.

The expression for the solution is

$$\phi(x,y,t) = \phi_o(x,y) + \lambda_p\phi_1(x,y,t) + \lambda_p^2\phi_2(x,y,t) + \cdots \lambda_p^N\phi_N(x,y,t) \quad (36)$$

where ϕ_o is the steady state solution, ϕ_1 the first order term, etc. The validity of this form of a solution is imbedded in the necessity that for large values of n

$$\lambda_p^n\phi_n(x,y,t) << \lambda_p^{n-1}\phi_{n-1}(x,y,t)$$

Equation (31) and (36) are substituted into equation (35) producing (N+1) differential equations in like terms of λ_p.

Fagela-Alabastro has solved the resulting equations for N = 2. Only the first order term will be considered here. Two differential equations remain to be solved:

$$\phi(x,y,t) = \phi_o(x,y) + \lambda_p\phi_1(x,y,t) + R_n \quad (37)$$

If R_n is sufficiently small the truncation is valid. It will be shown that the results of this investigation support this stand.

The equation for the steady state term, equivalent to the time average for a solution in the form of (37) is

$$\frac{4U_o y}{R}\frac{\partial\phi_o}{\partial x} = \mathcal{D}\frac{\partial^2\phi_o}{\partial y^2} \quad (38)$$

$$\phi_o(x,y = o) = 0$$

$$\phi_o(x,y = \infty) = 1$$

$$\phi_o(x = o,y) = 1$$

and for the first order periodic term:

$$\frac{\partial \phi_1}{\partial t} + \frac{4U_o y}{R} \frac{\partial \phi_1}{\partial x} + \frac{U_o y}{R} \gamma e^{i\omega t} \frac{\partial \phi_o}{\partial x} = \mathcal{D} \frac{\partial^2 \phi_1}{\partial y^2} \tag{39}$$

$$\phi_1(x, y = o, t) = 0$$

$$\phi_1(x, y = \infty, t) = 0$$

$$\phi_1(x = o, y, t) = 0$$

Steady Flow Solution

The solution to the steady state equation (38) is obtained through the implementation of a similarity transformation. The procedure is detailed in Appendix 3 and the results are given here. With the introduction of the transformed variable

$$\zeta = y \left(\frac{4}{9} \frac{U_o}{R\mathcal{D}x} \right)^{1/3} \tag{40}$$

equation (38) is reduced to an ordinary differential equation

$$\phi_o'' + 3\zeta^2 \phi_o' = 0 \tag{41}$$

whose solution is

$$\phi_o = \frac{3}{\Gamma(\frac{1}{3})} \int_o^{\zeta} \exp(-\zeta^3) d\zeta \tag{42}$$

originally obtained by Lévêque (1928).

The restraint upon this solution is related to the assumption of a linear velocity profile within the concentration layer which requires

that the Graetz Number

$$Gz = \frac{(L/D)}{ReSc} \tag{43}$$

be less than 10^{-2}. This introduces L, the equivalent rectangular length for a circular electrode, shown by Reiss (1962) to equal 82% of the electrode diameter. The validity of (42) is assured by the use of small electrodes and a liquid with its high Schmidt Number.

The solution for ϕ_o can be related to the mass transfer coefficient since

$$K_s = \mathcal{D} \frac{\partial \phi_o}{\partial y} \tag{44}$$

which leads to (see Appendix 3)

$$K_s = \mathcal{D} \frac{12^{1/3}}{\Gamma(\frac{1}{3})} \left(\frac{U_o}{R\mathcal{D}x}\right)^{1/3} \tag{45}$$

This is the local mass transfer coefficient which, when integrated over the electrode length, yields the spatial average mass transfer coefficient, the quantity obtainable from the measured current flowing through the cathode.

$$\langle K_s \rangle = \frac{\int_0^L K_s dx}{\int_0^L dx} \tag{46}$$

The result of the integration can be written in terms of the Graetz Number as

$$\langle K_s \rangle = \frac{3}{2} \cdot \frac{(3)^{1/3}}{\Gamma\left(\frac{1}{3}\right)} \cdot \frac{\mathcal{D}}{R} Gz^{-1/3} \tag{47}$$

Equation (47) is the steady state solution with which the electrode system was tested.

Since the harmonics of the pressure gradient driving the flow are sinusoidal, the first order term for the concentration profile can be expressed as

$$\phi_1(x,y,t) = f_\phi(x,y)e^{i\omega t} \tag{48}$$

Equation (48) is substituted into (39) to yield the differential equation for f_ϕ

$$\frac{\partial^2 f_\phi}{\partial y^2} - 4 \frac{U_o y}{R\mathcal{D}} \frac{\partial f_\phi}{\partial x} - \frac{i\alpha^2}{R^2} f_\phi = \frac{U_o y}{R\mathcal{D}} \gamma \frac{\partial \phi_o}{\partial x} \tag{49}$$

where

$$\alpha = \Omega \, Sc^{1/2} \tag{50}$$

A solution is obtained for both low and high frequencies by first non-dimensionalizing (49) by introducing

$$\xi = \frac{\mathcal{D}x}{U_o R^2} \alpha^3 i^{3/2} \tag{51}$$

as per McFeeley (1972) which gives

$$\frac{\partial^2 f_\phi}{\partial \eta^2} + \frac{4}{3} \eta^2 \frac{\partial f_\phi}{\partial \eta} - 4\eta\xi \frac{\partial f_\phi}{\partial \xi} - \xi^{2/3} f_\phi = \frac{1}{4} \gamma \frac{\partial^2 \phi_o}{\partial \eta^2} \tag{52}$$

where

$$\eta = y \left(\frac{U_o}{R\mathcal{D}x}\right)^{1/3} = \left(\frac{9}{4}\right)^{1/3} \zeta$$

Low Frequency Solution

The axial direction derivative, $\frac{df_\phi}{d\xi}$, is neglected as being small and a solution is assumed in the form of the perturbation

$$f_\phi(\eta,\xi) = f_\phi^o(\eta) + \xi^{2/3} f_\phi^1(\eta) + \xi^{4/3} f_\phi^2(\eta) + \cdots \tag{53}$$

with only the first two terms of the series contributing significantly. The remaining terms are neglected. McFeeley has solved (52) for the term f_ϕ^o and f_ϕ^1 by substituting (53) into (52), collecting like terms of ξ, and solving the resultant pair of differential equations. He obtains the result for low frequency

$$f_\phi = \frac{(12)^{1/3}}{12\Gamma\left(\frac{1}{3}\right)} \gamma\eta \exp\left(-\frac{4}{9}\eta^3\right) \left\{1 + \xi^{2/3} \left(a + \frac{\eta^3}{6}\right)\right\} \tag{54}$$

where a is an arbitrary constant of integration to be determined.

It can be shown that the Nusselt number for the fundamental fluctuating component is related to f_ϕ in the following way:

$$Nu_F = 2R\lambda_p \left.\frac{\partial \phi_1}{\partial y}\right|_{y=o} = 2R \frac{K_F}{\mathcal{D}} = \frac{2}{\psi^{1/3}} \lambda_p \left.\frac{\partial f_\phi}{\partial \eta}\right|_{\eta=o} \tag{55}$$

where

$$\psi = \frac{\mathcal{D}x}{U_o R^2} \tag{56}$$

and $K_F = \lambda_p K_f$ is the amplitude of the first harmonic fluctuation. The derivative of equation (54) is

$$\left.\frac{\partial f_\phi}{\partial \eta}\right|_{\eta=o} = \frac{(12)^{1/3}}{12\Gamma\left(\frac{1}{3}\right)}\ \gamma\ \{1 + \xi^{2/3}a\} \tag{57}$$

With this substitution into (55), along with equation (52) and (56), the definitions of η and ψ, the expression for the amplitude of the fluctuating Nusselt Number is

$$Nu_F = \frac{(12)^{1/3}}{6\Gamma\left(\frac{1}{3}\right)}\ \left(\frac{U_o R^2}{\mathcal{D}x}\right)^{1/3}\ \gamma\lambda_p \left\{1 + \frac{ai\alpha^2}{2}\ \left(\frac{\mathcal{D}L}{U_o R^2}\right)^{2/3}\right\} \tag{58}$$

Referring to equation (55) the amplitude of the local fluctuating mass transfer coefficient then becomes

$$K_F = \frac{(12)^{1/3}}{12\Gamma\left(\frac{1}{3}\right)}\ \gamma\ \left(\frac{U_o}{R\mathcal{D}x}\right)^{1/3}\ \mathcal{D}\lambda_p \left\{1 + ai\alpha^2\ \left(\frac{\mathcal{D}x}{U_o R^2}\right)^{2/3}\right\} \tag{59}$$

As was done for the steady state mass transfer coefficient, the spatial average of K_F is found to be

$$\langle K_F\rangle = \frac{(12)^{1/3}}{8\Gamma\left(\frac{1}{3}\right)}\ \gamma\ \left(\frac{U_o}{R\mathcal{D}L}\right)^{1/3}\ \mathcal{D}\lambda_p \left\{1 + \frac{ai\alpha^2}{2}\ \left(\frac{\mathcal{D}L}{U_o R^2}\right)^{2/3}\right\} \tag{60}$$

Recalling equation (43) and the expressions for Re and Sc, (60) is simplified by noting that

$$\frac{\mathcal{D}L}{U_o R^2} = 4Gz \tag{61}$$

Thus

$$\langle K_F \rangle = \frac{(12)^{1/3}}{8\Gamma\left(\frac{1}{3}\right)} \gamma \left(\frac{U_o}{R\mathcal{D}L}\right)^{1/3} \mathcal{D}\lambda_p \left\{1 + i2^{1/3} a\alpha^2 Gz^{2/3}\right\} \tag{62}$$

The mass transfer coefficient can be written directly from a differentiation of the perturbation solution, equation (37), as the sum of a steady component and a fluctuating component,

$$\langle K \rangle = \langle K_s \rangle + \lambda_p \langle K_f \rangle e^{i\omega t} \tag{63}$$

or for n harmonics

$$\langle K \rangle = \langle K_s \rangle + \sum_{n=1}^{N} \lambda_{p(n)} \langle K_{f(n)} \rangle e^{in\omega t} \tag{64}$$

The amplitude of each harmonic for the mass transfer coefficient naturally depends upon the amplitude of the pressure gradient causing that fluctuation. The magnitude of the deviation from the steady value is given as $\lambda_{p(n)} K_{f(n)}$. It should be noted that these fluctuations, being only of the first order, have a time average of zero and therefore do not contribute to the time averaged transfer which becomes identical to the steady flow value. The data support this assertion.

The functionality of K_f on n is through the α^2 term of equation (62), thus

$$\alpha^2 = \Omega^2 Sc = R^2 \frac{n\omega}{\mathcal{D}} \tag{65}$$

The results of McFeeley (1972) show that the low frequency range of validity of (62) is for values of $\alpha < 100$ ($\Omega < 2$).

Expressions for $\langle K_s \rangle$ and $\langle K_f \rangle$, equations (47) and (62) replace these terms in (64) and the low frequency solution becomes

$$\langle K \rangle = \frac{3}{2} \frac{(12)^{1/3}}{\Gamma\left(\frac{1}{3}\right)} \mathcal{D} \left(\frac{U_o}{RDL}\right)^{1/3} \left[1 + \frac{1}{12} \sum_{n=1}^{N} \gamma_n \lambda_{p(n)} (1 + i2^{1/3} a\alpha^2 Gz^{2/3}) e^{in\omega t} \right] \tag{66}$$

This is more conveniently written in the form of equation (18) as

$$\langle K \rangle = \langle K_s \rangle \left[1 + \sum_{n=1}^{N} \lambda_{m(n)} e^{in\omega t} \right] \tag{67}$$

where $\lambda_{m(n)}$ is the mass transfer ratio for the n^{th} pressure gradient harmonic and with reference to equation (63) is defined as

$$\lambda_m = \frac{\langle K_f \rangle}{\langle K_s \rangle} \quad \lambda_p = \frac{\langle K_F \rangle}{\langle K_s \rangle} \tag{68}$$

for each first order harmonic. This expression is a ratio of the amplitude of the fluctuating component (for each n) of the mass transfer coefficient to the steady value.

Comparing equations (66), (67), and (68) the mass transfer ratio then becomes

$$\lambda_{m(n)} = \lambda_{p(n)} \frac{\gamma_n}{12} \{1 + i2^{1/3} a\alpha^2 Gz^{2/3}\} \tag{69}$$

which can be reduced by considering the series expansion of $\gamma_n(\Omega)$ for small values of Ω. Recall that

$$\gamma_n = \frac{-8i^{1/2}}{\Omega} \frac{J_1(\Omega i^{3/2})}{J_o(\Omega i^{3/2})} \tag{31}$$

From Alabastro (1967) the series expansions of the Bessel functions

$$J_1(i^{3/2}\Omega) = i^{3/2}\left[\sum_{j=0}^{\infty} \frac{(-1)^j \Omega^{4(j+1)}}{2^{4(j+1)}(2j)!\Gamma(2j+2)} + i \sum_{j=0}^{\infty} \frac{(-1)^j \Omega^{4(j+3)}}{2^{4(j+3)}(2j+1)!(2j+3)}\right]$$

$$J_0(i^{3/2}\Omega) = \sum_{j=0}^{\infty} \frac{(-1)^j \Omega^{4(j+1)}}{2^{4j}((2j)!)^2} + i \sum_{j=0}^{\infty} \frac{(-1)^j \Omega^{4(j+2)}}{2^{4(j+2)}((2j+1)!)^2} \qquad (70)$$

are substituted into the expression for γ_n. Retaining only the first few terms which are significant,

$$\gamma_n = \frac{4\left[1 + \frac{i\Omega^2}{8} - \frac{\Omega^4}{192}\right]}{\left[1 + \frac{i\Omega^2}{4} - \frac{\Omega^4}{64}\right]} \qquad (71)$$

Further simplification results by making use of the binomial expansion

$$\frac{1}{1 + \frac{i\Omega^2}{4} - \frac{\Omega^4}{64}} = 1 - \left(\frac{i\Omega^2}{4} - \frac{\Omega^4}{64}\right) + \left(\frac{i\Omega^2}{4} - \frac{\Omega^4}{64}\right)^2 + \cdots \qquad (72)$$

and inserting this into (71). For small values of Ω, λ_n can then be expressed as

$$\gamma_n \simeq 4\left[1 - \frac{i\Omega^2}{8} - \frac{\Omega^4}{48}\right] \qquad (73)$$

This expression replacing γ_n in equation (69) reduces the equation for the low frequency mass transfer ratio to a form of the derivation obtained by Reiss (1962) for low frequency fluctuations. By comparing the two results McFeeley (1972) evaluated the constant (a)

and assigned the value

$$a = -\ 0.25285\ \left(\frac{3}{2}\right)^{1/3}\ \Gamma\ \left(\frac{1}{3}\right) \tag{74}$$

The mass transfer ratio is then

$$\lambda_{m(n)} = \lambda_{p(n)}\ \frac{\gamma_n}{12}\ \{1 - i\tau\alpha^2 Gz^{2/3}\} \tag{75}$$

with

$$\tau = \frac{0.50571\ \Gamma\ (\frac{1}{3})\ 3^{1/3}}{2} = 0.97695 \tag{76}$$

If a mass transfer pressure ratio is defined as

$$R_{mp} = \frac{\lambda_{m(n)}}{\lambda_{p(n)}} = \frac{\langle K_{f(n)}\rangle}{\langle K_s\rangle} = \frac{\gamma_n}{12}\ \{1 - i\tau\alpha^2\ Gz^{2/3}\} \tag{77}$$

then the magnitude of this quantity is a mass transfer to pressure amplitude ratio and

$$A_{mp} = M\{R_{mp}\} = M\left\{\frac{\gamma_n}{12}\ [1 - i\tau\alpha^2\ Gz^{2/3}]\right\} \tag{78}$$

where A_{mp} is the amplitude ratio used to fit the low frequency mass transfer data and M refers to the modulus. Since

$$\gamma_n = \frac{-8i^{1/2}}{\Omega}\ \frac{J_1(\Omega i^{3/2})}{J_0(\Omega i^{3/2})} \tag{31}$$

then

$$M\{\gamma_n\} = \frac{8\ M_1(\Omega)}{\Omega\ M_0(\Omega)} \tag{79}$$

where the $M_j(\Omega)$ are moduli of Bessel functions of order (j). These are tabulated by McLachlan (1941). Equation (78) then becomes

$$A_{mp} = \frac{2M_1(\Omega)}{3\Omega M_0(\Omega)} \left[1 + \tau^2\alpha^4\ Gz^{4/3}\right]^{1/2} \tag{80}$$

This is the equation used to model the low frequency mass transfer data.

The behavior of the low frequency solution, equation (77), as the frequency approaches zero, or equivalently as Ω goes to zero, is of interest.

Equation (54), the expression for the Nusselt or Sherwood Number is

$$Nu_F = 2R\lambda_p \left.\frac{\partial\phi_1}{\partial y}\right|_{y=o} = \frac{2RK_F}{\mathcal{D}} = \frac{2}{\psi^{1/3}} \lambda_p \left.\frac{\partial f_\phi}{\partial\eta}\right|_{\eta=o} \tag{54}$$

Substituting for ψ from (56) and rearranging yields

$$K_F = \frac{\mathcal{D}^{2/3}\ U_o^{1/3}}{R^{1/3}\ x^{1/3}} \lambda_p \left.\frac{\partial f_\phi}{\partial\eta}\right|_{\eta=o} \tag{81}$$

From equations (51, (57), and (73), as Ω approaches zero,

$$\left.\frac{\partial f_\phi}{\partial\eta}\right|_{\eta=o} = \frac{(12)^{1/3}}{3\Gamma\left(\frac{1}{3}\right)} \tag{82}$$

Then

$$K_F = \frac{\mathcal{D}^{2/3}\ U_o^{1/3}}{R^{1/3}x^{1/3}} \cdot \frac{(12)^{1/3}}{3\Gamma\left(\frac{1}{3}\right)} \cdot \lambda_p \tag{83}$$

and $$\langle K_F \rangle = \frac{3}{2}\left\{\left[\frac{\mathcal{D}^{2/3} U_o^{1/3}}{R^{1/3} L^{1/3}}\right]\left[\frac{(12)^{1/3}}{3\Gamma\left(\frac{1}{3}\right)}\right]\right\} \cdot \lambda_p \tag{84}$$

which is the spatial average over the electrode surface. The equivalent expression for $\langle K_s \rangle$ from equations (45) and (46) is

$$\langle K_s \rangle = \frac{3}{2}\,\mathcal{D}\,\frac{(12)^{1/3}}{\Gamma\left(\frac{1}{3}\right)}\left(\frac{U_o}{R\mathcal{D}L}\right)^{1/3} \tag{85}$$

Since $$\langle K_F \rangle = \lambda_p \langle K_f \rangle \tag{86}$$

dividing (84) by (85) yields, with reference to equation (68)

$$\frac{\langle K_f \rangle}{\langle K_s \rangle} = \frac{\lambda_m}{\lambda_p} = \frac{1}{3} \tag{87}$$

This is the low frequency asymptote of A_{mp}.

The slope with which the $\frac{1}{3}$ asymptotic value is reached can be obtained directly by differentiating the low frequency solution

$$R_{mp} = \frac{\gamma}{12}\left(1 - i\tau\alpha^2 Gz^{2/3}\right) \tag{77}$$

to obtain

$$\frac{\partial R_{mp}}{\partial \alpha} = -\left(\frac{i\gamma}{6}\,\tau\alpha Gz^{2/3} + \frac{i\gamma'}{12}\,\tau\alpha^2\, Gz^{2/3}\right) \tag{88}$$

which has the low frequency limit

$$\lim_{\alpha \to o} \frac{\partial R_{mp}}{\partial \alpha} = 0 \tag{89}$$

Therefore A_{mp} approaches the low frequency asymptote of $\frac{1}{3}$ with zero slope. This is noted on Figure (3) which displays the behavior of A_{mp} as a function of frequency. Very low frequency data were difficult to obtain because the motor could not deliver a constant angular frequency at the very low rotational speeds needed to generate values of α near zero.

High Frequency Solution

The solution to the differential equation for f_ϕ, equation (52), for large values of the frequency parameter, has been obtained by Fagela-Alabastro (1967) and Fortuna (1971) by neglecting the term $\frac{\partial f_\phi}{\partial \xi}$, the x-direction derivative, as suggested by Lighthill (1954) when the boundary layer problem of flow oscillations superimposed on a steady flow was first considered. When these solutions are placed in the desired form, e.g., $A_{mp} = \lambda_m/\lambda_p$, the result for the spatial average over the electrode surface becomes undefined at the leading edge. This dilemma is overcome by noting that the solution for low frequency, equation (77) is actually a truncation of the expansion

$$R_{mp} = \frac{\gamma}{12} \left(1 - i\tau\alpha^2\, Gz^{2/3} + i^2\tau^2\alpha^4\, Gz^{4/3} + \cdots \right) \tag{90}$$

a geometric progression equivalent to

$$R_{mp} = \frac{\gamma}{12} \frac{1}{1 + i\tau\alpha^2\, Gz^{2/3}} \tag{91}$$

for all values of the product $\tau\alpha^2\, Gz^{2/3}$. This solution also

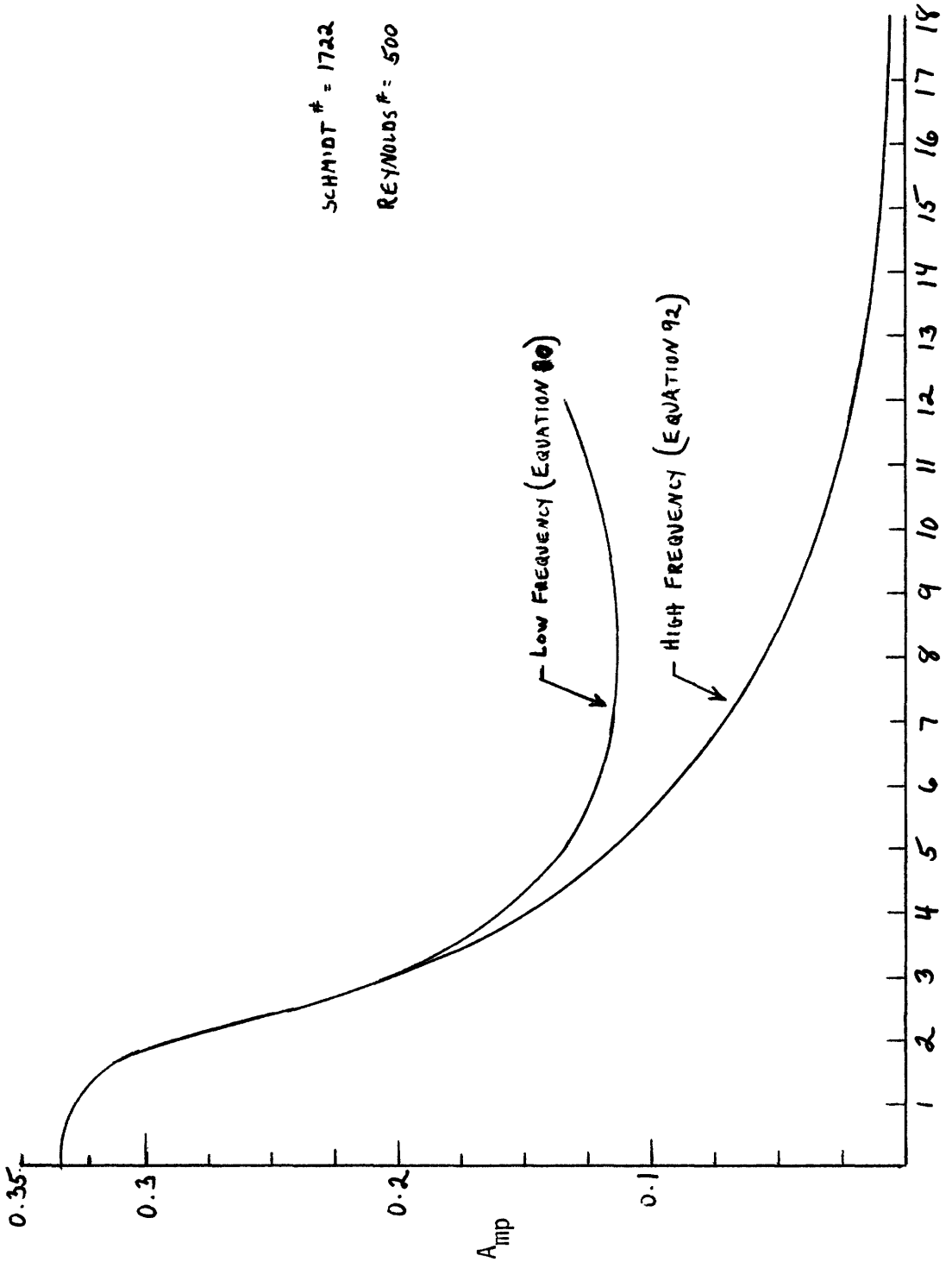

Figure 3. Mass Transfer to Pressure Amplitude Ratios.

satisfies (52), and in the form of (90) reduces to the low frequency solution, equation (77), for small values of α.

The high frequency mass transfer to pressure amplitude ratio then becomes

$$A_{mp} = M\{R_{mp}\} = \frac{2M_1}{3\Omega M_o} \cdot \frac{1}{(1 + \tau^2\alpha^4\ Gz^{4/3})^{1/2}} \tag{92}$$

McFeeley found that the high frequency solution in the form of (91) did not predict his data precisely, but with a correction that imparts a stronger dependence on the L/D ratio, a solution in the form

$$R_{mp} = \frac{\gamma}{12}\left(\frac{1}{1 + iz\left[\alpha^2\ Gz^{1/3}\ (\frac{L}{D})^{1/3}\right]^2}\right) \tag{93}$$

where z is an experimentally determined constant, correlated results in the high frequency range for all electrode lengths and Reynolds Numbers.

To place this solution into the form of (92) the variable x_2 is defined as

$$x_2 = \alpha^2\ Gz^{1/3}\ (\frac{L}{D})^{1/3} \tag{94}$$

such that the modulus of the right hand side of (93) is

$$M\left\{\frac{1}{\left(1 + iz\left[\alpha^2\ Gz^{1/3}\ (\frac{L}{D})^{1/3}\right]\right)}\right\} = M\left\{\frac{1}{1 + izx_2^2}\right\} \tag{95}$$

The modulus then becomes

$$M\left\{\frac{1}{1 + izx_2^2}\right\} = \frac{1}{(1 + z^2x_2^4)^{1/2}} \tag{96}$$

If the denominator is then expanded into the approximate series

$$(1 + z^2x_2^4)^{1/2} \simeq z_1 + z_2x_2 + z_3x_2^2 \tag{97}$$

and substituted into (96), the modulus of equation (93) then becomes

$$M\left\{\frac{\lambda_m}{\lambda_p}\right\} = A_{mp} = \frac{2M_1}{3\Omega M_o}\left(\frac{1}{z_1 + z_2x_2 + z_3x_3^2}\right) \tag{98}$$

where the values of z_1, z_2, and z_3 were found to be (McFeeley 1972)

$$z_1 = 1.147$$

$$z_2 = 4.625 \times 10^{-4}$$

$$z_3 = 7.456 \times 10^{-5}$$

One empirical reason for the discrepancy between the theoretical solution for high frequency, equation (92), and McFeeley's experimentally corrected form, equation (96), is that the increased dependence on the frequency parameter and the L/D ratio may reflect a correction for neglecting $\frac{\partial f_\phi}{\partial \xi}$ in equation (52).

Equation (92) was used as a mathematical model to compare the high frequency mass transfer amplitude data obtained from the electrode, where high frequency is considered to be in the range

$$\alpha > 100$$

$$\text{or} \quad \Omega > 2.$$

VII. RELATION OF MASS TRANSFER MEASUREMENTS TO THE INSTANTANEOUS SHEAR STRESS

The concentration boundary layer over the electrode surface is extremely thin relative to the radius of the pipe, thus permitting the mass balance for the ferricyanide ion to be written as

$$\frac{\partial C}{\partial t} + u\frac{\partial C}{\partial x} + v\frac{\partial C}{\partial y} = \mathcal{D}\left[\frac{\partial^2 C}{\partial x^2} + \frac{\partial^2 C}{\partial y^2}\right] \tag{99}$$

$$C(x, o, t) = 0$$

$$C(x, y = \infty, t) = C_B$$

$$C(o, y, t) = C_B$$

where C is the concentration of ionic species. Throughout the vicinity of the cathode the flow is fully developed and the velocity is changing in a uniformly periodic manner. The transverse velocity in this region vanishes, while the axial velocity and concentration assume the form of steady and fluctuating components.

$$u = \bar{U} + u' \qquad C = \overline{C} + c' \tag{100}$$

The bar represents a time average, defined for any quantity Q as

$$\overline{Q} = \frac{1}{T}\int_0^T QdT \qquad T \equiv \text{period of pulsation} \tag{101}$$

which is indistinguishable from the steady flow value for the linearized

treatment considered here. Thus $\overline{U}$ is identical to U_o, but the barred quantity is used to correspond to the physical consideration of time averaged flow.

As discussed earlier, the velocity profile within the concentration boundary layer is linear and related to S, the shear rate at the wall, represented by

$$S = \overline{S} + s_F e^{i\omega t} \tag{102}$$

for each harmonic. The functionality of the time average and fluctuating velocities within the concentration boundary layer then becomes

$$\overline{U} = \overline{S}y \qquad u' = s'y \tag{103}$$

where

$$s' = s_F e^{i\omega t} \tag{104}$$

The significance of the axial diffusion term of (99) has been investigated by Ling (1963) who has shown that it is negligible compared to the axial convective transport when

$$N_L = \frac{\overline{S}L^2}{\mathcal{D}} > 5000 \tag{105}$$

This restraint arises from the singular behavior at the trailing edge of the electrode surface, the effect of which is lost by the analytical solution to the steady flow form of equation (99). The axial diffusion term will be neglected in the mathematical model presented here, but results from the mass transfer analysis show that the condition (105) may not have been maintained at all times.

Making use of equations (100) and (103), the above assumption, and neglecting second order fluctuating terms, the conservation of mass equation (99) is transformed into two differential equations, one for the time average relation and the other for each of the fluctuating harmonic components. There results

$$\overline{Sy}\,\frac{\partial \overline{C}}{\partial x} = \mathcal{D}\,\frac{\partial^2 \overline{C}}{\partial y^2} \tag{106}$$

$$\overline{C}\,(o,\ y) = C_B$$

$$\overline{C}\,(x,\ \infty) = C_B$$

$$\overline{C}\,(x,\ o) = 0$$

and

$$\frac{\partial c_F}{\partial t} + \overline{Sy}\,\frac{\partial c_F}{\partial x} + s_F y\,\frac{\partial \overline{C}}{\partial x} = \mathcal{D}\,\frac{\partial^2 c_F}{\partial y^2} \tag{107}$$

$$c_F(x,\ \infty,\ t) = 0$$

$$c_F(o,\ y,\ t) = 0$$

$$c_F(x,\ o,\ t) = 0 \qquad (0 \le x \le L)$$

where c_F is the amplitude of the fluctuating component designated by

$$c' = c_F e^{i\omega t} \tag{108}$$

The solution to (106), equivalent to the solution for the steady state equation (38), is detailed in Appendix 3. The desired result, the magnitude of the shear rate as a function of the measured mass transfer coefficient is

$$\overline{S} = \left[\frac{\Gamma\left(\frac{1}{3}\right)\left(\frac{2}{3}\langle\overline{K}\rangle\right)}{(3)^{1/3}} \right]^3 \left(\frac{L}{D^2}\right) \tag{109}$$

where $\langle\overline{K}\rangle$ is the time averaged mass transfer coefficient spatially averaged over the electrode surface. It is presumed not to differ from $\langle K_s \rangle$, the steady flow average, because such deviations would manifest second order effects considered in these analyses to be negligible. The experimental data show that these deviations are generally not greater than 0.5% of $\langle K_s \rangle$.

Solution to the Fluctuating Concentration Field

The solution to (107) is extremely complex for the general time dependent case because no initial condition for time is available. By neglecting the second order terms of fluctuations, equation (99) was transformed into the linear equation (107). The concentration profile thus acts as a linear element responding to changes in the flow field induced by the oscillating shear stress.

The objective is to find a transfer function which relates the amplitude of the shear rate at the pipe wall to the magnitude of the mass transfer coefficient measured at the electrode surface flush with the wall. As will be shown, this transfer function takes the form of the spectral density function, a measure of the total power of the resultant current contributed by each frequency within its spectrum. The pulsatile motion of the flow field, comprised of integral frequencies, can then be analyzed by treating each frequency separately and individually.

Since the rigidity of the tubular walls ensure a linear system, precluding harmonic-harmonic interactions, the shear rate will respond linearly to the periodically undulating pressure gradient, acquiring the form specified by equation (104), for each (n)

$$s'_{(n)} = s_{F(n)} e^{in\omega t} \tag{110}$$

The concentration profile will in turn respond to the velocity gradient in a linear fashion. Thus for each frequency $\hat{c}$ is defined as

$$\frac{c'_{(n)}}{c_B} = \phi_n = \hat{c}_{(n)} e^{in\omega t} \tag{111}$$

Substitution of (110) and (111) into (107) yields the equation for $\hat{c}$ for n = 1,

$$i\omega\hat{c} + \bar{s}y \frac{\partial \hat{c}}{\partial x} + s_F y \frac{\partial \bar{C}}{\partial x} = \mathcal{D} \frac{\partial^2 \hat{c}}{\partial y^2} \tag{112}$$

If the time varying component of the mass transfer coefficient is written as

$$K' = K_F e^{i\omega t} \tag{113}$$

the amplitude, K_F, of the fluctuating mass transfer coefficient is related to $\hat{c}$ in the following way, with reference to equation (55)

$$\frac{K_F}{\mathcal{D}} = \frac{\lambda_p K_f}{\mathcal{D}} = \left.\frac{\partial \phi_1}{\partial y}\right|_{y=o} = \left.\frac{\partial \hat{c}}{\partial y}\right|_{y=o} \tag{114}$$

High Frequency Analysis

Fortuna and Hanratty (1971), employing methods originally suggested by Lighthill (1954) that at high frequencies the term $\overline{Sy}\,\frac{\partial \hat{c}}{\partial x}$ from (112) can be neglected, solved this differential equation for the fluctuating component and obtained the result for $(\frac{\partial \hat{c}}{\partial y})_{y=o}$ for turbulent flow, whose equivalent form for laminar flow in terms of λ_s, the ratio of the fluctuating shear rate to the steady shear rate, is

$$\left.\frac{\partial \hat{c}}{\partial y}\right|_{y=o} = \left[\left(\frac{\Lambda}{x^{4/3}\omega^{3/2}}\right)\left(\frac{\lambda_s}{\overline{S}^{1/2}}\right)\right] \tag{115}$$

where

$$\Lambda = \frac{2\nu^{1/3}\, Sc^{1/3}}{(9)^{1/3}\,\Gamma(\frac{1}{3})}$$

The mass transfer coefficient measured by the electrochemical method is a spatial average over the electrode surface. Therefore the term $\langle K_F \rangle$ must be considered which is evaluated as

$$\langle K_F \rangle = \mathcal{D}\left[\frac{1}{L}\int_0^L \left(\frac{\partial \hat{c}}{\partial y}\right)_{y=o} dx\right] \tag{116}$$

Since the integral is not defined at x = 0, the leading edge of the electrode surface, the relationship (114) cannot be established by this method. Therefore recourse was taken to the numerical solution of (107) obtained for all frequencies by Fortuna (1971) who showed that it reduced to the asymptotic solution (115) at high frequencies. Discussion of this solution follows the analysis for the low frequency range.

Low Frequency Solution

Following the formulation of Mitchell (1965), the amplitude coefficient of the oscillating component of concentration is expanded in a power series for low values of ω,

$$\hat{c} = \hat{c}_0 + \omega\hat{c}_1 + \omega^2\hat{c}_2 + \cdots \tag{117}$$

By substituting (117) into (112) and combining like terms in ω, the following equation is obtained for $\hat{c}_0$, the amplitude of the quasi-steady oscillation,

$$\overline{S}y \frac{\partial \hat{c}_0}{\partial x} + s_F y \frac{\partial \overline{C}}{\partial x} = \mathcal{D} \frac{\partial^2 \hat{c}_0}{\partial y^2} \tag{118}$$

The solution to (118), the quasi-steady solution for the concentration field is given by Mitchell (1965) as

$$\hat{c}_0 = s_F \frac{\partial \overline{C}}{\partial \overline{S}} \tag{119}$$

which leads to the quasi-steady relationship between K_F and s_F,

$$\frac{<K_{F_0}>}{<\overline{K}>} = \frac{1}{3} \frac{s_F}{\overline{S}} \tag{120}$$

where K_{F_0} is the quasi-steady undulating component of the mass transfer coefficient now described for the quasi-steady state as

$$K = \overline{K} + K' = \overline{K} + K_{F_0} e^{i\omega t} \tag{121}$$

At very low frequencies the adjustment of the concentration field to the changing velocity gradient will take place in phase with the velocity gradient. Equation (120) can then be written as

$$\frac{\langle K' \rangle}{\langle \overline{K} \rangle} = \frac{1}{3} \frac{s'}{\overline{S}} \tag{122}$$

The experimental conditions for which the quasi-steady solution is valid can be determined by considering the reduced form of (99)

$$\frac{\partial C}{\partial t} + u \frac{\partial C}{\partial x} = \mathcal{D} \frac{\partial^2 C}{\partial y^2} \tag{123}$$

Equation (122) is valid if and only if

$$\frac{\partial C}{\partial t} << \mathcal{D} \frac{\partial^2 C}{\partial y^2} \tag{124}$$

The condition (124) can be tested by applying an order of magnitude analysis to each term. The differentials are considered as finite differences, and with the period of oscillation representing the characteristic time, one obtains

$$\omega \Delta C << \mathcal{D} \frac{\Delta C}{\delta_C^2} \tag{125}$$

where δ_C is the thickness of the concentration boundary layer. It is then required that the following condition hold,

$$\omega << \frac{\mathcal{D}}{\delta_C^2} \tag{126}$$

The following values for the diffusion coefficient of ferricyanide ion in the experimental fluid have been reported

5.17×10^{-6} cm^2/sec (Reiss 1962)

4.32×10^{-6} cm^2/sec (McFeeley 1972)

For the magnitude of the concentration boundary layer thickness the following expression from Knudsen and Katz (1958) is used which relates the local Sherwood Number to the distance from the leading edge of the transfer element

$$Nu_x = \frac{(2R)K}{\mathcal{D}} = 1.077\ (ReSc)^{1/3}\ \left(\frac{2R}{x}\right)^{1/3} \tag{127}$$

Since δ_c is defined as

$$\delta_c = \frac{\mathcal{D}}{K} \tag{128}$$

the thickness of the mass transfer resistance layer for an electrode diameter of 0.05 cm and a Reynolds Number of 200 is calculated to be 5.89×10^{-3} cm. Using the average of the two values above for $\mathcal{D}$, (126) becomes

$$\omega << 0.11 \text{ rad/sec}$$

The motor employed in this investigation to pulse the flow was incapable of producing such low rotational speeds. The quasi-steady solution was therefore not applicable to the flow conditions since this state was unobtainable.

A solution to (112) was obtained, however, in the same form as (120), by introducing a correction factor to this quasi-steady solution. The

correction factor, a function of frequency and electrode length, was determined numerically by Fortuna and Hanratty (1971) and covers the full range of parameters used in this investigation. The complete response function in the form of (120) becomes valid at all frequencies by incorporating the factor $\hat{A}$ which is a ratio of the absolute value of the mass transfer rate to the quasi-steady rate, thus

$$\hat{A} = \frac{|\langle K_F \rangle|}{|\langle K_{F_o} \rangle|} = \frac{\int_o^L \left| \frac{\partial \hat{c}}{\partial y} \right|_{y=o} dx}{\int_o^L \left| \frac{\partial \hat{c}_o}{\partial y} \right|_{y=o} dx} \tag{129}$$

The corrected solution is described in the form of spectral density functions (the transfer function which relates shear rate to the mass transfer coefficient) from which the instantaneous rate of shear can be determined.

Determination of the Instantaneous Shear Rate

The solution relating the instantaneous shear rate to the instantaneous mass transfer coefficient, its experimentally measured response, is in the form of a correction to the quasi-steady solution (122). For very low frequencies, at any point on the electrode surface

$$\frac{K'}{\overline{K}} = \frac{1}{3} \frac{s'}{\overline{s}} \tag{130}$$

The mean squared value of K' is given by

$$\frac{\overline{K'^2}}{\overline{K}^2} = \frac{1}{9}\frac{\overline{s'^2}}{\overline{S}^2} \tag{131}$$

Since the fluctuating concentration field is related to the fluctuating velocity gradient at the wall through a linear equation (107), the spectral density for s', $W_{s(n)}$, can be related to the spectral density for K', $W_{K(n)}$, (see Appendix 5) at each frequency by the equation (Fortuna and Hanratty 1971),

$$W_{s(n)} = \left(\frac{9\overline{S}^2}{\langle\overline{K}^2\rangle}\right)\frac{W_{K(n)}}{\hat{A}^2_{(n)}} \tag{132}$$

where $\hat{A}^2$, a function of frequency and electrode diameter, is the correction factor previously specified which assures the validity of (132) for all frequencies. As ω approaches zero $\hat{A}^2$ equals unity and equation (132) reduces to the quasi-steady solution (130).

The spectral density function can be related to the amplitude of oscillation as shown in Appendix 5 by equations (A5-5) and (A5-6). This relationship, which removes the time averaged dependence of (132) then results in

$$s_F^2 = \left(\frac{9\overline{S}^2}{\langle\overline{K}^2\rangle}\right)\frac{K_F^2}{\hat{A}^2} \tag{133}$$

or taking the square roots,

$$s_F = \left(\frac{3\overline{S}}{\langle\overline{K}\rangle}\right)\frac{K_F}{\hat{A}} \tag{134}$$

which averaged over the electrode surface becomes

$$s_F = \frac{3\bar{S}}{\langle \bar{K} \rangle} \frac{\langle K_F \rangle}{\hat{A}} \tag{135}$$

Equation (135) is valid at each frequency, with the appropriate value of $\hat{A}$ inserted, and defines the relationship between the amplitude of the fluctuating mass transfer coefficient at any instantaneous point in its period to the magnitude of the shear rate at an equivalent time in its period. Since the undulations in the velocity gradient comprise the driving force for alterations in the concentration field, the change in the shear rate must precede the establishment of a new concentration profile. Thus there is a phase lag (the magnitude of which is dependent upon the frequency) between the shearing force and the measured mass transfer coefficient which is its response. The linearity of the system insures that the complete cycle of oscillations in these two entities will occur in the same period of time, but the peak in the amplitude of the shear stress at the electrode surface will anticipate the maximum in the periodic flow of current generated there. This phase difference can be accounted for by writing (135) in its time varying form for each harmonic, n

$$s_F \cos\left[(n\omega t - \Theta_{n_K}) - \delta_n\right] = \left(\frac{3\bar{S}}{\bar{K}\hat{A}}\right) K_F \cos\left(n\omega t - \Theta_{n_K}\right) \tag{136}$$

where Θ_{n_K} is the phase of the n^{th} harmonic of the fluctuating mass transfer coefficient, obtained by a Fourier analysis of the recorded signal, and δ_n

designates the phase lag between the time varying velocity gradient and the resultant mass transfer coefficient. Values for δ_n and the correction factor $\hat{A}$ were obtained at all frequencies considered in this investigation by Fortuna (1971). They appear on Figures 4 and 5. A simpler form for the graphical representation of the correction factor, $\hat{A}$, was obtained by McMichael (1973) who, by reducing equation (112) to a zero parameter differential equation (through a transformation of the coordinate system), was able to collapse the family of curves appearing on Figure 5 to the single curve of Figure 6. Figure 6 was the basis for determining corrections to the pseudo-steady solution.

Equation (136) was used to construct the experimental curves representing both the instantaneous shear and the ratio of the amplitude of the fluctuating component of the shear rate to the time averaged value. These results were compared to the theoretic values determined from the theory of Uchida (1956) as outlined in Appendix 4.

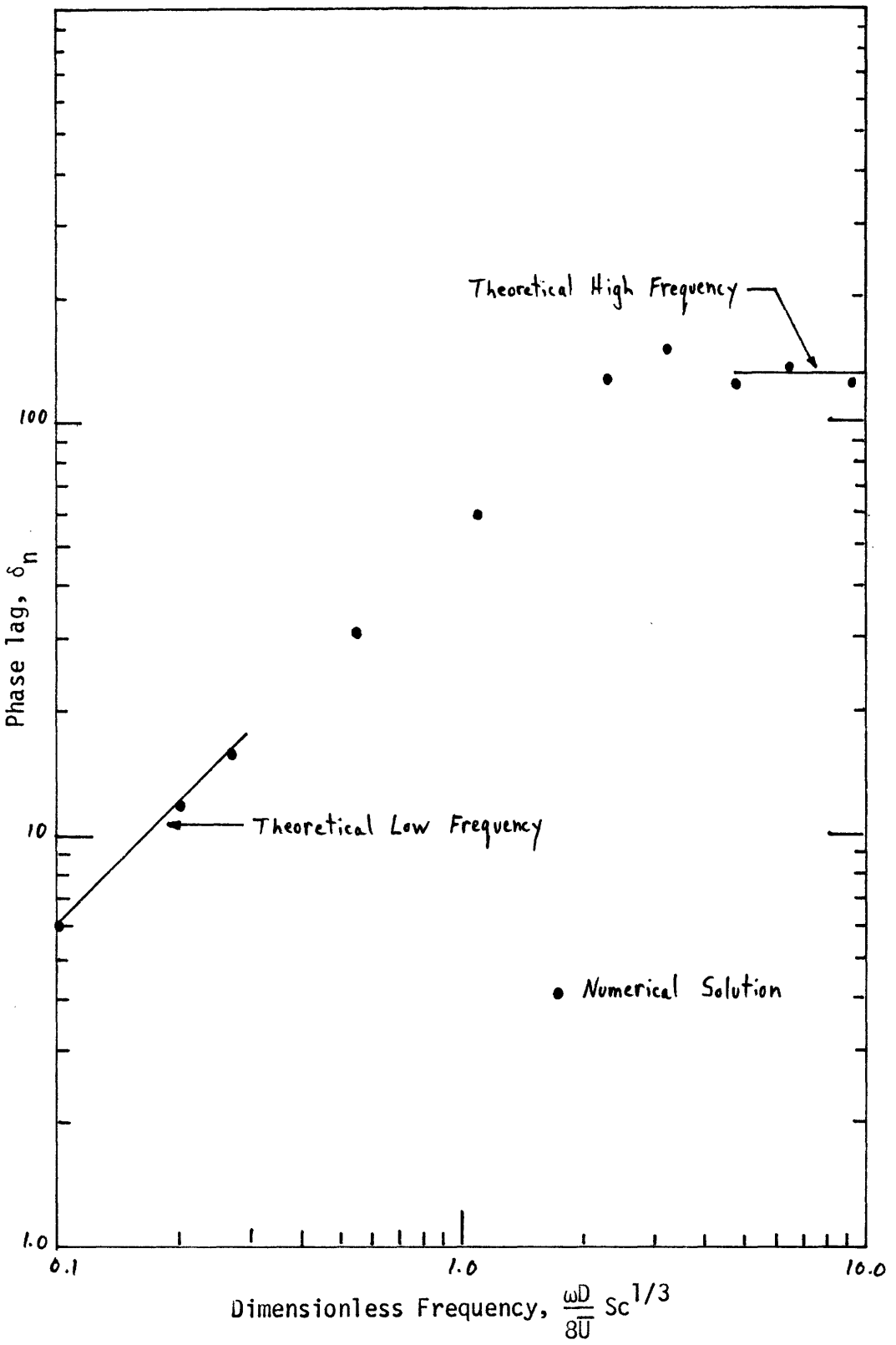

Figure 4. Phase Lag of Concentration Gradient $(\frac{\partial \hat{c}}{\partial y})_{y=0}$ with Velocity Gradient, S.

(From Fortuna and Hanratty, 1971)

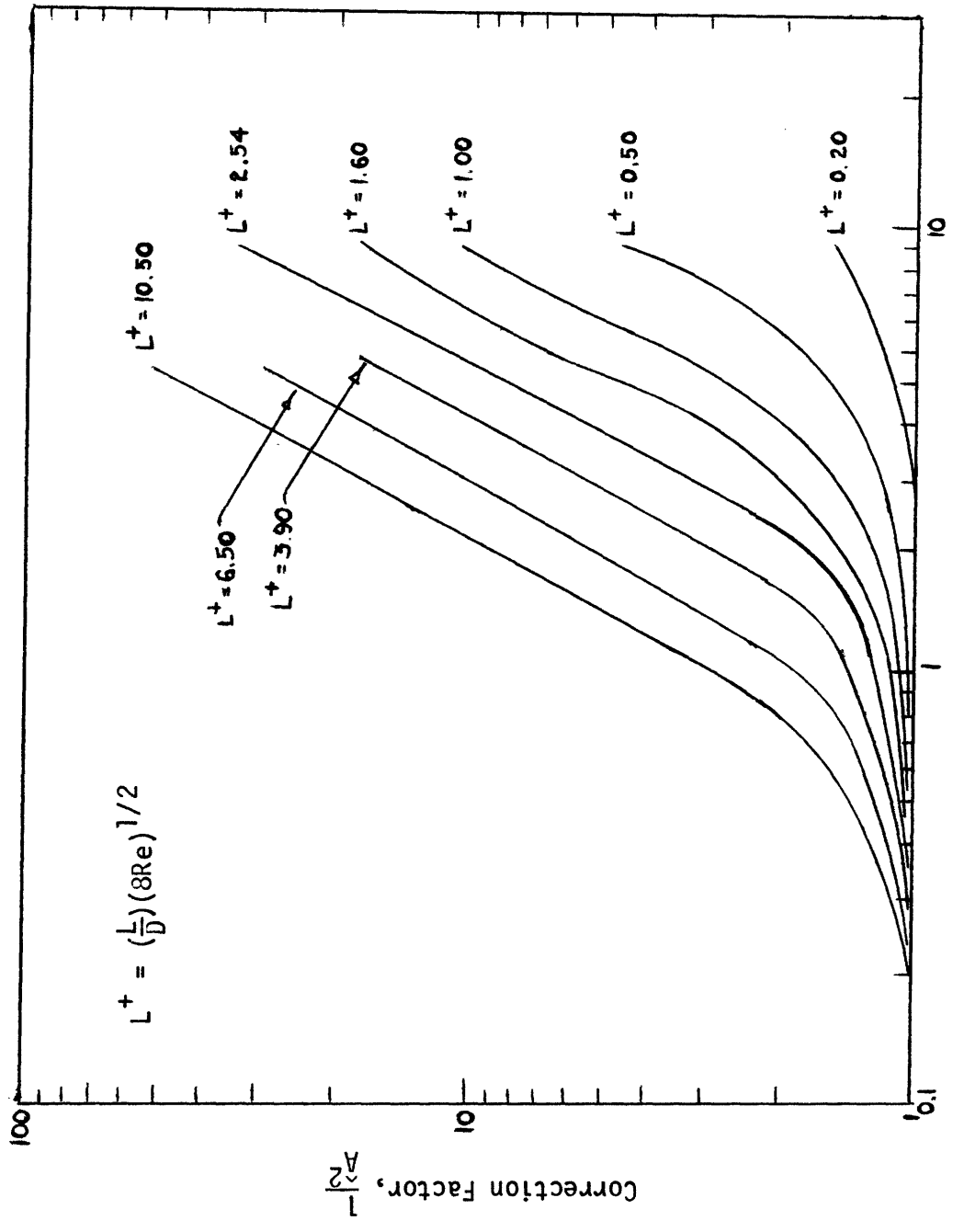

Figure 5. Correction Factor for Pseudo-Steady State Solution.
(From Fortuna and Hanratty, 1971)

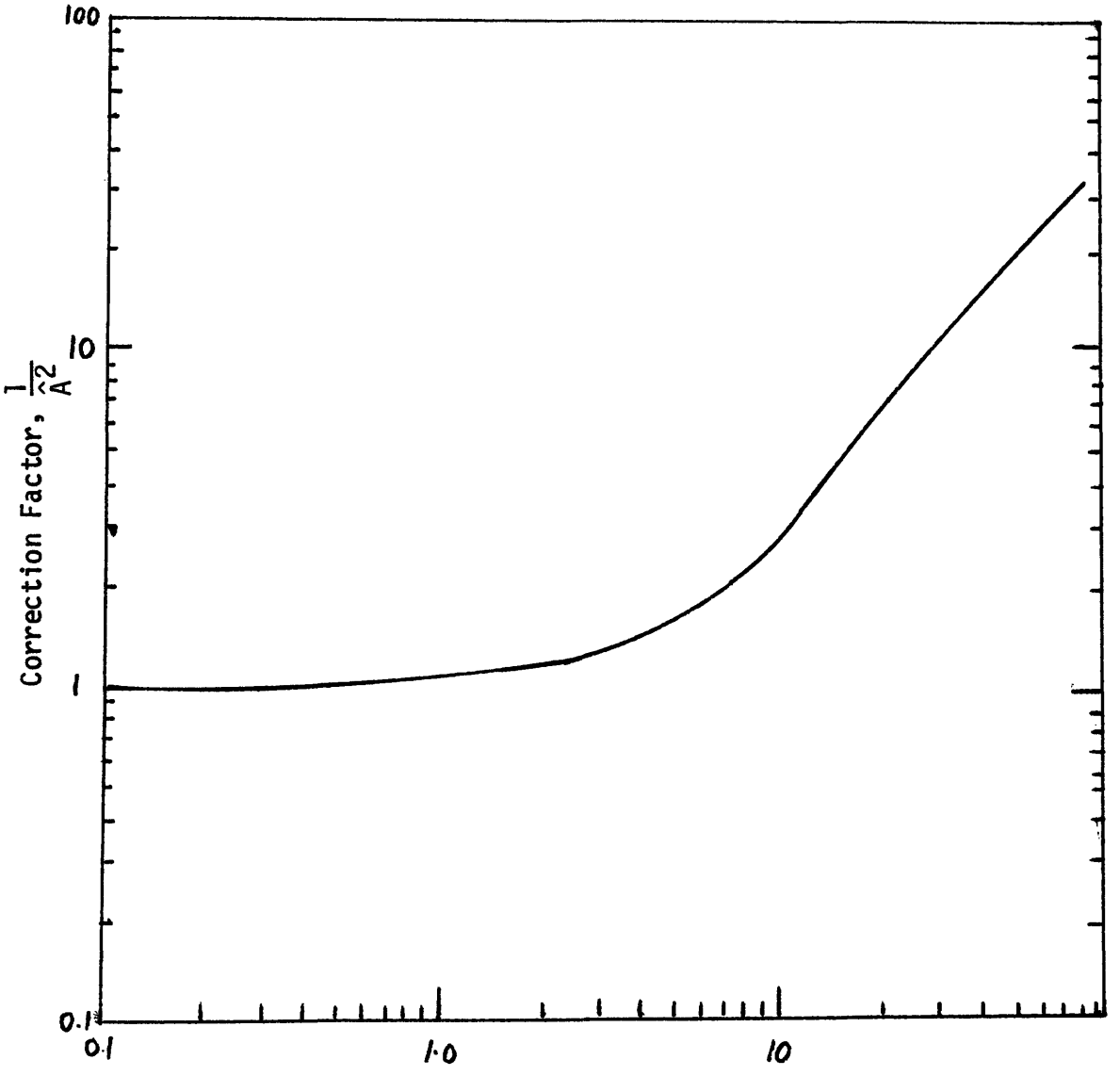

Figure 6. Zero Parameter Correction to the Pseudo-Steady State Solution.

VIII EXPERIMENTAL EQUIPMENT

Mass transfer measurements were made for steady flow (to test the consistency and precision of the experimental technique against the established theoretical predictions of Lévêque) and for pulsatile flow using three different sized circular electrodes imbedded in the wall of a horizontal tube. Laminar flow fields through the test section were produced by gravity feed from a constant head maintained by an overflow and recycling flow system. The flow rate was controlled by a downstream needle valve which permitted a maximum steady flow Reynold's Number of 1200.

Ferricyanide reduction at the cathode was accomplished by applying a potential from a constant voltage power supply between the test electrode and a downstream anode possessing a much larger surface area. The effective potential drop between the cathode and solution bulk was determined with the use of a proximal reference electrode. Mass transfer measurements were obtained from the current generated by the electrochemical reaction at the electrode surface. For steady flow this current was represented on a digital voltmeter as a potential drop across a precision resistor. The fluctuating current produced by the pulsatile flow was recorded as a voltage on an FM tape recorder, digitized, and separated into harmonic components by a Fourier analysis. Each frequency was then treated individually for its contribution to the wall shear rate.

Flow System

The flow system, containing an electrolyte, 2 Molar in sodium hydroxide, was constructed of non-corrosive PVC pipe and polyethylene tubing, and is shown schematically in Figure 7.

Storage capacity for the recycling constant head flow loop was provided by a polyethylene tank measuring 18" x 12" x 24" deep containing twenty-five gallons (94.64 liters) of electrolyte. A single outlet at the bottom of this vessel went directly to a pump (Chemtrol PVC centrifugal pump, 3475 RPM, 3/4 HP) which circulated the fluid to the constant head tank (dimensions: 12" x 12" x 12") situated eight feet above the straight pipe and test section. An adjustable portion of the pump outlet was returned to the storage tank via a by-pass line so that at the low flow rates employed (900 cc/min maximum) the surface of the constant head would experience no wave motion caused by excessive feed from the pump. The twenty-five gallon storage tank contained a total of four inlets: one for the by-pass return, one for the overhead tank overflow, another for the return from the test section, and the last, a tygon tube introducing nitrogen gas.

In order to prevent the reduction of oxygen dissolved in the electrolyte, which takes place at the same potentials as the reduction of ferricyanide, the electrolyte was saturated with nitrogen and the flow system was maintained in an inert nitrogen atmosphere, provided to both the storage vessel and overhead tank.

The combination of pump by-pass and constant head tank overflow

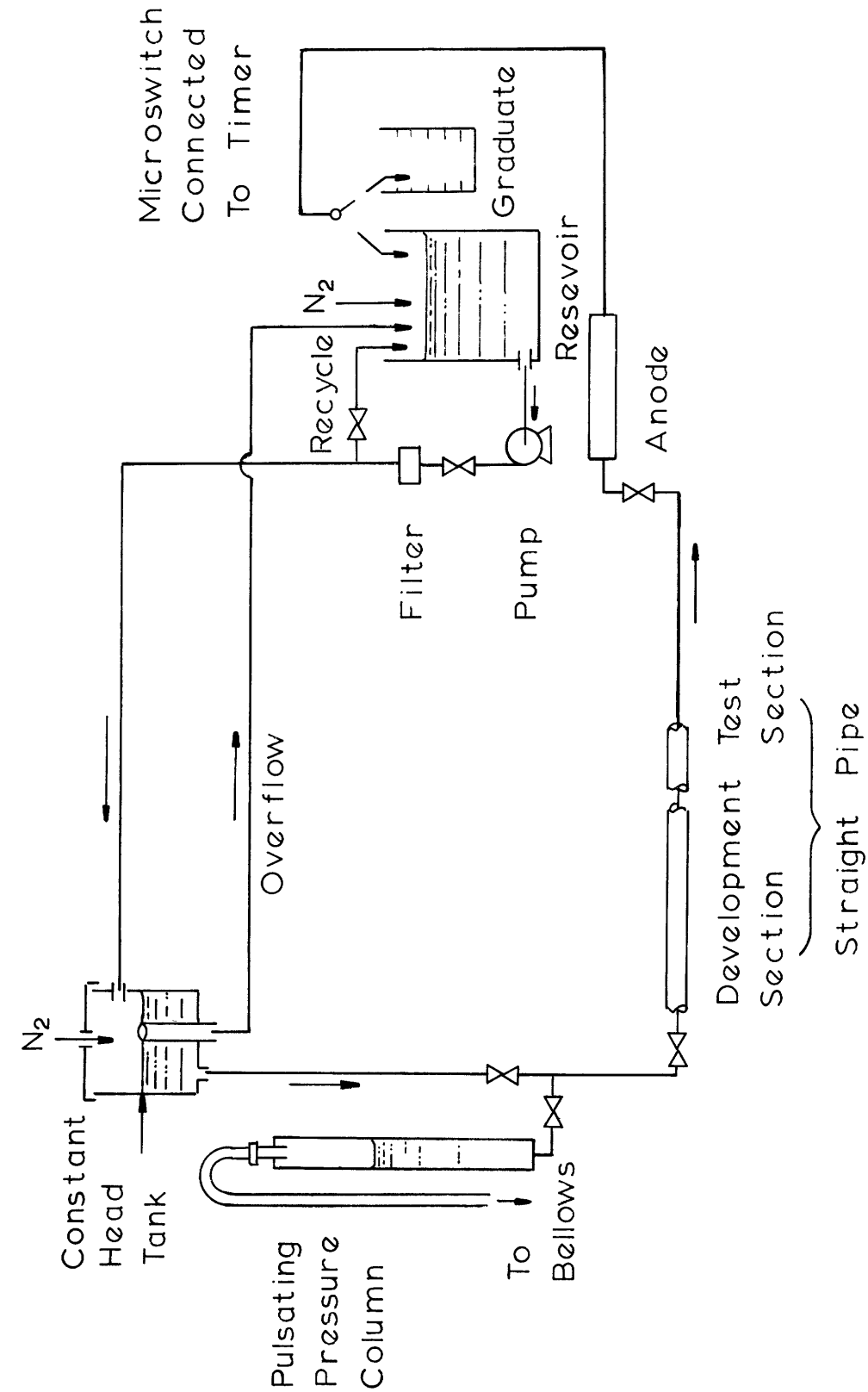

Figure 7. Schematic View of the Flow System.

was sufficient to insure a constant gravity-fed average flow of electrolyte, steady to within a maximum deviation of 0.2% (over four hours of running time) at the largest flow rates employed.

From the overhead tank the fluid flowed to a series of flow distributing valves. Opening the first admitted the electrolyte to a section of the system from where the flow could be shunted to both the pressure pulsing apparatus (when needed for non-steady flow) and the straight pipe test loop. The valve controlling flow to the test loop was preceded by a 90^{o} elbow in which a tap was bored for venting air out of the system before each run.

Entering the straight pipe section (1/2" Sch 40 PVC) the fluid passed through a hydrodynamic entry length of 335 cm or 205 pipe diameters. (The inner diameter of this section was measured with calipers and found to be 1.5799 cm). Since this horizontal length of pipe preceding the test section was the same for both steady and pulsatile flow, it was necessary that it be long enough to insure that a fully developed velocity profile entered the electrode test section. Establishment distance for the laminar flow field oscillates around the steady flow value of 0.0575 Re·D (Knudsen and Katz 1958) where Re is the Reynold's Number and D the pipe diameter, and is the longest when the velocity in the pipe is at its maximum. Florio and Mueller (1968) demonstrated that a developing pulsating flow can be considered as a superposition of a developing mean flow and a fully developed oscillating flow. Atabek and Chang considered theoretically the entrance length requirements for pulsatile flow (1961)

and utilized hot film anemometers to test the validity of their analysis (1964), but Denison et al (1970) have shown with the use of a directionally sensitive laser velocimeter that the theory of Atabek and Chang underpredicts the oscillatory flow development length, and for the flow parameters utilized in this work, the oscillating flow field is fully developed after an entry length of 0.1 Re·D (Reynold's Number based on time averaged flow rate) which for these experiments had a maximum value of 160 cm. A developing length of 335 cm was therefore more than sufficient for the establishment of all velocity profiles.

The test section was 42 cm long. It was followed by another straight section of pipe 120 cm in length, added to the flow loop to reduce end effects in the test section. This segment was attached through a 90^{o} elbow to a T which provided a means of draining the test loop while joining the test and end sections to the downstream anode.

The anode was fashioned in the following manner: nickel plates measuring 3" x 6" were sandwiched between two finely meshed nickel screens of the same dimensions and folded into an accordian-like shape. Five such folded sandwiches were tied together with nickel wire to form a cylindrical bundle, and ten of these bundles, bound so as to form an electrical unity, were inserted into a 2" I.D. Lucite tube. In this way over fifteen square feet of reactive electrode surface were available in a small volume to complete the electrolytic circuit, thereby insuring that the diffusional flux of ferricyanide ion to the much smaller test cathode would control the rate of the redox reaction. The anode section was elevated at a forty-five degree angle facilitating the removal of

gas entrapped within the flow system. Air bubbles were carried into the reservoir tank by the exiting electrolyte.

The temperature of the circulating fluid was not regulated. Temperature equilibrium between the flowing electrolyte and the surroundings was established after a warm-up period, but was subject to slow vascillations. Since the duration of any single run was shorter than the time between temperature variations,* the electrolyte temperature was constant for any one experiment and was recorded as a variable parameter. Temperature was monitored by a mercury thermometer inserted through a specially fabricated plug into the pipe upstream of the anode. Physical properties of the electrolyte (viscosity, density, diffusion coefficient) were therefore determined as a function of temperature.

Pressure Pulsing System

Oscillatory pressure gradients were obtained by pulsing the air pressure over a closed vertical column of electrolyte located adjacent to the gravity feed tank and connected to it through a tee and shunting ball valve as shown on Figure 7. The periodic variation of the height of this column was produced by the motion of a 12 in^2 Bellofram bellows, driven by a Bodine NSH 55 RH motor (48:1 gear ratio). Attached to the rotor of this motor was a brass cam cut into the shape of the curve $R = r + a \sin \Theta$. (R is the distance from the cam edge to the

* The maximum rate of temperature variation was $0.1^{o}C$ per 20 minutes so that for typical experimental runs of 5 minutes or less the temperature was effectively constant.

center of rotation; r = 3", a = 1/2"). As the cam rotated it produced linear sinusoidal motion in a cam follower. A horizontal steel lever arm, pivoting on a movable fulcrum, imparted the sinusoidal movement of the cam follower to the bellows. Adjusting the position of the fulcrum varied the amplitude of pulsation. In an attempt to reduce distortions in the pulse arising from small irregular movements in the linkage and bellows, a polyethylene bottle was connected in line between the bellows exhaust and the top of the pulsed column. It was thought that the air volume in the bottle, relatively larger than the volume of the tubing connection, would dampen out small deviations from a sinusoidal pulse. However, vibrations and distortions of unknown origin precluded the generation of any pure sine waves, but the resulting analysis difficulty was overcome by harmonic reduction through a Fourier analysis of the recorded pressure gradient.

Oscillatory pressure gradient measurements were made through .040" taps bored two feet (60.96 cm) apart; one located just upstream of the test electrodes and the other downstream of the test section. The inside of the pipe was smoothed after introducing these pressure taps. They were connected to a Celesco pressure transducer whose output was coupled with a compatable Celesco pressure demodulator and recorded on FM tape. Sensitivity of the transducer was 0.1 psi maximum range corresponding to an output of 10 volts.

Test Section

The test section consisted of eighteen circular electrodes (three

different sizes, six of each size) imbedded in the wall of (and electrically isolated from) three nickel tubes which could themselves be converted to relatively very large wall electrodes. See diagram of Figure 8.

Three two-inch lengths of nickel pipe were chosen so that their inner diameters were equivalent to the inner diameter (1.5799 cm) of the hydrodynamic development section. Into each of these, six holes were drilled circumferentially to contain two each of three different electrode sizes. As measured with micrometers, the diameters of these nickel wire electrodes were:

Electrode Size	Diameter (cm)
A	.0485
B	.0625
C	.0792

The first three-fourths of the distance through the wall was bored to a diameter considerably larger than the electrode to be placed there. This part of the hole was to contain a reservoir of epoxy to hold the nickel wire in place after being introduced into a hole which was then drilled one thousandth of an inch wider than the electrode diameter through the remaining wall.

Each of the test electrodes was dipped into electrically insulating epoxy and inserted into the slightly oversized hole so that they protruded into the interior of the pipe. When the epoxy coating dried the gap between the electrode and the drilled space was completely filled.

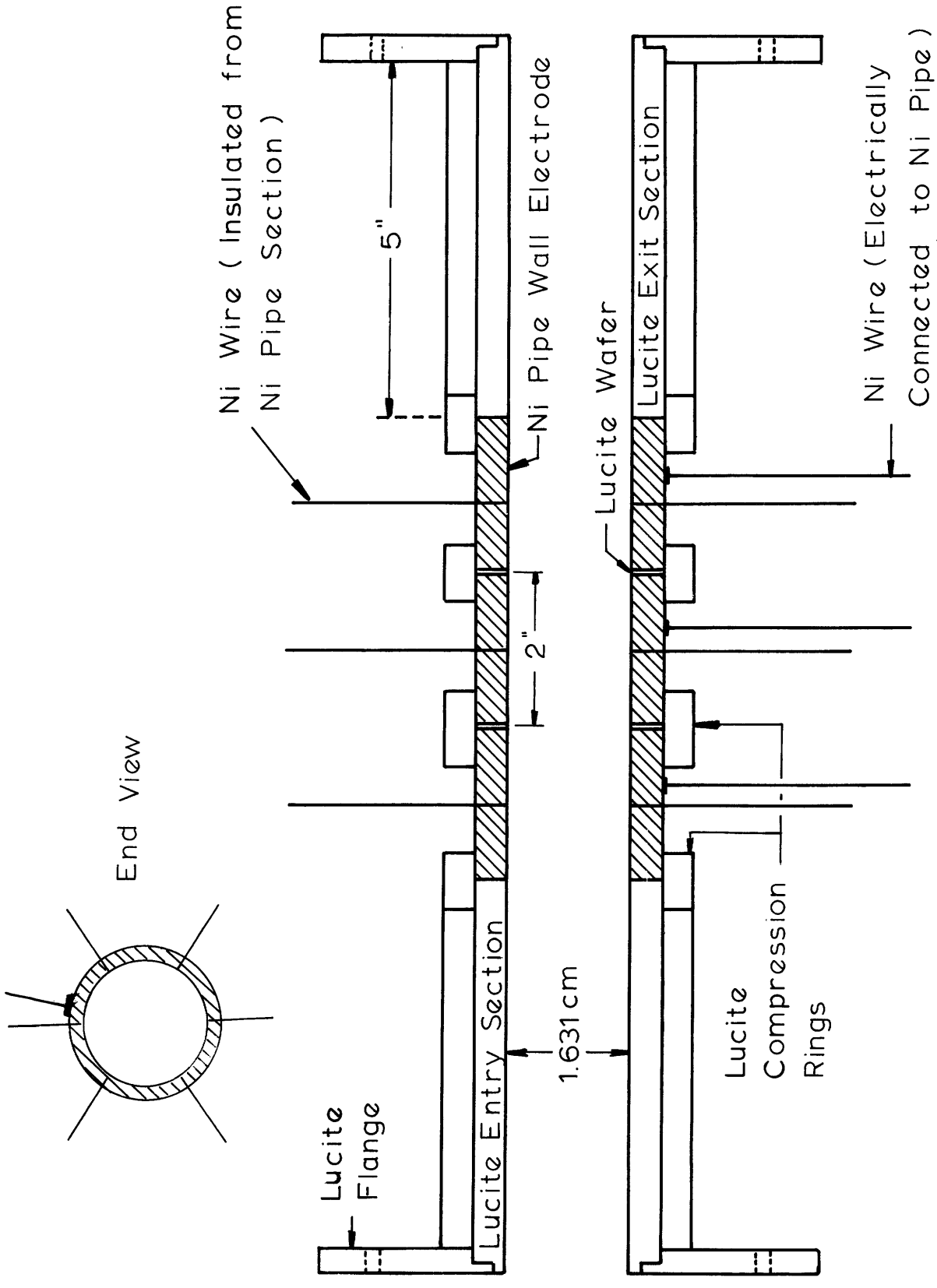

Figure 8. Electrode Test Section.

The larger hole was then filled with epoxy which when dry provided an extremely firm support for the thin wires.

Lucite wafers, .015 inches thick, were placed between the adjoined ends of the three nickel pipe sections to shield them electrically from one another. The inner diameter of the wafers conformed exactly to that of the nickel pipe lengths. Axial uniformity was assured by gluing around the wafer junctions short sections of Lucite tubing machined so as to match their inner diameters with the outer diameters of the nickel tubing. Each of the nickel pipe lengths were made electrically conductive by attaching a wire with electrically conductive epoxy to the outer surface. Two 5" Lucite entry and exit sections were afixed to the upstream and downstream ends of the nickel electrodes unit. Lucite compression rings were placed around these connections also.

The entire test section was partially wrapped in a larger sized PVC pipe appropriately drilled to accomodate the protruding electrode wires. Epoxy cement was then poured in between the partially enclosing pipe sections. When hardened it formed a single test section containing eighteen electrically insulated point electrodes and three sectional wall electrodes.

The entire inner wall of the test section was smoothed to a mirror-like finish by the Precision Honing Company. This process increased the inner diameter by .020" to 1.631 cm. As a result there was a radial step of .010" between the hydrodynamic entry length and the test section, but the 5" inlet to the upstream test electrodes was sufficient to restore a fully developed velocity profile within the test unit.

Frequent removal of the test section from the flow system for cleaning of the electrode surfaces was essential. Crest toothpaste was used as a mild abrasive for this purpose. Accordingly, the test section was connected in line with Lucite flanges.

Electronics

Measurements of the steady laminar flow mass transfer coefficient were simply obtained with the use of the circuitry of Figure 9. A D.C. constant voltage power supply maintained a steady potential between the cathode and downstream anode. The micro-ampere current generated at the surface of the test electrode passed through a Dana precision resistor ($\pm$ 0.01%) and was monitored as a constant voltage displayed on a Dana model 4430 digital voltmeter.

For pulsatile flow the circuit of Figure 10 was utilized both to maintain a constant voltage across the electrolytic cell, independent of the current drawn (to insure a diffusion controlled reaction), and to amplify and monitor the time varying current generated at the test cathode. The input to the electrical assembly (and to the electrode circuit) was a -0.55 voltage potential from a constant D.C. voltage power supply. An operational amplifier network maintained this voltage potential at a constant level. Passing through a series of pre-calibrated potentiometers, the variable current drawn at the electrode surface was recorded as a time-varying voltage on a Precision Instrument model 6200 FM tape recorder. The signal was subsequently digitized and analyzed for its Fourier components.

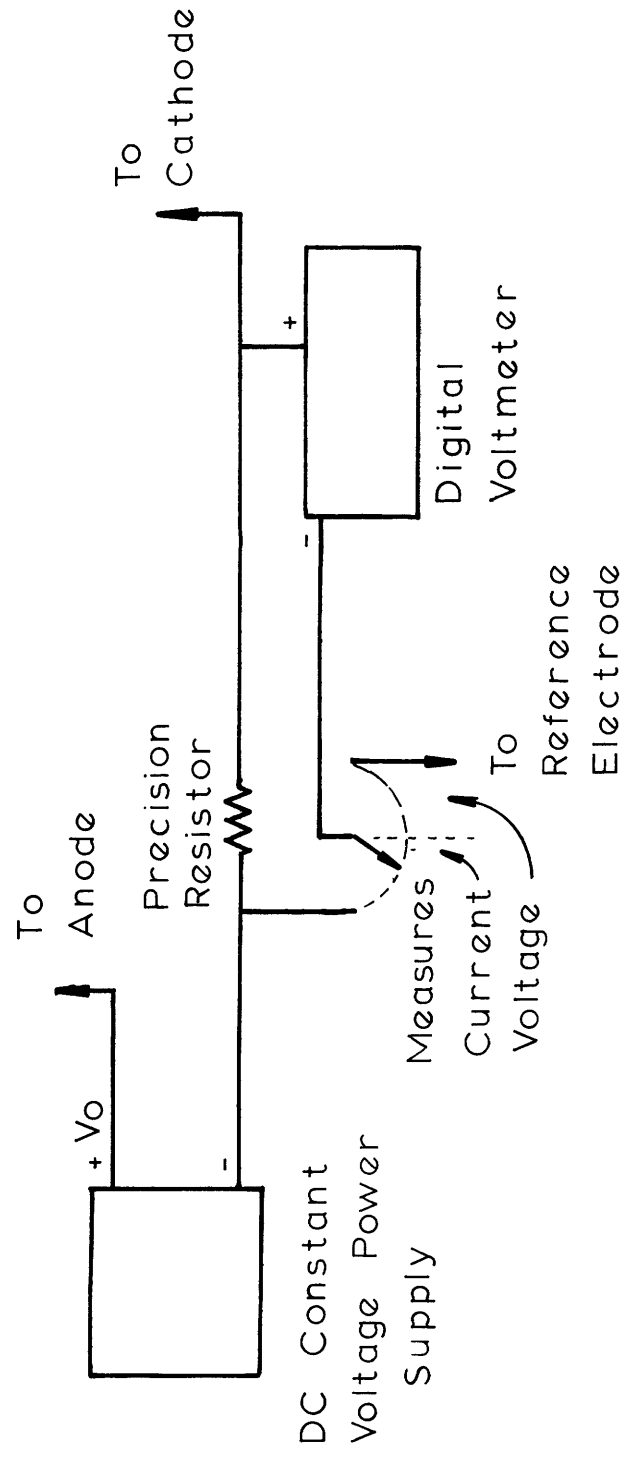

Figure 9. Circuitry for Steady Flow Current Measurements.

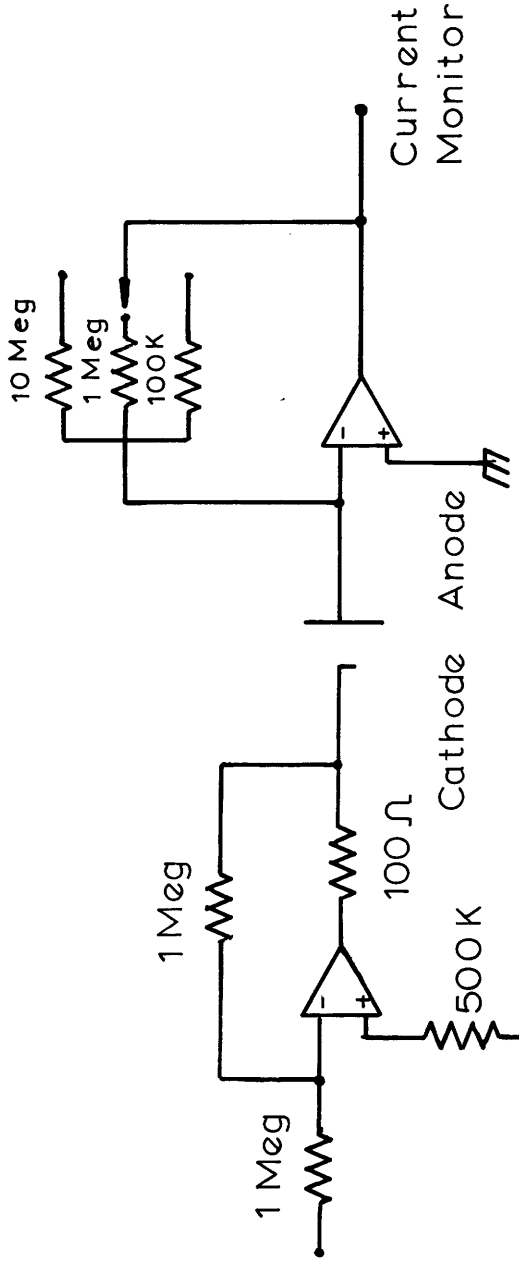

Figure 10. Circuitry for Pulsatile Flow Current Measurements.

IX. EXPERIMENTAL PROCEDURE

Calibration

The pressure transducer was calibrated *in situ* over the range 0 to 10.0 volts; all laminar flow pressure drops corresponded to an output less than 1 volt. Reynold's numbers were controlled by a needle valve and accurately determined with a graduate and micro-timer combination. Since calibration took place in the turbulent regime, the Blasius friction factor relationship was used to determine the pressure drop, and the pressure demodulator was adjusted accordingly (10 volts corresponded to 0.1 psi, linear in the range 0-10 volts). One calibration proved to be stable for several weeks.

The recording mechanism of the Precision Instrument FM tape recorder was calibrated by the method suggested by the manufacturer. Overload, accompanied by signal distortion, occurred when the input exceeded 3 volts RMS. Accordingly, amplification of any signal was controlled so as not to surpass this level.

Start Up

The electrolyte was made up of reagent grade chemicals and distilled water. Complexities accompanying the determination of ferricyanide and ferrocyanide ion concentrations by titration were cause to abandon that means of analysis. Instead, equal molar amounts of potassium ferrocyanide (water of hydration removed in a vacuum oven) and potassium ferricyanide were accurately weighed and dissolved in distilled water in a large drum calibrated for twenty-five gallons

(± 0.5%). Sodium hydroxide pellets, also carefully weighed, were added to the solution. After dissolution, addition of distilled water diluted the concentration of species, based on a total volume of 25 gallons, to 0.010 M for the ferricyanide and ferrocyanide ions and 2.0 M for the sodium hydroxide. When the electrolyte had cooled to room temperature it was charged to the reservoir tank, maintained in a nitrogen atmosphere, and used in the flow system for three weeks during which time no chemical degredation took place (Reiss 1962). After three weeks the electrolyte was replaced.

The electrolyte was circulated through the flow system for two hours before any experiment was begun to allow for electrolyte-room temperature equilibration to be established. Preliminary observations noted cathodic poisoning after the test electrodes had been monitored intermittently over a period of several hours. This was manifested as a continuous decrease in the drawn current under otherwise constant experimental conditions. However, no observable degredation occurred to electrodes in contact with the flowing electrolyte when not switched in to the external circuit during the several hours of observation. Attenuation of the current was eliminated by carefully cleaning the test section with toothpaste at the beginning of each day's runs. This agent acted as a water-soluble, sulfur-free mild abrasive, and it removed any residue which had presumably accumulated on the electrode surfaces. Other investigators (Reiss 1962, McFeeley 1972) have reported that reversing the polarity of the voltage applied between the cathode and an auxiliary electrode improved the response of the test electrode. This

treatment proved to be ineffective in this laboratory; however, daily cleaning achieved the same improved results.

Methods of Taking Data

All electronic equipment was turned on one hour prior to use. Current-voltage curves were measured for different electrode sizes and Reynold's numbers to establish the regions of applied voltage which produced diffusion limiting currents. Output of the D.C. constant voltage power supply was boosted incrementally and measured on the digital voltmeter. The resulting current was then displayed on the same voltmeter. Results from these tests showed that an applied voltage of - 0.55 volts insured a diffusion limited reaction under all flow conditions for the three electrode sizes. See Figure 2.

Measurements of steady flow mass transfer coefficients were performed only after the temperature of the flowing electrolyte had been noted. Flow rates were adjusted with a downstream needle valve and accurately determined with a graduate and micro-timer combination. Reynold's numbers varied from 100 to 1100. The use of a switching box facilitated connecting each of the eighteen electrodes, one at a time, into the current monitoring external circuit. A voltage potential as measured between the test cathode and proximal electrode was adjusted to a level of - 0.55 volts. Reaction rates at each of the cathodes were successively monitored by routing the drawn current through a precision resistor and displaying the resulting voltage drop on the same voltmeter. Ten to fifteen seconds were required for the measured current to reach

a constant value. In this manner, for any single flow rate, only six minutes were required to test the response of all electrodes.

At the beginning of each pulsatile flow experiment the constant stream response of the single test electrode to be monitored was noted for later comparison with the time averaged result. Using a motor speed control device the angular velocity of the rotating cam was arbitrarily set to a constant level, as was the amplitude of pulsation. The values of these parameters, thus established, were later determined from an analysis of the recorded motion of the rotating cam. Once the pulsating flow had come to a steady periodic state data acquisition was begun.

The constant voltage-current monitoring box permitted the recording of only one electrode's response for any single run. The time-varying current was monitored by an operational amplifier circuit and was then recorded directly on to one of the three data acquisition tracks of the FM tape recorder. The monitoring circuit served to convert micro-ampere currents to voltages on the order of unity. These recorded signals were later digitized by an EAI 680 analog computer, stored on disk and subjected to a Fourier analysis on an interfaced Interdata 70 digital computer.

To reduce errors which may have been introduced by non-periodic irregularities in tape motion, or unexpected fluctuations in the pulsating flow parameters, approximately 100 cycles of pulsation were recorded and digitized. A Fourier analysis was performed on the average of the results from the 100 cycles.

To insure that the analog to digital conversion program was initiated at the same point in each cycle, a triggering signal, recorded on a separate track of the tape, was played back through the computer simultaneously. This signal, synchronized with the cam's motion, was obtained with the use of a micro switch. A ball bearing connected to the switch was constantly in contact with the circumference of the cam. Once during each cycle the bearing, tracing a linearly sinusoidal pattern, would be displaced enough to close a circuit connecting the switch to the tape recorder. Designed to produce a rapid triggering signal, the circuit capacitors generated a voltage which rose to an amplitude of four volts in one millisecond. By utilizing this same spike to initiate and terminate the digitizing program (whose sampling rate was known), the fundamental frequency of pulsation could accurately be determined.

Recordings of the pressure pulse, obtained directly from the output of the demodulator, were digitized and Fourier analyzed in an identical manner. Frequencies and amplitudes of oscillation of both the mass transfer coefficient and the forcing pressure gradient were then directly comparable.

Electrolyte Physical Properties Analysis

After being charged to the reservoir tank, one liter of the electrolytic solution was removed for the measurement of temperature dependent densities and viscosities from which the kinematic viscosities, diffusion coefficients, and Schmidt numbers were determined.

Four volumetric flasks of twenty-five milliliter capacity, their volumes calibrated over a temperature range of $27^{o}C$ to $33^{o}C$, were used to measure solution densities at $28^{o}C$, $30^{o}C$, and $33^{o}C$ in a constant temperature bath. Densities at all other temperatures were linearly interpolated from the appropriate measured values. The same was done for viscosities.

Viscosities were determined in an Ostwald-Fenske viscometer which was calibrated with distilled water. Efflux time was approximately 100 seconds. The diffusion coefficient was then obtained as a function of both viscosity and temperature from the results of Eisenberg et al (1956),

$$\mathcal{D} = (2.50 \times 10^{-10} \ \frac{cm^2 - poise}{sec - {}^{o}K}) \ \frac{T}{\mu}$$

where

T is the temperature (^{o}K)

μ is the viscosity (poise)

X. RESULTS AND DISCUSSION

Steady Flow - Wall Electrodes

The test section was constructed with circular electrodes embedded in the wall of larger cylindrical electrodes for the purpose of evaluating mass transfer characteristics within a developing concentration boundary layer, especially for pulsatile flow where the effects of frequency and amplitude cause complex interactions between the concentration boundary layer initiated at the leading edge of the wall mass transfer section and that associated with the much smaller point electrode.

With a voltage potential applied between the wall electrode and the downstream anode, the current drawn (over 100 microamps) was large enough to cause a significant ohmic potential drop through the electrolytic fluid. As a result, only a very small voltage drop could be obtained across the concentration boundary layer (as measured by the reference electrode) and a diffusion controlled plateau region extending to -0.55 volts could not be attained. By augmenting the applied voltage potential between the test electrode and anode beyond thirty volts a diffusion plateau could slowly be approached. However, as the drawn current increased so did the ohmic potential drop through the fluid in the pipe with the result that the voltage at the leading edge of the cylindrical electrode differed from the level at the trailing edge. This change in voltage

along the length of the test electrode precluded the establishment of a diffusion controlled plateau over its entire surface. Inability to maintain a continuous diffusion controlled regime prevented the utilization of the wall electrodes; experiments with these were therefore abandoned.

Steady Flow - Circular Electrodes

Steady laminar flow measurements of interphase mass transfer were made to establish the validity of the electrochemical technique, and also to determine the behavorial consistency of the individual electrodes. To accomplish these purposes, measurements of the current produced at the electrode surface were compared to the theoretical predictions of Lévêque.

A form of his solution for a steady laminar flow field (for a cylindrical conduit) has previously been written as

$$\langle K_s \rangle = \frac{3}{2} \cdot \frac{(3)^{1/3}}{\Gamma\left(\frac{1}{3}\right)} \cdot \frac{\mathcal{D}}{R} Gz^{-1/3} \tag{47}$$

The mass transfer coefficient has also been related to the current by equation (4), rewritten here as

$$\langle K_s \rangle = \frac{I_s}{A_e F C_B} \tag{4}$$

to emphasize the spatially averaged mass transfer coefficient. Combining these two equations, with $A_e = \pi \frac{d^2}{4}$ and $Gz = \frac{.820d/D}{ReSc}$,

$$I_s = \frac{3}{4} \cdot \frac{1}{(.820)^{1/3}} \cdot \frac{(3)^{1/3}}{\Gamma\left(\frac{1}{3}\right)} \pi C_B F \mathcal{D}^{2/3} D^{-2/3} d^{5/3} Re^{1/3} \nu^{1/3} \qquad (137)$$

Equation (137) represents the theoretical prediction of the steady state current produced by the diffusion controlled electrochemical reaction. Inserting values of C_B = 0.010 moles/liter, F = 96,500 coulombs/equivalent weight, and D = 1.631 cm., this was simplified, in terms of the experimental parameter Q (flow rate in cc/min), to

$$I_s \text{ (microamps)} = 2.200 \times 10^6 \, d^{5/3} \mathcal{D}^{2/3} Q^{1/3} \qquad (138)$$

The current therefore reduces to an explicit functional dependence upon only the electrode diameter, diffusion coefficient, and volumetric flow rate. It is a weak function of small changes in temperature, increasing only 0.01 microamps for each 0.1°C rise in temperature over the range 27°C - 33°C.

To verify this relationship for the experimental system and electrode test section, data were taken for Reynolds Numbers in the range 160 to 1073 for each of the eighteen circular electrodes. The measured diameters of these test electrodes were

Electrode Number	Diameter (cm.)
A1-A6	0.0485
B1-B6	0.0625
C1-C6	0.0792

Measurements were taken over a period of several days to determine the effect, if any, of the age of the electrolytic fluid upon the electrode response. Currents read directly from the voltmeter were compared to theory with the use of equation (138).

Results from nine electrodes (three of each size) for a two day old electrolyte and a range of Reynolds Number from 330 to 1073 are shown on Figure 11. An unexpected observation is that the departure from theory is not independent of Reynolds Number but rather, for the range depicted, can be well represented by a line with negative slope. Each of the nine electrodes exhibits very similar behavior, differing from each other only in their vertical displacements from conformity with the predictions of equation (138). (Results from the other nine electrodes are not included in the figure since they are similar to those reported here and reveal no further information.)

The oblique orientation of these lines implies that the equivalent rectangular length for circular electrodes, given by Reiss (1962) as 0.820 d, is a function of Reynolds Number, at least in the laminar regime. For the range of Reynolds Numbers under consideration the deviation from Lévêque for any single electrode varies about 5% between end points; therefore an equivalent rectangular length, because of its cubic root dependence (equation 137), would necessarily have to vary by as much as 15%. For the precise determination of the absolute values of mass transfer coefficients and wall shear,

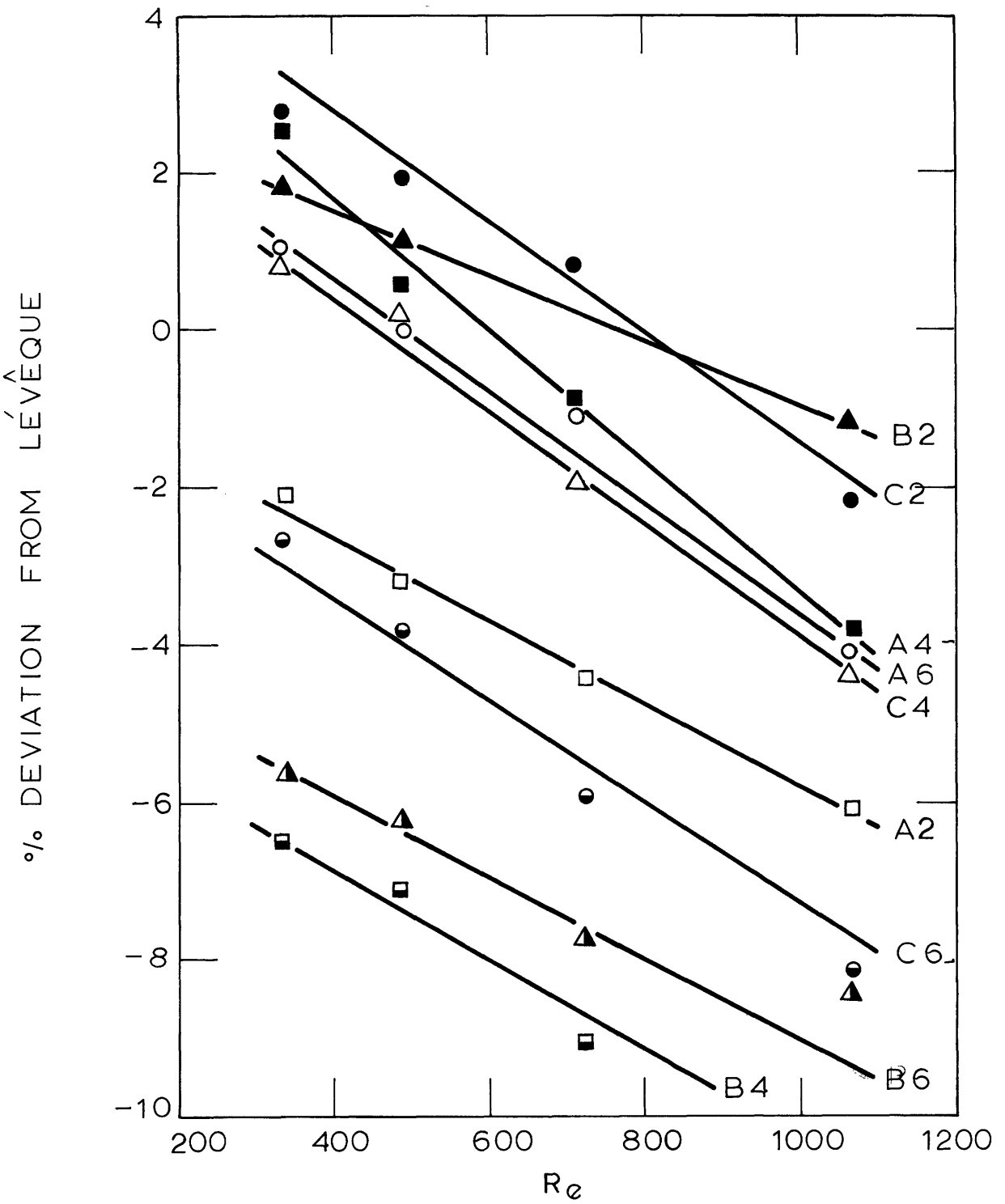

Figure 11. Effect of Reynolds Number on Steady Flow Electrode Response: 2 Day Old Electrolyte.

this functionality would have to be well quantified. However, the necessary analysis was not performed in this thesis for reasons to be stated later.

Focusing attention on the vertical arrangement of electrode responses, the likely explanation for these relatively larger departures from theory (compared to the Reynolds Number effect) is that the area assigned to each electrode is in error. Measured currents which were lower than predicted would be accounted for if the contact area between the electrode surface and the electrolyte was less than expected for a circular interface, or additionally, if the reacting surface was asymmetric, producing an unaccountable non-uniform concentration boundary layer. To test these possibilities several auxilliary electrodes were cast into epoxy, machined flush to the surface, and buffed to an extremely smooth finish. It could easily be observed that no electrode presented a circular area, but rather, each one exposed a different altered shape. Accordingly, on the basis of the results of Figure 11, each electrode could be assigned an effective diameter, one that would establish conformity between the current predicted by equation (138), based on a new effective area, and the measured response. Such a new diameter, specified at a particular Reynolds Number, would cause the family of lines of Figure 11 to collapse upon one another with deviations from theory not exceeding $\pm$ 3% (from the equivalent rectangular length effect). With this in mind, electrodes A2, A6, B2, and C4 were used to

determine steady flow shear rates since results from these electrodes daily fell within 6% of theory without an area adjustment, whereas there was day-to-day flutter in the percentage deviations from Lévêque for other electrodes as evidenced by Figure 12 where electrodes A4 and B4, for example, have shifted 3%.

Figure 12 is a repetition of the experiments depicted in Figure 11, but for a week-old electrolytic solution, and with an extended range of Reynolds Numbers. The most obvious change is the curvature imparted to the lines of Figure 11 with the inclusion of lower Reynolds Numbers. This phenomenon cannot be attributed to the age of the electrolyte because similar repetitive experiments over both shorter and larger intervals obtained the same non-linear effect. Again the family of curves can be collapsed to nearby a single curve with the introduction of an experimentally determined effective diameter to compensate for non-circular reacting surfaces.

The effect of the age of the electrolyte upon the electrode responses proved to be of no significance for a period of at least two weeks. As evidenced by Figures 11 and 12 there is uniform deviation between daily runs for a single electrode, but these changes differ between electrodes and show no day-to-day consistent behavior.

The conclusions to be drawn from Figures 11 and 12 are that each electrode, upon replacing its measured diameter with an effective diameter (which may change daily), chosen to eliminate significant

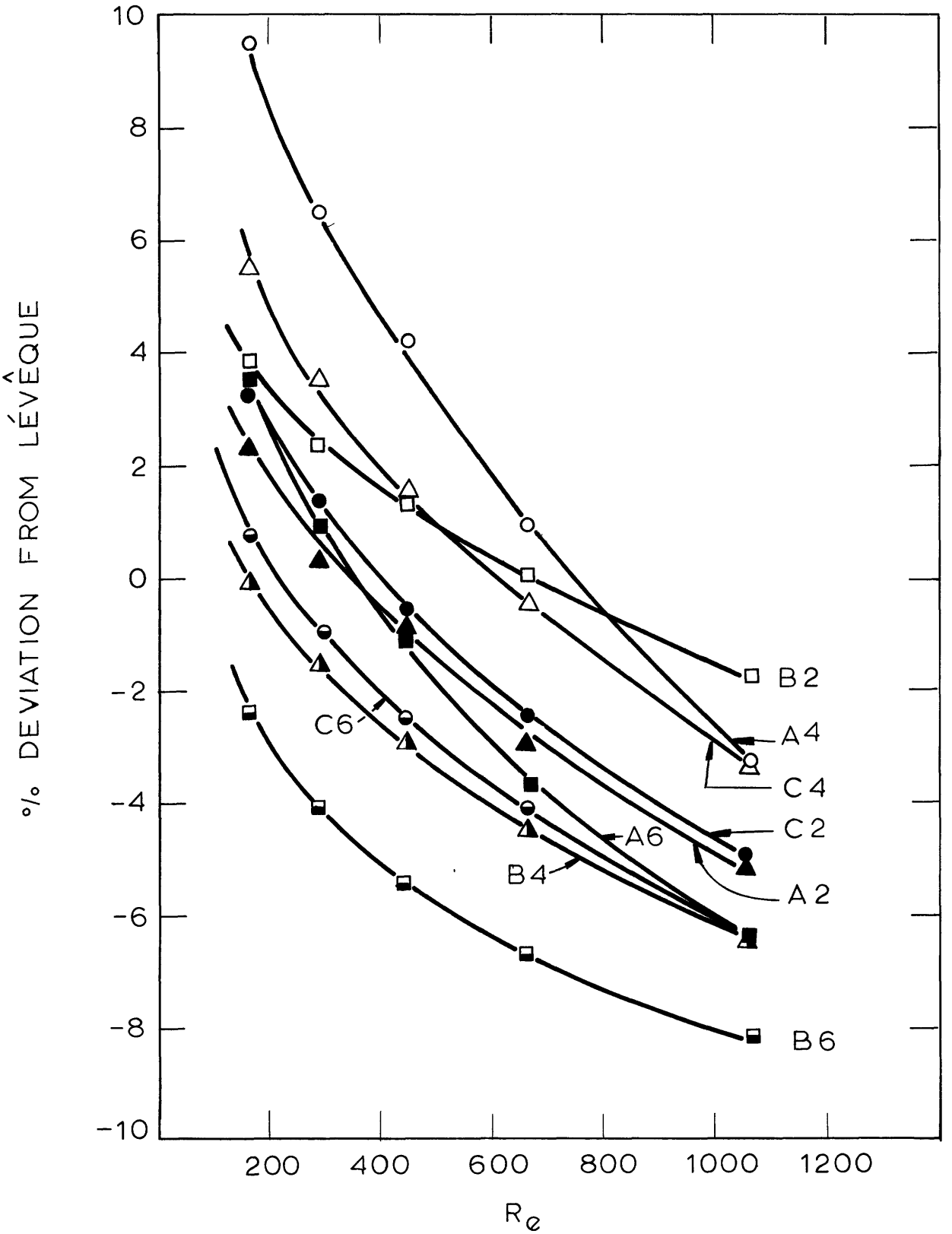

Figure 12. Effect of Reynolds Number on Steady Flow Electrode Response: 7 Day Old Electrolyte.

departures from theory, can serve as a bona-fide mass transfer measurement device whose accuracy can be further improved by incorporating a Reynolds Number dependent correction factor to transform the electrode diameter to an equivalent rectangular length.

As stated earlier, electrodes A2, A6, B2, and C4 were used to test the applicability of the electrochemical technique to the determination of wall shear stress on the basis of the proximity of their daily responses to the predictions of equation (138). Making no attempt to improve upon their genuine accuracy, no correction factors other than the constant 0.820 for the equivalent rectangular length were employed in determining the final results.

A transformation of the curves for these four electrodes from Figures 11 and 12 were redrawn on the universal plot, Figure 13, which is a graph of the mass transfer Nusselt Number vs. the Graetz Number where

$$\langle Nu \rangle = \frac{\langle K_s \rangle D}{\mathcal{D}} = \frac{I_s D}{C_B A_e F \mathcal{D}} \tag{139}$$

The solid line, representing equation (47) converted to the dimensionless form, equation (139), is described by

$$\langle Nu \rangle = \frac{3(3)^{1/3}}{\Gamma\left(\frac{1}{3}\right)} \, Gz^{-1/3} \tag{140}$$

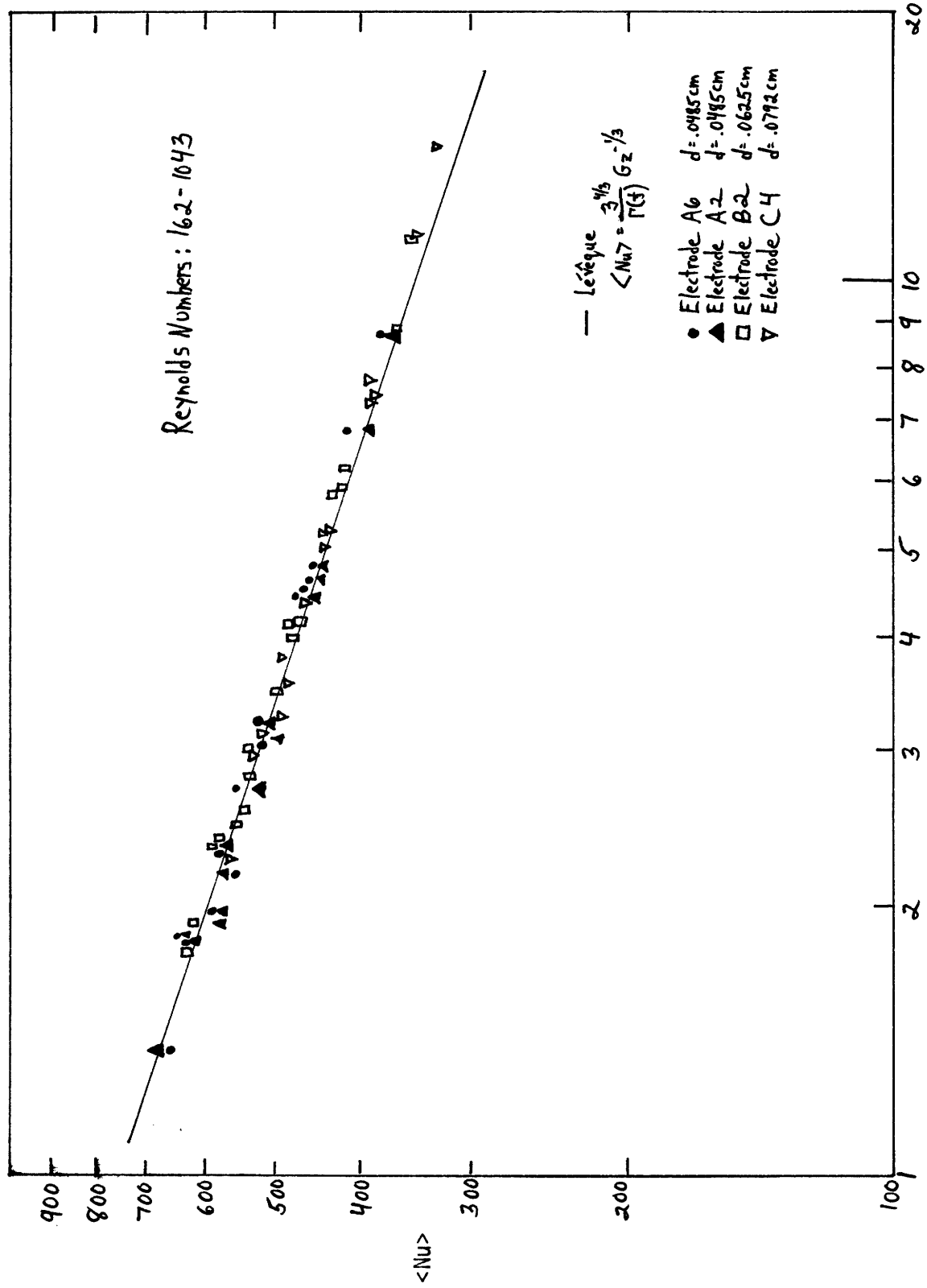

Figure 13. Steady Flow Mass Transfer Results.

All data obtained with these electrodes has been included in the graph; the maximum deviation for these electrodes with uncorrected diameters is 5.6%. A table of computed values is included in Appendix 6.

The necessity to correct for non-circular reaction areas and Reynolds Number becomes evident when considering Figure 14 where the experimentally determined wall shear rate is compared to the velocity gradient obtained from the parabolic velocity profile as

$$S = \frac{8\ U_o}{D} \tag{141}$$

Experimental values for S were computed by combining equation (A3-35) which relates the wall shear rate to the measured mass transfer coefficient by

$$S = \left[\frac{\Gamma(\frac{1}{3})\ (\frac{2}{3} <K_s>)}{3^{1/3}}\right]^3 \left(\frac{L}{\mathcal{D}^2}\right) \tag{A3-35}$$

with equation (138) to obtain the desired result

$$S = \frac{8}{81}\left[\Gamma(\tfrac{1}{3})\right]^3 <Nu>^3 \left[\frac{0.820d \cdot \mathcal{D}}{D^3}\right] \tag{142}$$

As can be seen by the cubic relationship between the Nusselt number and the wall shear rate in the above expression, the small errors observed in the experimental mass transfer coefficient are multiplied

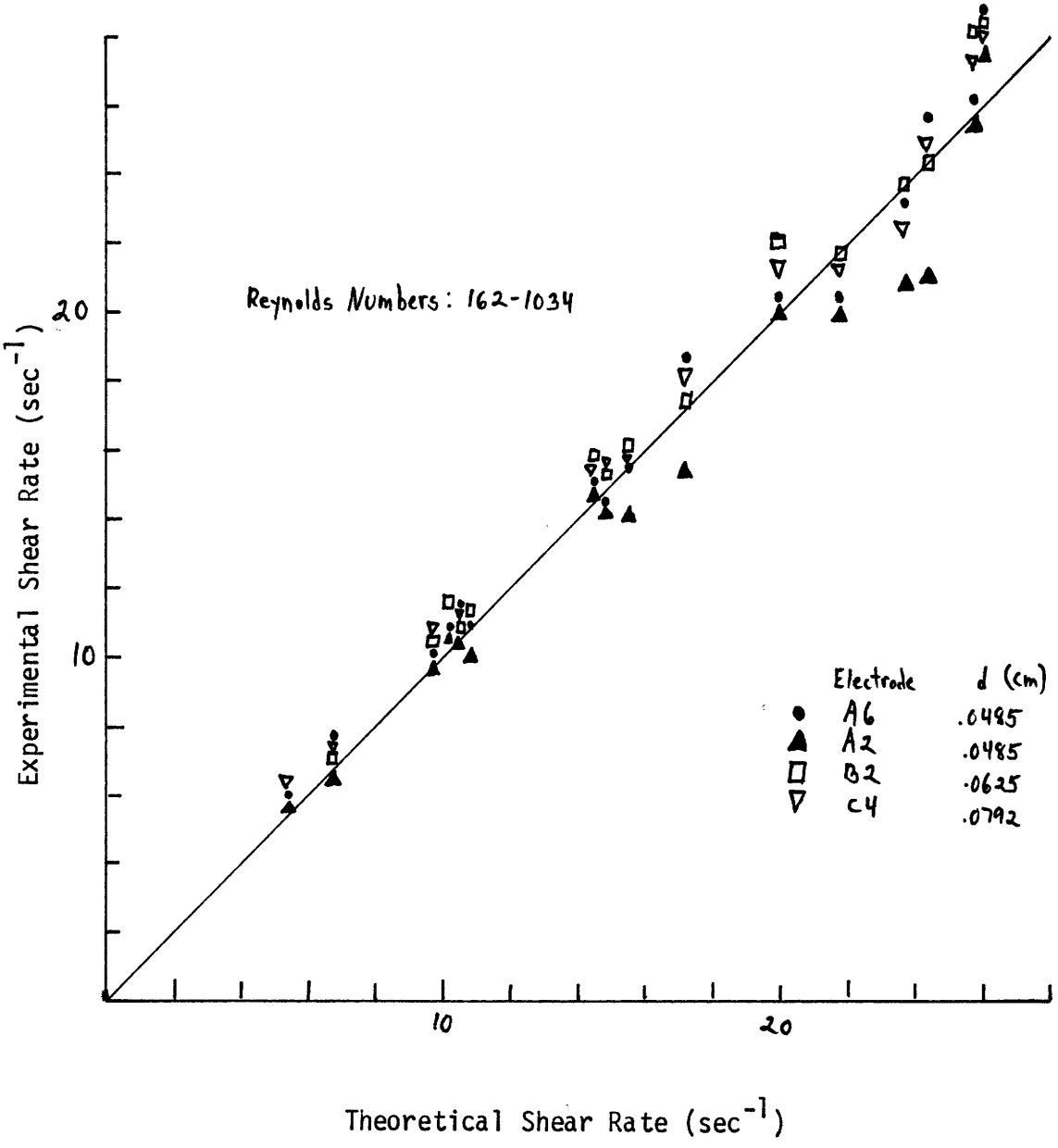

Figure 14. Steady Flow Wall Shear Results.

by a factor of three such that a reasonably good agreement with Lévêque (Figure 13) can depart considerably further from theory (by as much as 18% in Figure 14 - see table in Appendix 6). Consequently an accurate determination of the absolute value for the wall shear stress requires excellent mass transfer data, or alternately, well quantified correction factors both for non-circular electrode surface areas and for the Reynolds Number dependence of the equivalent rectangular length. It is appropriate to point out here that these correction factors were unnecessary for the treatment of pulsatile flow data, since the results for the case of non-steady flow are reported as a ratio of the amplitudes of oscillation of the fluctuating quantity to the time averaged value, thus nullifying the factors which would cause each of these values to depart from theory.

Pulsatile Flow

All signals generated by the experimental equipment under non-steady flow conditions were recorded directly on to a pre-calibrated FM tape. Consequently, all data were initially obtained in the form of periodic, time-varying voltages. The method of tape recording, aside from being essential because of the nature of the signals (no on-line computer hookup was available), actually served to simplify the analysis because of the direct proportionality between the mass transfer coefficient and the measured current, which, passing through the operational amplifier circuit, was recorded as a voltage. The relationship between the instantaneous mass transfer coefficient and the current, equation (6)

$$\bar{K} + K' = \frac{(\bar{I} + I')}{A_e F C_B} \tag{6}$$

is the basis for noting that the desired ratio of the fluctuating component of the mass transfer coefficient to the time-averaged value, λ_m, is equivalent to

$$\lambda_{m_{(n)}} = \frac{K_{F_{(n)}}}{\bar{K}} = \frac{I_{F_{(n)}}}{\bar{I}} \tag{143}$$

Thus it was necessary only to divide the amplitude of the fluctuating voltage for the nth integral multiple of the fundamental frequency to the DC level (time-average) to obtain λ_m for that particular harmonic.

Similarly, since the pulsating pressure gradient was recorded as a fluctuating voltage linearly related to $\frac{dp}{dx}$ in the laminar regime, the oscillatory pressure ratio, λ_p, was also directly obtained from a Fourier analysis of the digitized recording.

Nine electrodes, three of each size, were used for mass transfer measurements at several different fundamental frequencies covering a range of the dimensionless frequency parameter, Ω, from 6.215 to 7.107. The pressure pulsing system, incapable of producing a sine wave at these frequencies (despite many attempts to make it do so), actually generated an oscillatory pressure gradient composed of at least ten harmonics of significance.

This can be observed in the tables of Appendix 8 where the complete results of experimental runs numbered #8, #9, and #10 are listed. The first entry under the heading of dimensionless frequency is the value of Ω produced by the rotating cam. Successive values were obtained as $\Omega_n = n\Omega_1$ where Ω_1 is the fundamental. Note that values for the pressure ratio, λ_p, are predominantly in the range 0.2 to 3, considerably larger than those employed by McFeeley (1972), but smaller than the constraints of flow reversal (see Appendix 2) or allowable values for the perturbation parameter, also λ_p, discussed in the theoretical section and reported as a function of Ω by Fagela-Alabastro and Hellums (1969).

Three electrodes were chosen for the purpose of presenting the tabled results of Appendix 8 in graphical form; A2 and B2 because of

their demonstrated conformity with theory in the steady flow experiments, and C2, arbitrarily chosen to represent those electrodes which deviated from the predictions of Lévêque for steady flow but which can nevertheless justifiably be utilized for the measurement of non-steady mass transfer coefficients, reported in the form of λ_m, since the factors (presumed to be constant) which would cause both K_F and $\bar{K}$ (or alternately, K_s) to depart from steady-flow or quasi-steady theory are eliminated by the division process. Alternate choices to C2 could have been made, but with no significant differences of any kind, as careful inspection and comparison of electrode data will reveal.

The values of A_{mp}, drawn from Tables A8-1, A8-2, and A8-3 (electrode A2), are plotted against the theoretical model for high frequency, equation (92), computed with parameter values as depicted on the graph, Figure 15. (Values for M_0 and M_1 were obtained from McLachlin, 1961). Results for electrodes B2 (Tables A8-9 to A8-11) and C2 (Tables A8-17 to A8-19) are similarly presented on Figures16 and 17 respectively. Agreement with theory is excellent for values of Ω beyond 16, whereas A_{mp} values within the intermediate range of frequency parameters ($6<\Omega\leq 16$) are considerably more scattered and are not well represented by equation (92). McFeeley (1972) also found that his data ($4<\Omega<8$) did not conform well with the high frequency model in this region. As reference to Figure 3 will illustrate, the low frequency model for A_{mp}, equation (80), is equivalent to the high frequency solutions equation (92), up to a Ω

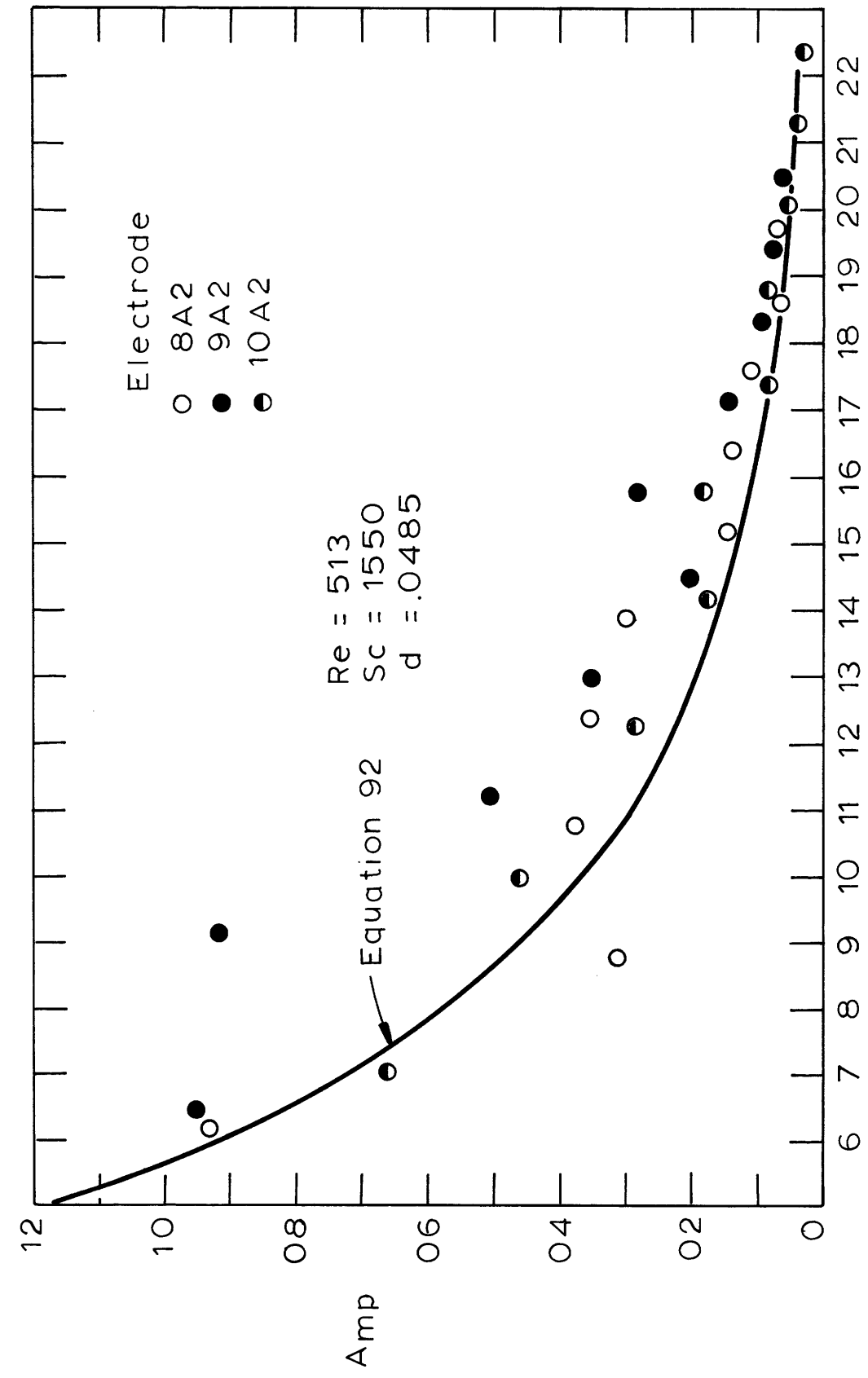

Figure 15. Experimental Vs. Theoretical A_{mp} for Electrode A2.

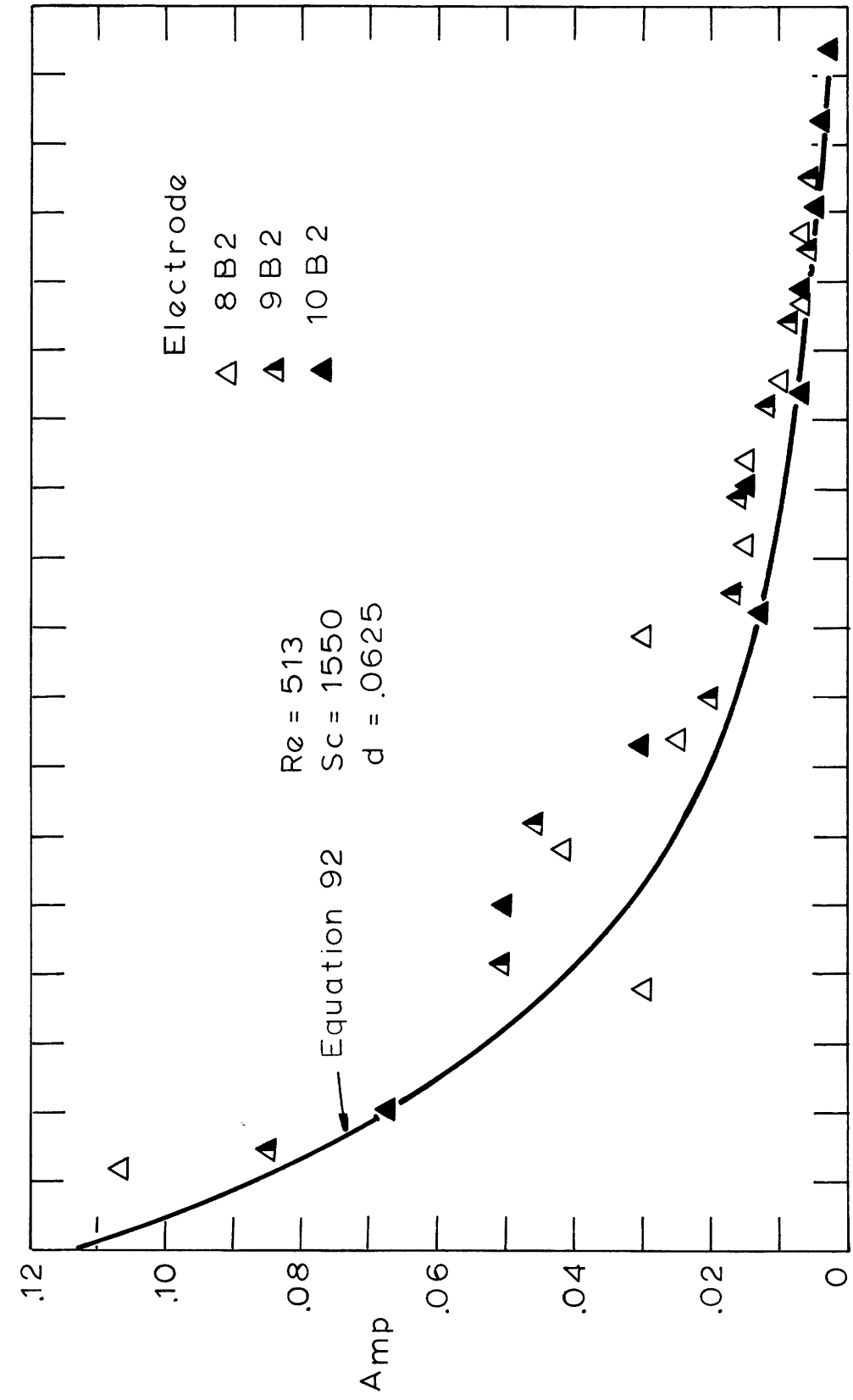

Figure 16. Experimental Vs. Theoretical A_{mp} for Electrode B2.

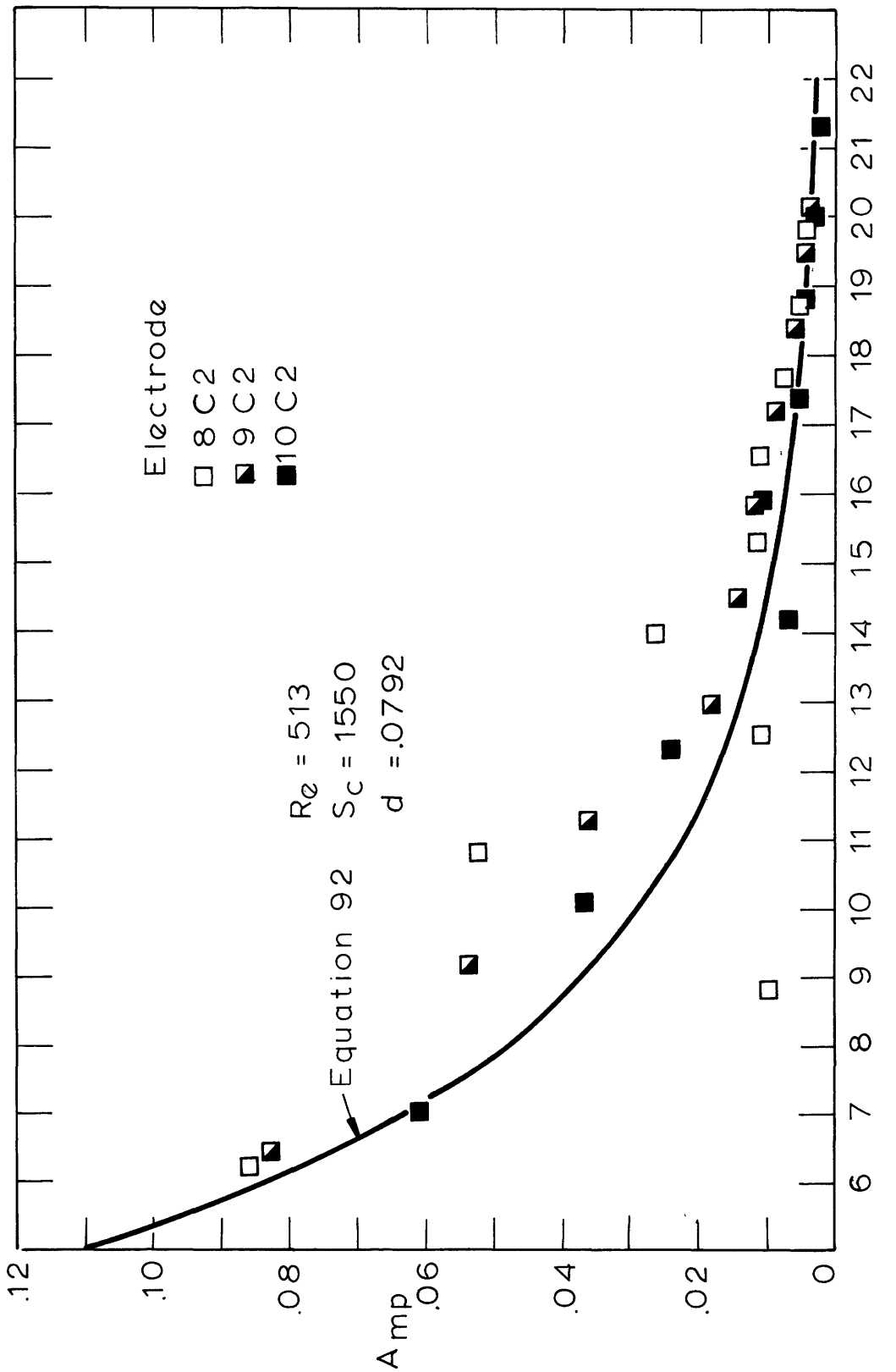

Figure 17. Experimental Vs. Theoretical A_{mp} for Electrode C2.

value of 2. This is equivalent to stating that the perturbation term, $\tau\alpha^2 Gz^{2/3}$ in equation (90) is small such that second order terms are negligible. In fact this parameter is less than 0.01 for $\Omega<2$ for the physical parameters used in this investigation, but beyond a value of 2 for the frequency parameter, its magnitude increases sharply, terminating the applicability of (80) as can be seen readily by comparing equation (77) to equation (90) for large values of this parameter. Since the high frequency solution is in fact also written as equation (90), (it satisfied the differential equation (52) in this form), the final expression for the high frequency model for A_{mp}, equation (92), is applicable at all values of Ω. A region of invalidity can therefore not be ascribed to the solid curves of Figures 15, 16, and 17, although some fault in its derivation may eventually be found which will point to a region of invalidity in the range ($6<\Omega<16$) where an intermediate frequency solution may be required*. The function which correlated McFeeley's data, equation (98) fails to improve agreement with the experimental

---

* McFeeley states that the high frequency solution, equation (92), can be derived independently of the low frequency solution by expressing the series expansion for $f_\phi(n, \xi)$, equation (53), with $1/(1 + \tau\xi^{2/3})$, $1/(1 + \tau^2\xi^{4/3})$, etc. as the perturbation parameter. This is effectively an expansion in $1/(1 + \Omega^2)$ which for high frequencies supports the consideration of only the first order term. Similarly for low frequencies ($\Omega<2$) consideration of only the first order term of equation (53) is sufficient. But for intermediate frequencies higher order terms are of comparable magnitude and should be accounted for. Thus, if the above contention of McFeeley is true, there is a intermediate frequency region where neither the low frequency nor the high frequency models are accurate. This appears to be the case on Figures 15, 16, and 17.

results reported here. Curves described by equation (98) fall below those of equation (92) and therefore depart even further from the experimental A_{mp} values.

Regarding the large scatter in the data in the frequency range $8<\Omega<10$, there was a relatively large error in the results from the second harmonic from several electrodes because of the low signal level for that particular harmonic compared to the inherent level of noise introduced by both the digitizing analog computer and the method of averaging when performing a Fourier analysis on a digitized signal. This point is illustrated in Table 1 which is the result of the Fourier analysis of the pressure signal for run $^{\#}9$, electrode A2 (=electrode 9A2). The '0' harmonic represents the time-averaged voltage; only every fourth harmonic corresponds to an integral harmonic of the real signal since the digitized values from four complete periods of oscillation were treated as a single curve for averaging purposes. (Technical difficulties prevented the averaging of more than four periods). Harmonic '4' therefore corresponds to the fundamental of the recorded signal, harmonic '8' is the second harmonic, etc. It is harmonic 8 of Table 1 that contributes an amplitude of the same magnitude as background and signal averaging noise (harmonics 7, 9, and 10). The accuracy of λ_p for the second harmonic is therefore of questionable accuracy; an unusually low value is the result, as can be noted in Table A8-2 and even more so on Figure 15. The analogous Fourier analysis for the mass transfer

PRESSURE DIFFERENTIAL DATA ANALYSIS
NUMBER OF POINTS PER CYCLE IN THE FOURIER ANALYSIS= 99
NUMBER OF CYCLES IN REAL TIME PER CYCLE IN THE FOURIER ANALYSIS= 4

HARMONIC	AMPLITUDE	PHASE(DEG)
0	0.0585	
1	0.0025	-47.8
2	0.0020	-13.5
3	0.0021	-6.4
4	0.0475	42.6
5	0.0006	-29.3
6	0.0005	-6.8
7	0.0011	4.4
8	0.0018	-4.8
9	0.0014	-19.4
10	0.0012	22.5
11	0.0015	-11.0
12	0.0134	60.8
13	0.0018	40.5
14	0.0019	26.2
15	0.0020	24.0
16	0.0061	1.4
17	0.0008	24.0
18	0.0000	18.7
19	0.0020	31.7
20	0.0068	54.7
21	0.0016	36.1
22	0.0017	39.5
23	0.0012	45.6
24	0.0042	-36.8
25	0.0037	55.4
26	0.0020	68.3
27	0.0032	-80.2
28	0.0322	-58.2
29	0.0036	-0.1
30	0.0015	-40.9
31	0.0011	-78.1
32	0.0348	66.9
33	0.0040	58.9
34	0.0044	63.5
35	0.0044	89.2
36	0.0263	40.1
37	0.0119	77.3
38	0.0107	79.6
39	0.0219	80.9
40	0.1600	-81.9

TABLE 1.

FOURIER ANALYSIS OF PRESSURE DIFFERENTIAL FOR ELECTRODE 9A2.

MASS TRANSFER COEFFICIENT DATA ANALYSIS
NUMBER OF POINTS PER CYCLE IN THE FOURIER ANALYSIS= 99
NUMBER OF CYCLES IN REAL TIME PER CYCLE IN THE FOURIER ANALYSIS= 4

HARMONIC	AMPLITUDE	PHASE(DEG)
0	0.3583	
1	0.0019	74.5
2	0.0008	-72.6
3	0.0010	-66.8
4	0.0277	-13.1
5	0.0004	40.7
6	0.0005	47.0
7	0.0004	-62.2
8	0.0010	28.4
9	0.0001	-77.2
10	0.0003	-15.5
11	0.0001	29.0
12	0.0042	-38.6
13	0.0004	-36.2
14	0.0001	-45.9
15	0.0006	11.6
16	0.0013	60.0
17	0.0002	17.1
18	0.0005	-54.5
19	0.0003	-63.9
20	0.0008	-58.4
21	0.0004	-79.1
22	0.0001	-52.0
23	0.0003	-7.5
24	0.0007	10.5
25	0.0004	-80.9
26	0.0001	25.0
27	0.0002	46.8
28	0.0028	-4.8
29	0.0006	-53.2
30	0.0004	-68.8
31	0.0002	-35.6
32	0.0020	-83.4
33	0.0004	71.5
34	0.0005	-82.7
35	0.0003	-56.3
36	0.0012	58.8
37	0.0005	-63.0
38	0.0003	-58.9
39	0.0012	-60.1
40	0.0067	-55.0

TABLE 2.

FOURIER ANALYSIS OF MASS TRANSFER COEFFICIENT FOR ELECTRODE 9A2.

PRESSURE DIFFERENTIAL DATA ANALYSIS
NUMBER OF POINTS PER CYCLE IN THE FOURIER ANALYSIS= 99
NUMBER OF CYCLES IN REAL TIME PER CYCLE IN THE FOURIER ANALYSIS= 4

HARMONIC	AMPLITUDE	PHASE(DEG)
0	0.0500	
1	0.0023	-25.8
2	0.0022	-9.9
3	0.0021	-17.4
4	0.0490	44.8
5	0.0021	3.0
6	0.0017	-8.9
7	0.0023	-31.4
8	0.0023	37.3
9	0.0022	6.8
10	0.0022	0.9
11	0.0711	7.2
12	0.0141	43.3
13	0.0023	19.5
14	0.0016	8.3
15	0.0022	32.1
16	0.0096	-14.6
17	0.0021	0.5
18	0.0024	26.3
19	0.0016	-0.6
20	0.0103	39.7
21	0.0021	1.4
22	0.0020	3.4
23	0.0023	40.4
24	0.0056	-45.9
25	0.0035	17.0
26	0.0030	55.3
27	0.0033	47.3
28	0.0036	-82.3
29	0.0034	21.3
30	0.0059	-38.4
31	0.0014	-11.7
32	0.0413	47.1
33	0.0057	17.7
34	0.0043	59.4
35	0.0026	7.3
36	0.0016	24.3
37	0.0107	32.4
38	0.0124	48.5
39	0.0159	70.3
40	0.1629	82.1

TABLE 3.

FOURIER ANALYSIS OF PRESSURE DIFFERENTIAL FOR ELECTRODE 9B4.

PRESSURE DIFFERENTIAL DATA ANALYSIS
NUMBER OF POINTS PER CYCLE IN THE FOURIER ANALYSIS= 99
NUMBER OF CYCLES IN REAL TIME PER CYCLE IN THE FOURIER ANALYSIS= 4

HARMONIC	AMPLITUDE	PHASE(DEG)
0	0.0462	
1	0.0016	-61.3
2	0.0040	-58.1
3	0.0012	1.4
4	0.0478	48.4
5	0.0016	-65.9
6	0.0029	89.3
7	0.0007	-25.8
8	0.0036	-89.2
9	0.0094	22.0
10	0.0095	83.1
11	0.0006	-47.7
12	0.0176	39.8
13	0.0012	28.8
14	0.0029	-36.6
15	0.0006	-5.3
16	0.0066	-6.6
17	0.0026	-48.5
18	0.0039	29.2
19	0.0013	3.2
20	0.0069	48.2
21	0.0026	52.6
22	0.0021	-73.2
23	0.0021	-44.9
24	0.0102	-26.5
25	0.0004	-39.2
26	0.0047	71.2
27	0.0030	77.2
28	0.0030	-75.9
29	0.0005	36.2
30	0.0030	-57.2
31	0.0010	75.6
32	0.0040	44.1
33	0.0051	21.8
34	0.0028	-13.2
35	0.0010	-26.2
36	0.0060	26.3
37	0.0076	51.4
38	0.0083	61.7
39	0.0168	82.9
40	0.1620	88.8

TABLE 4.

FOURIER ANALYSIS OF PRESSURE DIFFERENTIAL FOR ELECTRODE 9C2.

MASS TRANSFER COEFFICIENT DATA ANALYSIS
NUMBER OF POINTS PER CYCLE IN THE FOURIER ANALYSIS= 99
NUMBER OF CYCLES IN REAL TIME PER CYCLE IN THE FOURIER ANALYSIS= 4

HARMONIC	AMPLITUDE	PHASE(DEG)
0	0.5775	
1	0.0033	83.4
2	0.0019	80.1
3	0.0015	-87.7
4	0.0495	-18.9
5	0.0006	-88.7
6	0.0003	70.0
7	0.0007	79.6
8	0.0024	40.9
9	0.0001	47.2
10	0.0004	26.6
11	0.0003	50.1
12	0.0081	-62.5
13	0.0003	89.6
14	0.0005	85.4
15	0.0003	-86.0
16	0.0015	66.4
17	0.0003	-42.4
18	0.0009	87.9
19	0.0002	54.9
20	0.0012	-87.8
21	0.0001	16.9
22	0.0003	-32.7
23	0.0009	-34.0
24	0.0015	2.9
25	0.0009	2.0
26	0.0001	-1.5
27	0.0005	-10.9
28	0.0035	-34.7
29	0.0004	-86.3
30	0.0001	28.7
31	0.0001	46.7
32	0.0035	75.5
33	0.0002	62.6
34	0.0002	-65.9
35	0.0002	38.8
36	0.0018	44.3
37	0.0006	-67.6
38	0.0007	-72.0
39	0.0011	-69.9
40	0.0081	-64.2

TABLE 5.

FOURIER ANALYSIS OF MASS TRANSFER COEFFICIENT FOR ELECTRODE 9C2.

coefficient appears on Table 2. Here the second harmonic (harmonic '8') is considerably lower than the first or the third, but appreciably above the noise level. Nevertheless, the ratio which determines A_{mp} is of course adversely affected by a spurious pressure result. Another example of a low amplitude pressure signal is in Table 3 (electrode 9B4). To compare these low magnitude signals to those which produce more consistent results, Tables 4 and 5 which list the pressure gradient and mass transfer analyses for electrode 9C2 have been included. Together these tables illustrate how the cause for a relatively large deviation among rather consistent and well-behaved data points can be pinpointed. A very low pressure signal for the second and sometimes the fifth harmonic, along with an occasional low mass transfer signal, accounted for almost all of the experimental scatter observable in Figures 15, 16, and 17.

The relationship between the measure mass transfer coefficient, characterized as $A_{mp}\ (\frac{\lambda_m}{\lambda_p})$, and the instantaneous wall shear rate, described as the analogous ratio $\frac{\lambda_s}{\lambda_p}$, is expressed by equation (A4-15) as

$$A_{sp} = \frac{\lambda_s}{\lambda_p} = \frac{3}{\hat{A}}\ A_{mp} \qquad \text{(A4-15)}$$

where $\hat{A}$ is a correction factor for the frequency response of the concentration boundary layer to changes in the velocity gradient for conditions removed from the pseudo-steady state (Fortuna and Hanratty,

1971). As shown on Figure 6, $\hat{A}$ decreases as both frequency and electrode size increase (for a constant Schmidt Number). The position along the horizontal axis (denoted as XAXIS in Appendix 8) was calculated for each harmonic and electrode size, and the resulting value of $\hat{A}$ was inserted into equation (A4-15) to yield the graph of Figure 18 which represents the conversion of A_{mp} from Figures 15, 16, and 17 to A_{sp}. For comparative purposes, the results from electrode 8C4 have been added to Figure 18. (Recall that electrode C4 previously manifested very good agreement with the steady flow predictions of Lévêque). The solid line represents the unassailable theoretical predictions of Uchida (1956) for A_{sp} as a function only of the frequency parameter, equation (A4-12).

A remarkable observation from Figure 18 is that the data fall uniformly, with frequency, well below their expected positions along the curve, although a merging effect is evident at the lower end of the frequency range represented. The scatter arising from the analysis of low signal levels as discussed earlier is apparent and should be overlooked in view of the consistency of behavior for all electrode sizes especially in the upper frequency range. Clearly, attention must be focused on the correction factor, $\hat{A}$, since these graphed points represent the rather well modeled A_{mp} data of the previous figures. The large differences between the experimental results and theoretical predictions for A_{sp} in the intermediate and higher frequency region, suggest that $\hat{A}$, described by the curve,

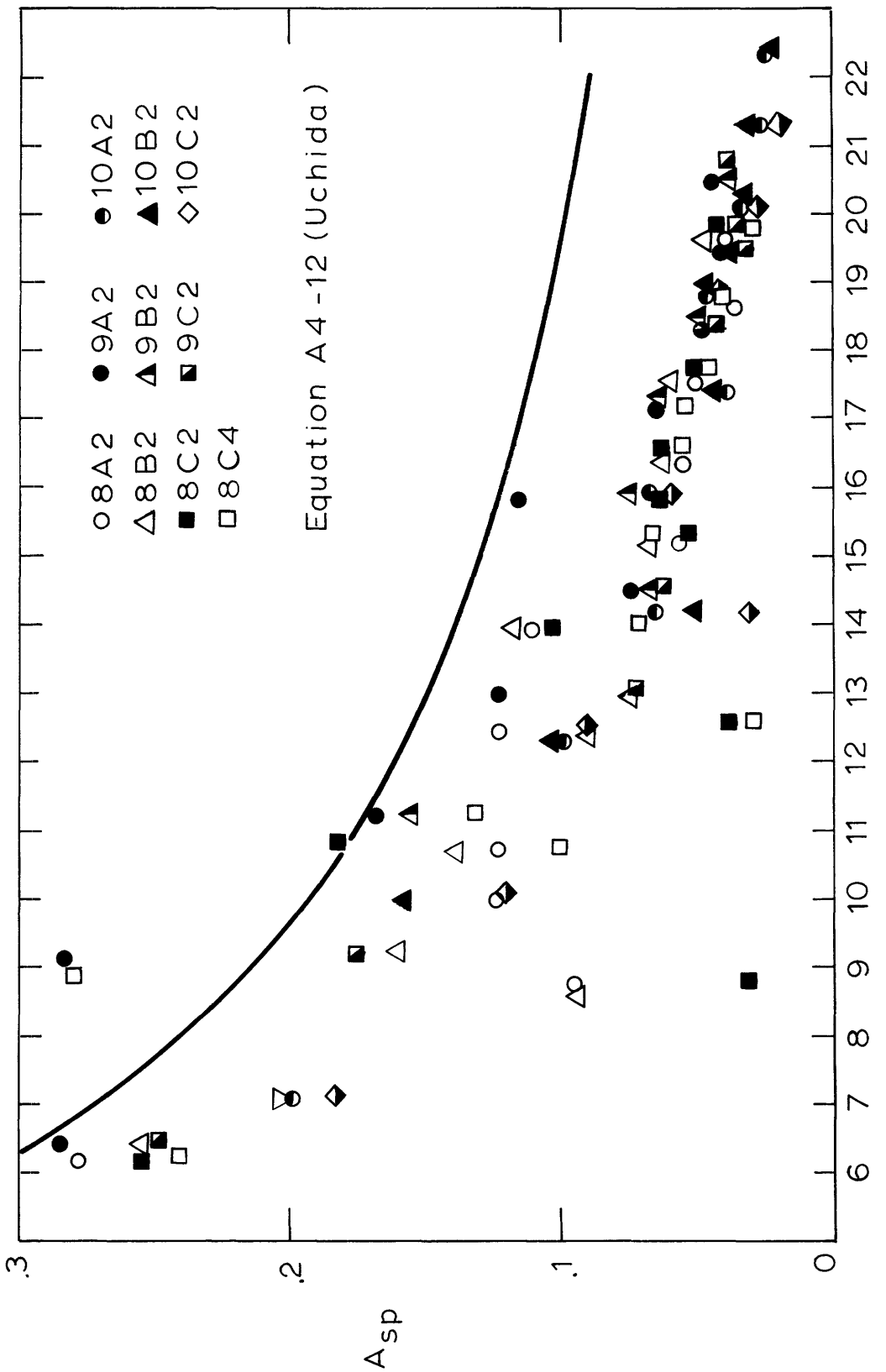

Figure 18. Experimental Vs. Theoretical Values for A_{sp}.

Figure 6, a transformation of the numerical results of Fortuna (1971), Figure 5, insufficiently compensates for the effects of frequency upon the response of the concentration boundary layer to shifts in the velocity gradient.* If so, it would be necessary to employ a steeper rising curve than Figure 6, (one that would impart larger corrections for the frequency response of the concentration boundary layer), for the experimental determination of pulsatile shear stress. On Figure 19 is such a curve, a plot of the values of $\hat{A}$ that would be required to establish conformity between the experimental values of A_{sp} and those described by equation (A4-12). The basis for determining the experimental values of $\hat{A}$ was a curve drawn through the data of Figure 18.

These experiments are the first attempt to test the validity and applicability of the numerically derived correction factor for the non-pseudo-steady state frequency response of the concentration boundary layer. Only for the laminar regime can this be accomplished since it is for only laminar pulsatile flow that a theoretical model for comparison of A_{sp} results (equation A4-12) is available. Although

---

* As to whether the size of the electrode is reflected correctly in $\hat{A}$, this is difficult to determine because of the overwhelming influence of the frequency parameter upon the term $GzSc^{3/2}\Omega^3$; the clustering of results from different electrodes suggest that the functional dependence of $\hat{A}$ on the Graetz Number is appropriate or at least less significant than its dependence upon Ω.

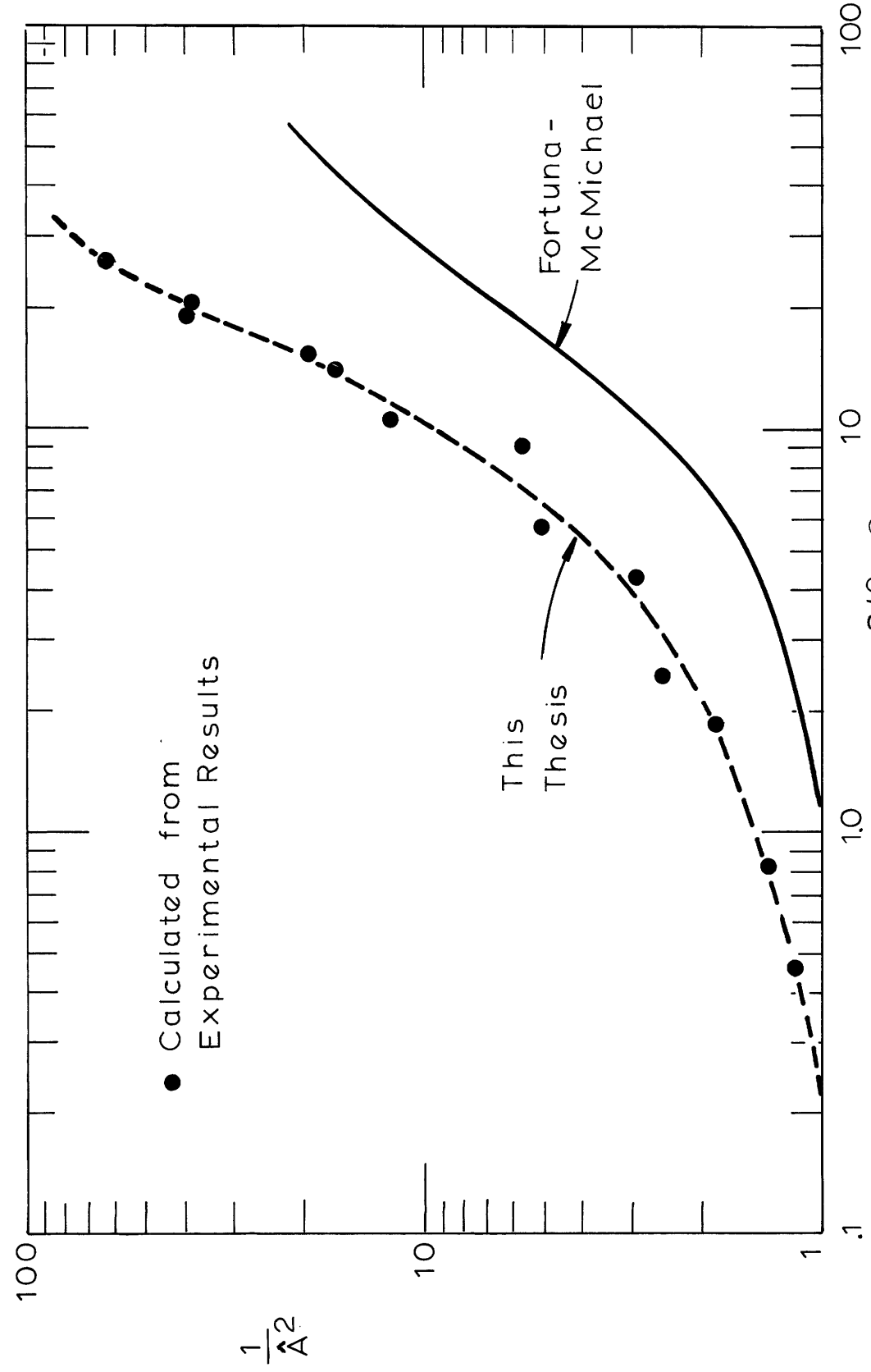

Figure 19. Experimental Correction to the Pseudo-Steady State Solution.

the results depicted in Figure 18 cast some doubt on the validity of the values for $\hat{A}$ calculated by Fortuna, it would be premature to conclude that Fortuna's results, described by Figure 6, are in error; the experimental conditions under which A_{sp} values were determined may have exceeded the range of applicability of the frequency response correction factor. The differential equation (99),

$$\frac{\partial C}{\partial t} + u \frac{\partial C}{\partial x} + v \frac{\partial C}{\partial y} = \mathcal{D}\left[\frac{\partial^2 C}{\partial x^2} + \frac{\partial^2 C}{\partial y^2}\right] \qquad (99)$$

from which $\hat{A}$ was eventually derived, was simplified to the form

$$\frac{\partial c_F}{\partial t} + \bar{S}y \frac{\partial c_F}{\partial x} + s_F y \frac{\partial \bar{C}}{\partial x} = \mathcal{D} \frac{\partial 2 c_F}{\partial y^2} \qquad (107)$$

by neglecting second order terms, such as u'c', as being small compared to both u' and c'. Indeed, for very low oscillatory pressure ratios, the undulating component of the fluid velocity would also be minute (equation 24), but as can be seen from the tables of Appendix 8, values for λ_p rarely fell below 0.1 and lay predominantly in the range 0.20 to 3, so that the amplitude of fluctuating velocity (within-the concentration boundary layer) was comparable to the time averaged flow above the electrode surface. This would certainly augment the term u'c' beyond the level of insignificance and would require its inclusion within the theoretical framework for the analysis of a pulsatile concentration boundary layer. Accordingly, it is impossible

to refute the validity of the correction factors previously reported (they may well be correct for very small oscillatory pressure ratios), but at the same time it is very difficult to assess the quantitative effect of significant second order terms without a more complete analysis of the concentration boundary layer frequency response problem. It seems likely, judging from the results reported here, that the inclusion of second order effects in such an analysis would have a marked effect on $\hat{A}$, shifting the lower curve of Figure 19 upwards and to the left so that its position would fall on or near the experimental curve (dashed line).

However, for experimental A_{mp} values that are well represented by equation (92), such as those of Figures 15, 16, and 17, an alternate correction factor can be derived, one that transforms A_{mp} to A_{sp}, thus providing a means of obtaining pulsatile shear stress data. Recalling equation (79)

$$M\{\gamma_n\} = \frac{8M_1(\Omega)}{\Omega\, Mo(\Omega)} \tag{79}$$

it can easily be shown, with reference to equations (25), (A2-8), (A4-6), and (A4-12), that

$$M\{\gamma_n\} = \frac{8}{\Omega}\sqrt{D^2 + E^2} = 4\,\sigma_t = 4\,A_{sp} \tag{144}$$

Then equation (92) can be rewritten as

$$A_{mp} = \frac{A_{sp}}{3(1 + \tau^2\alpha^4 Gz^{4/3})^{1/2}} \tag{145}$$

Rearranging (145) yields an alternate experimental route to A_{sp},

$$A_{sp} = 3(1 + \tau^2\alpha^4 Gz^{4/3})^{1/2} A_{mp} \tag{146}$$

where the term $(1 + \tau^2\alpha^4 Gz^{4/3})^{1/2}$ is an effective correction factor, of the form $\frac{1}{\hat{A}}$, for the frequency response of the concentration boundary layer. This term reduces to the same form as that given by Mitchell (1965) for the analytical representation of $\hat{A}$ at low values of $GzSc^{3/2}\Omega^3$. The analytical form of (146) is applicable at all frequencies; the results of this thesis demonstrate excellent agreement with Uchida at high values (>10) of $GzSc^{3/2}\Omega^3$.

Equation (146) is not restrictive to a cylindrical tube if the velocity gradient for the tube, implicit in $M\{\gamma_n\}$ and A_{sp} (equation 144) is removed by rearranging (146) to yield the general expression for converting non-steady electrochemical mass transfer data to shear stress results,

$$\frac{A_{sp}}{A_{mp}} = \frac{\lambda_s}{\lambda_m} = 3(1 + \tau^2\alpha^4 Gz^{4/3})^{1/2} \tag{147}$$

or equivalently,

$$S_F = 3(1 + \tau^2\alpha^4 Gz^{4/3})^{1/2}\bar{S}\ \frac{K_F}{\bar{K}} \tag{148}$$

It is clear then (from Figures 15, 16, and 17) that at higher frequencies, agreement with Uchida is excellent, and that for complex geometries it is necessary only to measure the mass transfer ratio and the steady flow shear rate to determine the ampliture of the fluctuating wall shear stress. Thus the need to measure the pressure gradient has been eliminated, and the diffusion controlled electrode has been shown to be a very effective shear stress measuring device.

XI. CONCLUSIONS AND RECOMMENDATIONS

Steady laminar flow measurements of interphase mass transfer were made to establish the validity of the electrochemical technique for measuring wall shear stress, and also to determine the behavorial consistency of the individual electrodes.

It was found that experimental departures from the theoretical predictions of Lévêque (for a steady laminar flow field in a cylindrical conduit) could be accounted for by two factors:

1) The equivalent rectangular length for circular electrodes ($L = .820d$) is not a constant within the laminar regime - electrode responses showed a consistent dependence upon the Reynolds number, reflecting a 15% variation about the value of .820 in the range $200<Re<1100$. Failure to account for this Reynolds number effect on the equivalent rectangular length can contribute errors of 5% in the measurement of mass transfer coefficients, and errors of 15% to the determination of steady flow wall shear.

2) The assumption that the electrode surfaces were circular and therefore symmetric was erroneous. Surface areas were found to be distorted from the circular shape, producing non-uniform concentration boundary layers with the effect that less current was drawn than expected. From the results of the steady flow experiments it was concluded that each electrode can serve as a bona-fide mass transfer measurement device. This requires that data analysis be

based on a 'corrected' diameter (rather than the electrodes measured diameter) chosen to eliminate significant departures from expected behavior. Accuracy can be further improved by incorporating a Reynold number-dependent correction factor to transform the electrode diameter to an equivalent rectangular length.

These correction factors were unnecessary for the analysis of pulsatile flow data, since the results for the case of non-steady flow were reported as a ratio of the amplitude of oscillation of the fluctuating quantity to the time-averaged value, thus nullifying the factors which would cause each of these to depart from theory.

It was found that the high frequency solution characterizing the effects of the amplitude and frequency of pulsation upon the fluctuating mass transfer coefficient, was an accurate model for the high frequency mass transfer data.

It was necessary to account for the frequency response of the concentration boundary layer when determining the fluctuating wall shear rate from the measured fluctuating mass transfer coefficient. This required the use of a correction factor for the non-pseudo-steady-state.

The numerical solution of Fortuna and Hanratty (1971) for this correction factor failed to produce agreement between the experimental results for the fluctuating wall shear rate and the exact analytical expression of Uchida (1956) for pulsatile wall shear. The use of oscillatory pressure ratios in the range 0.2 to 3 may have exceeded the restrictions of Fortuna and Hanratty's analysis, in which case the

experimental data reflect large contributions from the second order fluctuating terms such as u'c'. These must be considered in further analyses of the concentration boundary layer frequency response problem.

An alternate correction factor in analytical form was derived from the high frequency model for mass transfer. This correction term is effectively a transfer function between the experimental mass transfer coefficient and the fluctuating wall shear rate. It yields excellent agreement with Uchida for low and high frequencies and can be adjusted for the intermediate frequency range. In its general form the transfer function eliminates the need to measure the time-varying pressure gradient and is applicable to arbitrary geometries with arbitrary laminar flow fields.

It is strongly suggested that the technique of utilizing diffusion-controlled electrodes for the determination of pulsatile wall shear stress be applied to more complex models representative of the human arterial system. The available analysis for evaluating pulsatile shear stress phenomena in geometries such as a bifurcation can provide quantitative and meaningful information regarding the causal relationship between wall shear stress and atherogenesis.

APPENDIX 1

SOLUTION FOR THE OSCILLATING VELOCITY PROFILE

Appendix 1

Solution for the Oscillating Velocity Profile

The equation of motion whose solution is sought is given by

$$\frac{\partial u}{\partial t} = -\frac{1}{\rho} \cdot \frac{\partial p}{\partial x} + \frac{\nu}{r} \frac{\partial}{\partial r} \left(r \frac{\partial u}{\partial r}\right) \tag{A1-1}$$

where the pressure gradient is defined as

$$-\frac{1}{\rho} \cdot \frac{\partial p}{\partial x} = P_s \left[1 + \sum_{n=1}^{N} \lambda_{p(n)} \cos (n\omega t - \Theta_n) \right] \tag{A1-2}$$

and Θ_n is the phase difference between a frequency component n and the fundamental frequency. Since the flow is contained by rigid walls, the response of the fluid to this exciting force will be periodic at the same frequency as the disturbance. The linearity of the system together with the linear form of the equation of motion (A1-1), (no convective acceleration terms are present), permits a solution to be constructed by a superposition of all frequencies of oscillation. The N harmonic components are treated individually thereby permitting the arbitrary establishment of the origin of the period for each frequency. Each Θ_n is therefore made to vanish and for the sake of simplicity in calculation (A1-2) can be written in the form

$$-\frac{1}{\rho} \cdot \frac{\partial p}{\partial x} = P_s \left[1 + \sum_{n=1}^{N} \lambda_{p(n)} e^{in\omega t} \right] \tag{A1-2b}$$

where only the real part has any physical significance.

The composite pulse can be reconstructed by summing the real parts of (A1-2b) and reinserting each θ_n to account for the phase differences among the component frequencies.

Responding linearly to the pressure gradient, each harmonic of the time varying velocity will acquire the form

$$u_n(r, t) = u_n(r)e^{in\omega t} \tag{A1-3}$$

where $u_n(r)$ is a complex coefficient. With (A1-2b) and (A1-3) substituted into (A1-1), the following equation results:

$$in\omega u_n = P_s\lambda_n + \frac{\nu}{r}\frac{d}{dr}\left(r\frac{du_n}{dr}\right) \tag{A1-4}$$

Let

$$\eta = \frac{r}{R}$$

Then

$$iu_n = \frac{P_s\lambda_n}{\omega n} + \frac{1}{\Omega^2}\cdot\frac{1}{\eta}\frac{d}{d\eta}\left(\eta\frac{du_n}{d\eta}\right) \tag{A1-5}$$

where

$$\Omega^2 = R^2\cdot\frac{n\omega}{\nu}$$

Multiplying by Ω^2 and carrying out the indicated differentiation,

$$(\beta - \Omega^2 iu_n) + \frac{1}{\eta}\frac{du_n}{d\eta} + \frac{d^2u_n}{d\eta^2} = 0 \tag{A1-6}$$

with

$$\beta = \frac{P_s\lambda_{p(n)}}{n\omega}\cdot\Omega^2 = \frac{P_s\lambda_{p(n)}R^2}{\nu} \tag{A1-7}$$

This equation is closely related to Bessel's equation whose equation of the general form

$$x^2 \frac{d^2y}{dx^2} + x \frac{dy}{dx} + (c^2x^2 - q^2)y = 0 \qquad \text{(A1-8)}$$

has the solution (for q = 0, or any integer) in terms of Bessel functions:

$$y = F_q(Dx);\ F_q(x) = C_1J_q(x) + C_2Y_q(x) \qquad \text{(A1-9)}$$

Equation (A1-6) can be put in this form with the substitution

$$w_n = u_n - \frac{\beta}{i\Omega^2} \qquad \text{(A1-10)}$$

which yields

$$\eta^2 \frac{d^2w_n}{d\eta^2} + \eta \frac{dw_n}{d\eta} + (-i\Omega^2\eta^2 - 0)w_n = 0 \qquad \text{(A1-11)}$$

Hence q = 0, $D^2 = -i\Omega^2$, $D = i^{3/2}\Omega$, and

$$w_n = C_1J_o(i^{3/2}\Omega\eta) + C_2Y_o(i^{3/2}\Omega\eta) \qquad \text{(A1-12)}$$

At $\eta = 0$, u_n and hence w_n must be finite. Since $Y_o(0) \to \infty$, c_2 must be zero. Then

$$w_n = u_n - \frac{\beta}{i\Omega^2} = C_1J_o(i^{3/2}\Omega\eta) \qquad \text{(A1-13)}$$

At $\eta = 1$, with no slip at the wall, $u_n = 0$. Thus

$$-\frac{\beta}{i\Omega^2} = C_1J_o(i^{3/2}\Omega\eta) \qquad \text{(A1-14)}$$

and

$$C_1 = -\frac{\beta}{i\Omega^2} \cdot \frac{1}{J_o(i^{3/2}\Omega\eta)} \tag{A1-15}$$

Then

$$u_n = \frac{\beta}{i\Omega^2}\left[1 - \frac{J_o(i^{3/2}\Omega\eta)}{J_o(i^{3/2}\Omega)}\right] \tag{A1-16}$$

or, substituting for β:

$$u_n = \frac{-iP_s\lambda_{p(n)}R^2}{\Omega^2\nu}\left[1 - \frac{J_o(i^{3/2}\Omega\eta)}{J_o(i^{3/2}\Omega)}\right] \tag{A1-17}$$

From relations governing Poiseuille flow it can be shown that

$$U_o = \left(\frac{dp}{dx}\right)_s \cdot \frac{R^2}{8\mu} \tag{A1-18}$$

Combined with

$$P_s = -\frac{1}{\rho} \cdot \left(\frac{dp}{dx}\right)_s \tag{A1-19}$$

equation (A1-17) becomes

$$u_n = \frac{-8i\lambda_{p(n)}U_o}{\Omega^2}\left[1 - \frac{J_o(i^{3/2}\Omega\eta)}{J_o(i^{3/2}\Omega)}\right] \tag{A1-20}$$

This is the desired solution which is the same as equation (23).

APPENDIX 2

CRITICAL VALUES OF PULSATILE FLOW PARAMETERS

Appendix 2

Critical Values of Pulsatile Flow Parameters

The analysis of the fluctuating current generated at the electrode requires that the velocity gradient at the surface retain a positive value throughout the period of pulsation. The mathematical model stemming from the conservation of mass equation maintains that the mass transfer coefficient is directly linked to the shear rate, being driven and altered by it. However, if the shear rate should vanish instantaneously at some point of time in its cyclic oscillation, the flow of current would not cease, as is implied by the model (and equations 109 and [136]), but would continue for ferricyanide ions could still diffuse through the momentarily quiescent fluid. The shear rate dependence of the mass transfer process is then destroyed at which time not only the validity but the meaning of the measured signal becomes questionable.

It is therefore desirable to quantify the relationship between the pulsatile parameters, λ_p and Ω, which represents an upward barrier or physical constraint upon the flow conditions, where the velocity gradient at the wall vanishes, and beyond which the hydrodynamic boundary layer reverses its direction.

Consider a single frequency of oscillation so that the time varying pressure gradient, expressed by equation (15) becomes

$$-\frac{1}{\rho}\cdot\frac{\partial p}{\partial x} = P_s[1 + \lambda_p \cos(\omega t - \Theta)] \qquad \text{(A2-1)}$$

The fluctuating velocity, described in its general harmonic form by equation (29), is then written as

$$\frac{u'}{U_o} = \lambda_p \left\{ \frac{8\beta}{\Omega^2} \cos(\omega t - \Theta) + \frac{8(1 - A)}{\Omega^2} \sin(\omega t - \Theta) \right\} \quad \text{(A2-2)}$$

where

$$A = \frac{\text{ber}(\Omega)\cdot\text{ber}(\Omega \frac{r}{R}) + \text{bei}(\Omega)\cdot\text{bei}(\Omega \frac{r}{R})}{\text{ber}^2(\Omega) + \text{bei}^2(\Omega)}; \quad B = \frac{\text{bei}(\Omega)\cdot\text{ber}(\Omega \frac{r}{R}) - \text{ber}(\Omega)\cdot\text{bei}(\Omega \frac{r}{R})}{\text{ber}^2(\Omega) + \text{bei}^2(\Omega)}$$

(A2-3)

Equation (A2-2) is added to the familiar Poiseuille solution for the steady flow to obtain the instantaneous velocity at any point in the conduit (beyond the flow development region), then

$$\frac{u}{U_o} = 2\left(1 - \frac{r^2}{R^2}\right) + \lambda_p \left\{ \frac{8\beta}{\Omega^2} \cos(\omega t-\Theta) + \frac{8(1-A)}{\Omega^2} \sin(\omega t-\Theta) \right\} \quad \text{(A2-4)}$$

The conditions at which the velocity gradient at the wall vanishes are determined from the requirement that

$$\frac{du}{dr} = 0 \quad \text{at} \quad r = R \quad \text{(A2-5)}$$

Differentiating equation (A2-4) and evaluating the result at the wall yields,

$$\lambda_p = \frac{\Omega}{2[D \sin(\omega t-\Theta) - E \cos(\omega t-\Theta)]} \quad \text{(A2-6)}$$

where using the notation

$$ber'(\Omega) = \frac{d(ber\ \Omega)}{d\Omega};\ bei'(\Omega) = \frac{d(bei\ \Omega)}{d\Omega} \qquad (A2\text{-}7)$$

E and D are

$$E = \frac{ber(\Omega)\cdot bei(\Omega) - bei(\Omega)\cdot ber'(\Omega)}{ber^2(\Omega) + bei^2(\Omega)},\ D = \frac{ber(\Omega)\cdot ber'(\Omega) + bei(\Omega)\cdot bei'(\Omega)}{ber^2(\Omega) + bei^2(\Omega)} \qquad (A2\text{-}8)$$

The minimum value of λ_p for which flow reversal is at its critical point is given as

$$M\{\lambda_p\} = \frac{\Omega}{2(D^2 + E^2)^{1/2}} \qquad (A2\text{-}9)$$

The critical values for λ_p are plotted against Ω on the accompanying graph. Beyond a value of unity for Ω, the relationship is nearly linear with a slope of 0.5. It is clear that in the physiological range of the frequency parameter for various regions of the aorta ($3 < \Omega < 14$), the value of the pressure amplitude ratio can safely exceed unity without causing the shear rate at the wall to vanish.

The relationship (A2-9) defines the critical limits for λ_p and Ω dictated by the range of validity of the experimental technique. The graph then, represents an absolute limit for the values of these parameters, but does not provide or imply the limits beyond which the fluctuating quantities become large enough in magnitude to acquire significance and belie the linearization process by which the differential equation describing the conservation of mass within the concentration boundary layer (equation 99) was simplified. These analytically

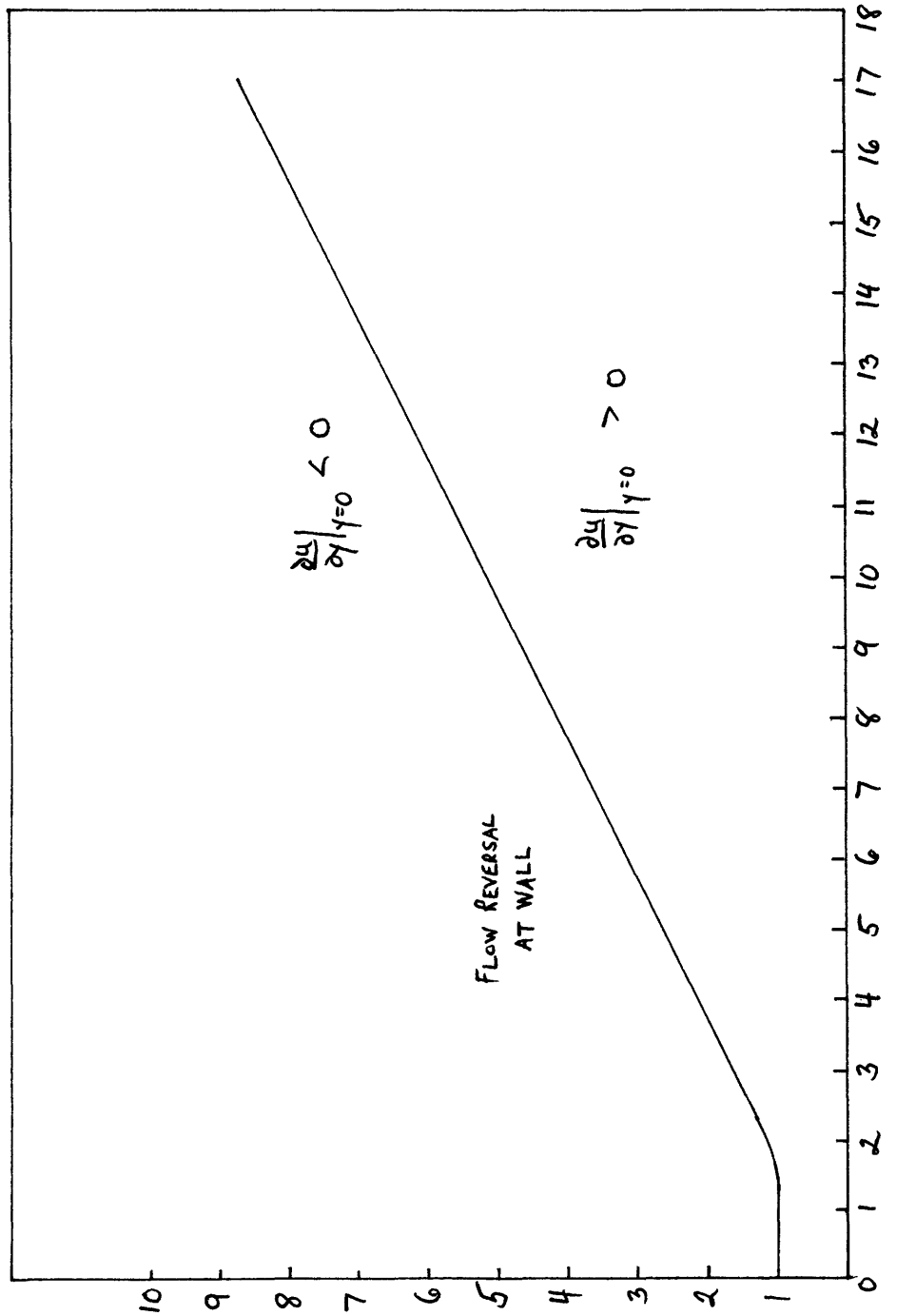

Figure A2-1. Relationship of Flow Parameters for $\frac{\partial u}{\partial y}\Big|_{y=0} = 0$.

restrictive limits are lower than those imposed by (A2-9) and are manifested by a significant deviation in the time average of a measured fluctuating quantity from its steady flow value. They were determined from the experimental data.

APPENDIX 3

DERIVATION OF THE RELATIONSHIP BETWEEN THE MASS TRANSFER COEFFICIENT AND THE WALL SHEAR RATE

Appendix 3

Derivation of the Relationship Between the Mass Transfer Coefficient and the Wall Shear Rate

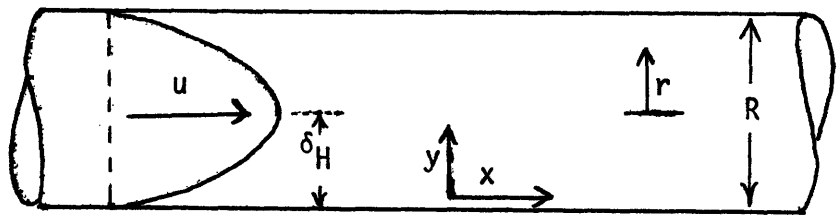

Coordinate System

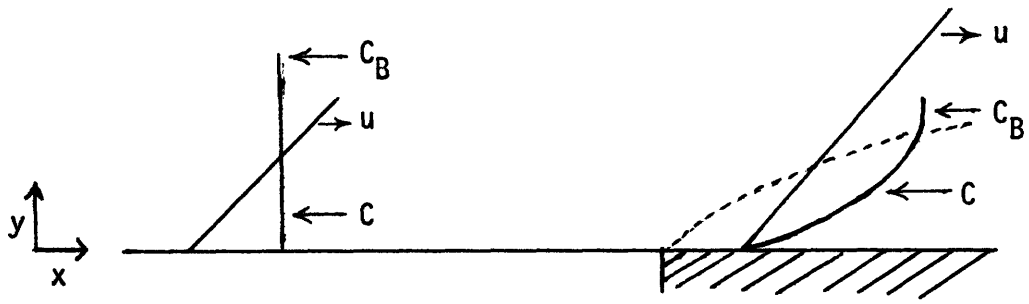

Profiles in and Near the Mass Transfer Section

Steady Flow Solution

Consider a steady fully developed flow confronting the leading edge of the electrode surface. There are no transient perturbations and radial velocities have vanished. The conservation of mass within the developing concentration boundary layer is then written for this cylindrical system as

$$u \frac{\partial C}{\partial x} = \mathcal{D} \left[\frac{\partial^2 C}{\partial r^2} + \frac{1}{r} \frac{\partial C}{\partial r} \right] \tag{A3-1}$$

where $\mathcal{D}$ is the diffusion coefficient, a constant for the flow considered here. Since the Schmidt number, $\frac{\nu}{\mathcal{D}}$, is much greater than unity,

$$\delta_C << \delta_H$$

and within the concentration boundary layer distances radial from the wall will be very small such that with

$$y = R - r,$$

the following is true: $y << R$

Therefore

$$r = R - y$$

and (A3-2)

$$\frac{\partial y}{\partial r} = - 1$$

With (A3-2) substituted into the right hand side of (A3-1) there is obtained

$$u \frac{\partial C}{\partial x} = \frac{\partial^2 C}{\partial y^2} - \frac{1}{R - y} \frac{\partial C}{\partial y} \tag{A3-3}$$

A comparison of the orders of magnitude of the terms on the right hand side of (A3-3) simplifies this equation to

$$u \frac{\partial C}{\partial x} = \frac{\partial^2 C}{\partial y^2} \tag{A3-4}$$

with boundary conditions

$$C(x \leq o,\ y) \quad = C_B$$

$$C(x \geq o,\ y = o) = C_W$$

$$C(x > o,\ y = \infty) = C_B$$

which demonstrates that curvature can be neglected.

Since the dramatic changes in concentration are confined to a very thin layer adjacent to the wall, the velocity can be considered to relate linearly to the distance from the wall with a slope equal to the gradient at the wall.

$$u = Sy \tag{A3-5}$$

where

$$S = \left(\frac{\partial u}{\partial y}\right)_{y=o} \equiv \text{wall shear rate}$$

Introducing the dimensionless variable

$$\Theta = \frac{C - C_W}{C_B - C_W} \tag{A3-6}$$

along with (A3-5) into (A3-4) yields

$$Sy \frac{\partial \Theta}{\partial x} = \mathcal{D} \frac{\partial^2 \Theta}{\partial y^2} \tag{A3-7}$$

$$\Theta(x = o,\ y) \quad = 1$$

$$\Theta(x > o,\ y = o) = 0$$

$$\Theta(x > o,\ y = \infty) = 1$$

The solution is obtained as follows:

Let $\Theta = f(\zeta)$ where $\zeta = y/\delta_c$ (A3-8)

The concentration boundary layer thickness can be found by dimensional analysis,

$$S\delta_c \frac{\Delta\Theta}{x} = \mathcal{D} \frac{\Delta\Theta}{\delta_c^2} \tag{A3-9}$$

or

$$\delta_c = \left(\frac{\mathcal{D}x}{S}\right)^{1/3} \tag{A3-10}$$

If we let

$$\delta_c = \left(\frac{9\mathcal{D}x}{S}\right)^{1/3} \tag{A3-11}$$

then

$$\zeta = y\left(\frac{S}{9\mathcal{D}x}\right)^{1/3} \tag{A3-12}$$

and

$$\frac{\partial\Theta}{\partial x} = \frac{\partial\Theta}{\partial\zeta} \cdot \frac{\partial\zeta}{\partial x} = \frac{\partial\Theta}{\partial\zeta}\left[-\frac{1}{3x}\zeta\right] \tag{A3-13}$$

The second order differential

$$\frac{\partial^2\Theta}{\partial y^2} = \frac{\partial^2\Theta}{\partial\zeta^2}\left(\frac{\partial\zeta}{\partial y}\right)^2 \tag{A3-14}$$

along with (A3-13) is substituted into (A3-7) and the result is simplified algebraically to obtain

$$\frac{\partial^2\Theta}{\partial\zeta^2} + 3\zeta^2 \frac{\partial\Theta}{\partial\zeta} = 0 \tag{A3-15}$$

$$\Theta(x = o,\ \zeta \to \infty) = 1$$

$$\Theta(x > o,\ \zeta = o) = 0$$

Let $p = \frac{d\Theta}{d\zeta}$, then (A3-15) becomes

$$\frac{dp}{d\zeta} + 3\zeta^2 p = 0 \qquad \text{(A3-16)}$$

whose solution is easily found to be

$$p = \frac{d\Theta}{d\zeta} = C_1 \, \mathrm{EXP}(-\zeta^3) \qquad \text{(A3-17)}$$

then

$$\Theta = C_1 \int_0^{\zeta} \mathrm{EXP}(-\zeta)^3 \, d\zeta \qquad \text{(A3-18)}$$

C_1 is found from the boundary condition $\Theta = 1$ when $\zeta = \infty$, thus

$$1 = C_1 \int_0^{\infty} \mathrm{EXP}(-\zeta^3) \, d\zeta \rightarrow C_1 = \frac{1}{\int_0^{\infty} \mathrm{EXP}(-\zeta^3) d\zeta} \qquad \text{(A3-19)}$$

so that

$$\Theta = \frac{C - C_W}{C_B - C_W} = \frac{\int_0^{\zeta} \mathrm{EXP}(-\zeta^3) d}{\int_0^{\infty} \mathrm{EXP}(-\zeta^3) d\zeta} \qquad \text{(A3-20)}$$

This can be simplified to gamma function form by noting that

$$\Gamma(\alpha) = \int_0^{\infty} z^{\alpha-1} \, \mathrm{EXP}(-z) dz \qquad \text{(A3-21)}$$

Let $z = \zeta^3$, then $\zeta = z^{1/3}$

and $d\zeta = \frac{1}{3} z^{-2/3} \, dz$

Thus

$$\int_0^\infty \mathrm{EXP}(-\zeta^3)d\zeta = \int_0^\infty \frac{1}{3} z^{1/3-1}\, \mathrm{EXP}(-z)dz = \frac{1}{3}\Gamma\left(\frac{1}{3}\right) \qquad \text{(A3-22)}$$

Hence

$$\frac{C - C_W}{C_B - C_W} = \frac{\int_0^\zeta \mathrm{EXP}(-\zeta^3)d\zeta}{\frac{1}{3}\Gamma\left(\frac{1}{3}\right)} \qquad \text{(A3-23)}$$

where

$$\zeta = y\left(\frac{S}{9\mathcal{D}x}\right)^{1/3}$$

If N is designated to be the flux of ferricyanide ion per unit electrode surface area per unit time then

$$N = -\mathcal{D}\left(\frac{\partial C}{\partial y}\right)_{y=o} = -\mathcal{D}\,(C_B - C_W)\left(\frac{\partial \Theta}{\partial y}\right)_{y=o} = K_S(C_B - C_W) \qquad \text{(A3-24)}$$

where K_S is defined as the steady state mass transfer coefficient. Then

$$\left|\frac{K}{\mathcal{D}}\right| = \left(\frac{\partial \Theta}{\partial y}\right)_{y=o} \qquad \text{(A3-25)}$$

The right hand side of (A3-25) is determined as follows:

$$\frac{\partial \Theta}{\partial y} = \frac{\partial \Theta}{\partial \zeta} \cdot \frac{\partial \zeta}{\partial y} = \frac{\partial \Theta}{\partial \zeta} \cdot \left(\frac{S}{9\mathcal{D}x}\right)^{1/3} \qquad \text{(A3-26)}$$

From (A3-17)

$$\frac{\partial \Theta}{\partial \zeta} = \frac{\mathrm{EXP}(-\zeta^3)}{\frac{1}{3}\Gamma\left(\frac{1}{3}\right)} \qquad \text{(A3-27)}$$

and since $\zeta = 0$ when $y = 0$

$$\left(\frac{\partial\Theta}{\partial y}\right)_{y=0} = \left(\frac{\partial\Theta}{\partial\zeta}\right)_{\zeta=0} \left(\frac{S}{9\mathcal{D}x}\right)^{1/3} = \frac{1}{\frac{1}{3}\,\Gamma\left(\frac{1}{3}\right)} \left(\frac{S}{9\mathcal{D}x}\right)^{1/3} \tag{A3-28}$$

Combining (A3-28) with (A3-25) the steady state mass transfer coefficient is found to be

$$K_s = \frac{3^{1/3}}{\Gamma\left(\frac{1}{3}\right)} \left(\frac{S\mathcal{D}^2}{x}\right)^{1/3} \tag{A3-29}$$

and

$$S = \left[\frac{\Gamma\left(\frac{1}{3}\right) K_s}{3^{1/3}}\right]^3 \left(\frac{x}{\mathcal{D}^2}\right) \tag{A3-30}$$

For steady flow in a tube the velocity gradient at the wall is

$$S = \frac{4U_o}{R} \tag{A3-31}$$

where U_o is the average velocity. With this value of the shear rate introduced into (A3-29) the expression for the steady state mass transfer coefficient becomes

$$K_s = \mathcal{D}\,\frac{(12)^{1/3}}{\Gamma\left(\frac{1}{3}\right)} \left(\frac{U_o}{R\mathcal{D}x}\right)^{1/3} \tag{A3-32}$$

which is the same as equation (45).

To determine the wall shear rate from the measured electrode response the spatial average of K_s must be considered. Integrating equation (A3-29) over the electrode surface yields,

$$\langle K_s \rangle = \frac{3}{2} K_s \Big|_{x=L} \tag{A3-33}$$

Then

$$\langle K_s \rangle = \frac{3}{2} \cdot \frac{3^{1/3}}{\Gamma(\frac{1}{3})} \left(\frac{SD^2}{L} \right)^{1/3} \tag{A3-34}$$

and

$$S = \left[\frac{\Gamma(\frac{1}{3}) \ (\frac{2}{3} \langle K_s \rangle)}{3^{1/3}} \right]^3 \ (\frac{L}{D^2}) \tag{A3-35}$$

where L = 0.82 d.

APPENDIX 4

EXACT SOLUTION FOR THE TRANSIENT AND INSTANTANEOUS SHEAR RATE

Appendix 4

Exact Solution for the Transient and Instantaneous Shear Rate

The transient behavior of the wall shear stress can be determined by performing the differentiation, $\frac{\partial u}{\partial r}$, of equation (28). By superposing the steady value of the shear stress, obtained from the friction factor for laminar flow as

$$\tau_s = f \cdot \frac{1}{2} \rho U_o^2 = \frac{1}{2} \rho U_o^2 \cdot \frac{16}{Re} \tag{A4-1}$$

the result, originally obtained by Uchida (1956) is

$$\tau = (\frac{1}{2} \rho U_o^2) \cdot \frac{16}{Re} \left[1 + \sum_{n=1}^{N} a_n \left\{ \frac{2E}{\Omega} \cos n\omega t + \frac{2D}{\Omega} \sin n\omega t \right\} + \sum_{n=1}^{N} b_n \left\{ \frac{2E}{\Omega} \sin n\omega t - \frac{2D}{\Omega} \cos n\omega t \right\} \right] \tag{A4-2}$$

where D and E are defined in equation (A2-8) and the a_n and b_n terms are obtained from equation (14). For a periodic pressure gradient expressed as

$$-\frac{1}{\rho} \cdot \frac{\partial p}{\partial x} = P_s \left[1 + \sum_{n=1}^{N} \lambda_{p(n)} \cos (n\omega t - \Theta_n) \right] \tag{A4-3}$$

equation (A4-2) becomes

$$\tau = \tau_s \left[1 + \sum_{n=1}^{N} \lambda_{p(n)} \left\{ \frac{2E}{\Omega} \cos (n\omega t - \Theta_n) + \frac{2D}{\Omega} \sin (n\omega t - \Theta_n) \right\} \right] \tag{A4-4}$$

or, combining the cosine and sine terms,

$$\tau = \tau_s \left[1 + \sum_{n=1}^{N} \lambda_{p(n)} \sigma_T \cos (n\omega t - \Theta_n - \delta_T) \right] \tag{A4-5}$$

where

$$\sigma_T = \sqrt{\left(\frac{2E}{\Omega}\right)^2 + \left(\frac{2D}{\Omega}\right)^2} \tag{A4-6}$$

and

$$\delta_T = \tan^{-1} \frac{D}{E}$$

For each n (A4-5) can be written as

$$\tau = \tau_s(1 + \lambda_{p(n)} \sigma_T \cos (n\omega t - \Theta_n - \delta_T)) \tag{A4-7}$$

The shear rate can be expressed in the same form by dividing (A4-7) by the viscosity μ, hence for any frequency

$$S_n = \overline{S} (1 + \lambda_{p(n)} \sigma_T \cos (n\omega t - \Theta_n - \delta_T)) \tag{A4-8}$$

or equivalently,

$$S_n = \overline{S} + s_{F(n)} \cos (n\omega t - \Theta_n - \delta_T) \tag{A4-9}$$

where

$$s_{F(n)} = \overline{S} \lambda_{p(n)} \sigma_T \tag{A4-10}$$

The oscillatory shear rate amplitude ratio is obtained after dividing (A4-10) by the time average (equivalent to the steady flow value) of the shear rate. Thus for each frequency

$$\frac{s_F}{\overline{S}} = \lambda_s = \lambda_p \sigma_T \tag{A4-11}$$

which when rearranged yields the final result

$$A_{sp} = \frac{\lambda_s}{\lambda_p} = \sigma_T \tag{A4-12}$$

Since σ_T is a function of frequency, the value of A_{sp} will also depend on the frequency of the harmonic under consideration. It is plotted on the accompanying graph (Figure A4-1).

Equations (A4-8) and (A4-12) were used respectively as a theoretical comparison for the transient shear rate as determined experimentally from equation (136) and for the oscillatory amplitude ratio obtained from equation (135). Rearranging (135) there is obtained

$$\frac{S_F}{\bar{S}} = \frac{3}{\hat{A}} \frac{K_F}{\bar{K}} \tag{A4-13}$$

or

$$\lambda_s = \frac{3}{\hat{A}} \lambda_m \tag{A4-14}$$

Dividing (A4-14) by λ_p,

$$\frac{\lambda_s}{\lambda_p} = A_{sp} = \frac{3}{\hat{A}} A_{mp} \tag{A4-15}$$

A_{mp} is determined from the experimental data and A_{sp} is then calculated. The results from (A4-15) were compared to the theory (A4-12).

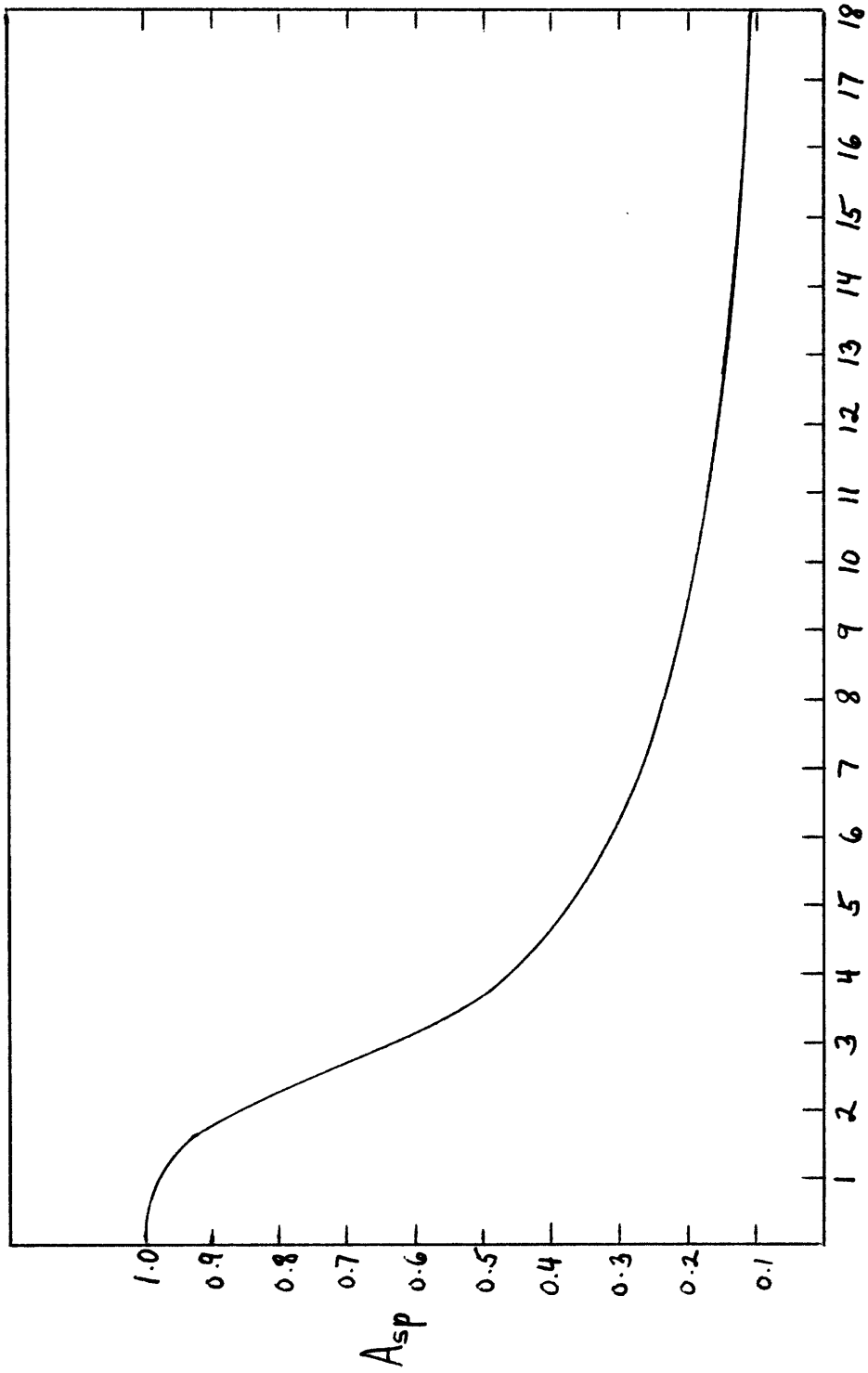

Figure A4-1. Shear Rate to Pressure Amplitude Ratios (Equation A4-12).

APPENDIX 5

DESCRIPTION OF FLUCTUATING QUANTITIES

Appendix 5

Description of Fluctuating Quantities

The deviation of the instantaneous mass transfer coefficient from its time averaged value, $\overline{K}$, has been designated as K' (equation 113). This is the first harmonic fluctuation whose time average is zero. The quantity resulting from squaring the magnitude of this fluctuation and averaging the result over the period of pulsation will be finite, however. The root mean square (RMS) of this fluctuating power is defined as

$$\text{RMS} = \overline{K'^2} = \left[\frac{1}{T}\int_0^T K'^2\, dt\right]^{1/2} \qquad \text{(A5-1)}$$

where T is the period of oscillation.

The relative intensity of a property of the undulating field is the ratio of the RMS value to the time average value, thus for the pulsatile velocity profile the intensity is given by

$$\frac{\overline{u'^2}}{\overline{U}} \qquad \text{(A5-2)}$$

The quantity which acts as the transfer function connecting mass transfer to the wall velocity gradient is the spectral density function which, for the mass transfer coefficient, is defined as

$$\overline{K'^2} = (\text{RMS})^2 = \int_0^\infty W_{K(n)}\, dn \qquad \text{(A5-3)}$$

This describes the distribution of the power of the fluctuating signal among the various frequencies. Since each harmonic of the flow is an integral multiple of the fundamental frequency, (A5-3) can properly be written as

$$\overline{K'^2} = \int_0^\infty W_{K(n)}dn = \sum_{n=1}^{N} W_{K(n)}dn \qquad \text{(A5-4)}$$

Furthermore, for a sine wave of a single frequency,

$$\overline{K'^2} = W_{K(n)} = (RMS)^2 \qquad \text{(A5-5)}$$

This spectral density function for each frequency of pulsation is related to the amplitude of the n^{th} harmonic of the fluctuating mass transfer coefficient in the following way,

$$\overline{K'^2_{(n)}} = (RMS)^2_{(n)} = \frac{K^2_{F(n)}}{2} \qquad \text{(A5-6)}$$

APPENDIX 6

ELECTROLYTE PHYSICAL PROPERTIES DATA

Table A6-1.

ELECTROLYTE PHYSICAL PROPERTY DATA

Component	Concentration
Sodium Hydroxide	2.000 M
Potassium Ferricyanide	0.010 M
Potassium Ferrocyanide	0.010 M

$T^{o}C$	μ(centipoise)	ρ(g/cc)	$\mathcal{D}x10^{6}(cm^{2}/sec)$	Schmidt#
27.0	1.1924	1.0783*	6.2898	1758.40
28.0	1.1699	1.0790	6.4322	1685.27
29.0	1.1466	1.0797*	6.5847	1612.83
30.0	1.1178	1.0804	6.7767	1526.73
31.0	1.0882	1.0807*	6.9840	1441.78
32.0	1.0666	1.0811*	7.1489	1380.06
33.0	1.0433	1.0814	7.3325	1315.74

*Represents values linearly interpolated from measured quantities. Properties at all other temperatures not listed here were similarly interpolated.

APPENDIX 7

SAMPLES OF RESULTS FROM STEADY FLOW EXPERIMENTS

Table A7-1.

SAMPLES OF STEADY FLOW MASS TRANSFER RESULTS

Reynolds	T°C	Electrode	Current (Amps x 10^6) Leveque	Experimental	% Error	Graetz x 10^8	Nusselt
162.21	27.4	A2	2.53	2.59	2.4	8.70	373.38
162.21	27.4	A6	2.53	2.62	3.6	8.70	377.70
161.97	27.3	B2	3.85	4.00	3.9	11.18	348.03
161.47	27.2	C4	5.71	6.03	5.6	14.15	327.19
200.06	26.6	A2	2.69	2.68	-0.37	6.82	393.21
200.06	26.6	A6	2.69	2.83	5.2	6.82	415.28
200.06	26.6	B2	4.11	4.21	2.4	8.79	371.96
199.70	26.5	C4	6.09	6.35	4.3	11.12	350.13
292.58	27.2	A2	3.08	3.09	0.32	4.78	447.11
292.58	27.2	A6	3.08	3.11	0.97	4.78	450.00
293.38	27.3	B2	4.70	4.81	2.3	6.17	418.51
293.38	27.3	C4	6.97	7.22	3.6	7.82	391.20
329.88	28.8	A2	3.24	3.17	-2.2	4.54	442.53
329.88	28.8	A6	3.24	3.27	0.93	4.54	456.49
329.88	28.8	B2	4.95	5.04	1.8	5.86	423.68
329.88	28.8	C4	7.34	7.47	1.8	7.42	391.05
436.90	27.3	A2	3.52	3.54	0.57	3.22	511.49
436.90	27.3	A6	3.52	3.56	1.1	3.22	514.38
436.90	27.3	B2	5.36	5.53	3.2	4.14	481.15
436.90	27.3	C4	7.96	8.18	2.8	5.25	443.22
519.37	27.3	A2	3.72	3.59	-3.5	2.71	518.71
519.37	27.3	A6	3.72	3.83	3.0	2.71	553.39
519.37	27.3	B2	5.68	5.71	0.53	3.49	496.81
519.37	27.3	C4	8.43	8.59	1.9	4.42	465.44

Table A7-1. (continued)

603.98	27.4	A2	3.92	3.92	0.0	2.34	565.11
603.98	27.4	A6	3.92	3.95	0.77	2.34	569.43
603.98	27.4	B2	5.98	6.18	3.3	3.01	536.49
603.98	27.4	C4	8.88	9.08	2.3	3.81	490.87
740.04	27.5	A2	4.20	4.00	-4.8	1.91	575.37
740.04	27.5	A6	4.20	4.27	1.7	1.91	614.21
740.04	27.5	B2	6.41	6.39	-0.31	2.49	553.50
740.04	27.5	C4	9.51	9.56	0.53	3.13	515.68
816.33	29.0	A2	4.39	4.48	2.1	1.85	622.44
816.33	29.0	A6	4.39	4.63	5.5	1.85	643.28
816.33	29.0	B2	6.70	6.96	3.9	2.39	582.30
816.33	29.0	C4	9.95	10.24	2.9	3.02	533.52
1034.02	27.6	A2	4.70	4.65	-1.1	1.38	667.35
1034.02	27.6	A6	4.70	4.64	-1.3	1.38	665.91
1034.02	27.6	B2	7.17	7.22	0.70	1.77	623.97
1035.92	27.7	C4	10.66	10.69	0.28	2.25	574.06

Table A7-2.

CALCULATED WALL SHEAR RATES

(Corresponding to Data of Table A7-1)

Reynolds	Electrode	Wall Shear Rate (sec^{-1}) Poiseuille	Experimental	% Error
162.21	A2	5.35	5.75	7.5
162.21	A6	5.35	5.95	11.2
161.97	B2	5.35	5.99	11.9
161.47	C4	5.35	6.30	17.6
200.06	A2	6.70	6.60	-1.6
200.06	A6	6.70	7.77	15.9
200.06	B2	6.70	7.20	7.4
199.70	C4	6.70	7.59	13.3
292.58	A2	9.70	9.84	1.4
292.58	A6	9.70	10.03	3.4
293.38	B2	9.70	10.41	7.4
293.38	C4	9.70	10.78	11.1
329.88	A2	10.58	9.89	-6.5
329.88	A6	10.58	10.85	2.6
329.88	B2	10.58	11.18	5.7
329.88	C4	10.58	11.14	5.3
436.90	A2	14.44	14.75	2.1
436.90	A6	14.44	15.00	3.9
436.90	B2	14.44	15.82	9.5
436.90	C4	14.44	15.67	8.5
519.37	A2	17.17	15.38	-10.4
519.37	A6	17.17	18.68	8.8
519.37	B2	17.17	17.42	1.5
519.37	C4	17.17	18.15	5.7

Table A7-2. (continued)

603.98	A2	19.93	19.93	0.0
603.98	A6	19.93	20.40	2.4
603.98	B2	19.93	21.98	10.3
603.98	C4	19.93	21.33	7.1
740.04	A2	24.37	21.09	-13.5
740.04	A6	24.37	25.65	5.3
740.04	B2	24.37	24.19	-0.74
740.04	C4	24.37	24.79	1.7
816.33	A2	26.07	27.64	5.8
816.33	A6	26.07	30.51	17.0
816.33	B2	26.07	29.16	11.9
816.33	C4	26.07	28.42	9.0
1034.02	A2	33.99	32.98	-3.0
1034.02	A6	33.99	32.76	-3.6
1034.02	B2	33.99	34.73	2.2
1035.92	C4	33.99	34.35	1.1

APPENDIX 8

TABLES OF EXPERIMENTAL RESULTS FOR PULSATILE FLOW

$$* \quad XAXIS = GzSc^{3/2}\ \Omega^{3}$$

TABLE A8-1. PULSATILE FLOW RESULTS FOR RUN #8, ELECTRODE A2.

ELECTRODE	DIMENSIONLESS FREQUENCY	REYNOLDS NUMBER	SCHMIDT NUMBER	MASS TRANSFER RATIO	PRESSURE RATIO	AMP	XAXIS	CORRECTION FACTOR	ASP	UCHIDA	PER CENT ERROR
8A2	6.215	504.40	1619.18	0.0724	0.7737	0.0935	0.467	1.000	0.2806	0.3046	-7.87
8A2	8.789	504.40	1619.18	0.0045	0.1454	0.0311	1.321	0.979	0.0954	0.2186	-56.34
8A2	10.764	504.40	1619.18	0.0109	0.2876	0.0378	2.426	0.919	0.1233	0.1799	-31.45
8A2	12.429	504.40	1619.18	0.0021	0.0600	0.0357	3.735	0.868	0.1235	0.1564	-21.04
8A2	13.896	504.40	1619.18	0.0044	0.1458	0.0299	5.220	0.818	0.1096	0.1404	-21.92
8A2	15.222	504.40	1619.18	0.0037	0.2408	0.0154	6.862	0.754	0.0615	0.1284	-52.15
8A2	16.442	504.40	1619.18	0.0062	0.4522	0.0138	8.647	0.681	0.0608	0.1191	-48.99
8A2	17.577	504.40	1619.18	0.0065	0.6114	0.0106	10.564	0.610	0.0520	0.1116	-53.43
8A2	18.644	504.40	1619.18	0.0033	0.4984	0.0067	12.606	0.553	0.0363	0.1053	-65.57
8A2	19.652	504.40	1619.18	0.0142	2.0167	0.0071	14.764	0.501	0.0423	0.1000	-57.74

TABLE A8-2. PULSATILE FLOW RESULTS FOR RUN #9, ELECTRODE A2.

ELECTRODE	DIMENSIONLESS FREQUENCY	REYNOLDS NUMBER	SCHMIDT NUMBER	MASS TRANSFER RATIO	PRESSURE RATIO	AMP	XAXIS	CORRECTION FACTOR	ASP	UCHIDA	PER CENT ERROR
9A2	6.484	513.08	1560.05	0.0772	0.8115	0.0951	0.512	1.000	0.2854	0.2926	-2.45
9A2	9.170	513.08	1560.05	0.0029	0.0314	0.0919	1.447	0.970	0.2841	0.2099	35.34
9A2	11.231	513.08	1560.05	0.0117	0.2298	0.0509	2.659	0.910	0.1679	0.1726	-2.75
9A2	12.968	513.08	1560.05	0.0037	0.1041	0.0353	4.094	0.855	0.1238	0.1501	-17.51
9A2	14.499	513.08	1560.05	0.0023	0.1162	0.0199	5.721	0.801	0.0746	0.1348	-44.63
9A2	15.883	513.08	1560.05	0.0020	0.0719	0.0283	7.521	0.730	0.1162	0.1232	-5.69
9A2	17.155	513.08	1560.05	0.0078	0.5507	0.0141	9.477	0.647	0.0653	0.1142	-42.84
9A2	18.340	513.08	1560.05	0.0055	0.5947	0.0092	11.579	0.580	0.0476	0.1070	-55.57
9A2	19.452	513.08	1560.05	0.0033	0.4501	0.0073	13.817	0.523	0.0420	0.1010	-58.40
9A2	20.505	513.08	1560.05	0.0188	2.7365	0.0069	16.182	0.470	0.0439	0.0960	-54.28

TABLE A8-3. PULSATILE FLOW RESULTS FOR RUN #10, ELECTRODE A2.

ELECTRODE	DIMENSIONLESS FREQUENCY	REYNOLDS NUMBER	SCHMIDT NUMBER	MASS TRANSFER RATIO	PRESSURE RATIO	AMP	XAXIS	CORRECTION FACTOR	ASP	UCHIDA	PER CENT ERROR
10A2	7.097	527.19	1474.68	0.0567	0.8550	0.0664	0.635	1.000	0.1991	0.2688	-25.92
10A2	10.037	527.19	1474.68	0.0054	0.1151	0.0467	1.796	0.949	0.1476	0.1924	-23.28
10A2	12.292	527.19	1474.68	0.0114	0.3971	0.0287	3.299	0.883	0.0976	0.1581	-38.27
10A2	14.194	527.19	1474.68	0.0008	0.0467	0.0179	5.079	0.822	0.0653	0.1375	-52.50
10A2	15.870	527.19	1474.68	0.0057	0.2992	0.0189	7.099	0.745	0.0760	0.1233	-38.35
10A2	17.384	527.19	1474.68	0.0062	0.7328	0.0085	9.331	0.653	0.0391	0.1128	-65.37
10A2	18.777	527.19	1474.68	0.0124	1.4175	0.0087	11.759	0.576	0.0455	0.1046	-56.53
10A2	20.074	527.19	1474.68	0.0137	2.4054	0.0057	14.367	0.510	0.0335	0.0979	-65.82
10A2	21.291	527.19	1474.68	0.0035	0.9139	0.0038	17.143	0.452	0.0255	0.0926	-72.49
10A2	22.443	527.19	1474.68	0.0201	6.0671	0.0033	20.078	0.406	0.0245	0.0878	-72.11

TABLE A8-4. PULSATILE FLOW RESULTS FOR RUN #8, ELECTRODE A4.

ELECTRODE	DIMENSIONLESS FREQUENCY	REYNOLDS NUMBER	SCHMIDT NUMBER	MASS TRANSFER RATIO	PRESSURE RATIO	AMP	XAXIS	CORRECTION FACTOR	ASP	UCHIDA	PER CENT ERROR
8A4	6.215	504.40	1619.18	0.0615	0.6689	0.0920	0.467	1.000	0.2760	0.3046	-9.39
8A4	8.789	504.40	1619.18	0.0031	0.1467	0.0214	1.321	0.979	0.0656	0.2186	-69.97
8A4	10.764	504.40	1619.18	0.0098	0.1919	0.0511	2.426	0.919	0.1667	0.1799	-7.31
8A4	12.429	504.40	1619.18	0.0022	0.0675	0.0332	3.735	0.868	0.1147	0.1564	-26.69
8A4	13.896	504.40	1619.18	0.0033	0.0661	0.0492	5.220	0.818	0.1805	0.1404	28.55
8A4	15.222	504.40	1619.18	0.0031	0.2133	0.0146	6.862	0.754	0.0581	0.1284	-54.78
8A4	16.442	504.40	1619.18	0.0057	0.4217	0.0134	8.647	0.681	0.0593	0.1191	-50.27
8A4	17.577	504.40	1619.18	0.0057	0.5713	0.0100	10.564	0.610	0.0489	0.1116	-56.16
8A4	18.644	504.40	1619.18	0.0033	0.5335	0.0062	12.606	0.553	0.0336	0.1053	-68.11
8A4	19.652	504.40	1619.18	0.0123	1.7917	0.0068	14.764	0.501	0.0410	0.1000	-59.04

TABLE A8-5. PULSATILE FLOW RESULTS FOR RUN #9, ELECTRODE A4.

ELECTRODE	DIMENSIONLESS FREQUENCY	REYNOLDS NUMBER	SCHMIDT NUMBER	MASS TRANSFER RATIO	PRESSURE RATIO	AMP	XAXIS	CORRECTION FACTOR	ASP	UCHIDA	PER CENT ERROR
9A4	6.493	514.56	1551.49	0.0677	0.8408	0.0806	0.511	1.000	0.2417	0.2922	-17.30
9A4	9.182	514.56	1551.49	0.0028	0.0308	0.0905	1.445	0.970	0.2797	0.2096	33.42
9A4	11.246	514.56	1551.49	0.0094	0.2707	0.0347	2.655	0.910	0.1144	0.1724	-33.64
9A4	12.985	514.56	1551.49	0.0024	0.1086	0.0220	4.087	0.856	0.0770	0.1499	-48.66
9A4	14.518	514.56	1551.49	0.0024	0.1439	0.0170	5.712	0.802	0.0635	0.1346	-52.83
9A4	15.904	514.56	1551.49	0.0026	0.1247	0.0205	7.508	0.730	0.0841	0.1230	-31.62
9A4	17.178	514.56	1551.49	0.0066	0.5701	0.0116	9.461	0.648	0.0536	0.1141	-53.04
9A4	18.364	514.56	1551.49	0.0055	0.6911	0.0079	11.559	0.581	0.0409	0.1069	-61.78
9A4	19.478	514.56	1551.49	0.0031	0.5662	0.0055	13.793	0.523	0.0313	0.1009	-68.96
9A4	20.531	514.56	1551.49	0.0159	2.8968	0.0055	16.155	0.471	0.0350	0.0959	-63.56

TABLE A8-6. PULSATILE FLOW RESULTS FOR RUN #10, ELECTRODE A4.

ELECTRODE	DIMENSIONLESS FREQUENCY	REYNOLDS NUMBER	SCHMIDT NUMBER	MASS TRANSFER RATIO	PRESSURE RATIO	AMP	XAXIS	CORRECTION FACTOR	ASP	UCHIDA	PER CENT ERROR
10A4	7.097	527.19	1474.68	0.0462	0.8129	0.0568	0.635	1.000	0.1705	0.2688	-36.57
10A4	10.037	527.19	1474.68	0.0026	0.0960	0.0268	1.796	0.949	0.0847	0.1924	-55.96
10A4	12.292	527.19	1474.68	0.0109	0.3741	0.0293	3.299	0.883	0.0994	0.1581	-37.12
10A4	14.194	527.19	1474.68	0.0008	0.0636	0.0126	5.079	0.822	0.0459	0.1375	-66.63
10A4	15.870	527.19	1474.68	0.0048	0.2980	0.0163	7.099	0.745	0.0655	0.1233	-46.88
10A4	17.384	527.19	1474.68	0.0055	0.7042	0.0078	9.331	0.653	0.0359	0.1128	-68.18
10A4	18.777	527.19	1474.68	0.0094	1.3907	0.0068	11.759	0.576	0.0353	0.1046	-66.22
10A4	20.074	527.19	1474.68	0.0114	2.4207	0.0047	14.367	0.510	0.0276	0.0979	-71.78
10A4	21.291	527.19	1474.68	0.0025	0.8420	0.0030	17.143	0.452	0.0197	0.0926	-78.74
10A4	22.443	527.19	1474.68	0.0138	5.4265	0.0025	20.078	0.406	0.0188	0.0878	-78.63

TABLE A8-7. PULSATILE FLOW RESULTS FOR RUN #8, ELECTRODE A6.

ELECTRODE	DIMENSIONLESS FREQUENCY	REYNOLDS NUMBER	SCHMIDT NUMBER	MASS TRANSFER RATIO	PRESSURE RATIO	AMP	XAXIS	CORRECTION FACTOR	ASP	UCHIDA	PER CENT ERROR
8A6	6.215	504.40	1619.18	0.0565	0.6711	0.0841	0.467	1.000	0.2524	0.3046	-17.13
8A6	8.789	504.40	1619.18	0.0030	0.1254	0.0238	1.321	0.979	0.0731	0.2186	-66.56
8A6	10.764	504.40	1619.18	0.0081	0.2457	0.0330	2.426	0.919	0.1077	0.1799	-40.10
8A6	12.429	504.40	1619.18	0.0017	0.0571	0.0294	3.735	0.868	0.1018	0.1564	-34.90
8A6	13.896	504.40	1619.18	0.0030	0.1080	0.0274	5.220	0.818	0.1006	0.1404	-28.37
8A6	15.222	504.40	1619.18	0.0024	0.2037	0.0118	6.862	0.754	0.0470	0.1284	-63.41
8A6	16.442	504.40	1619.18	0.0052	0.3920	0.0134	8.647	0.681	0.0589	0.1191	-50.60
8A6	17.577	504.40	1619.18	0.0057	0.6078	0.0094	10.564	0.610	0.0462	0.1116	-58.62
8A6	18.644	504.40	1619.18	0.0022	0.4964	0.0045	12.606	0.553	0.0242	0.1053	-77.03
8A6	19.652	504.40	1619.18	0.0102	1.8353	0.0056	14.764	0.501	0.0333	0.1000	-66.70

TABLE A8-8. PULSATILE FLOW RESULTS FOR RUN #10, ELECTRODE A6.

ELECTRODE	DIMENSIONLESS FREQUENCY	REYNOLDS NUMBER	SCHMIDT NUMBER	MASS TRANSFER RATIO	PRESSURE RATIO	AMP	XAXIS	CORRECTION FACTOR	ASP	UCHIDA	PER CENT ERROR
10A6	7.097	527.19	1474.68	0.0422	0.8357	0.0505	0.635	1.000	0.1516	0.2688	-43.59
10A6	10.037	527.19	1474.68	0.0031	0.1131	0.0271	1.796	0.949	0.0856	0.1924	-55.53
10A6	12.292	527.19	1474.68	0.0095	0.4258	0.0223	3.299	0.883	0.0757	0.1581	-52.10
10A6	14.194	527.19	1474.68	0.0014	0.0981	0.0141	5.079	0.822	0.0514	0.1375	-62.64
10A6	15.870	527.19	1474.68	0.0024	0.3010	0.0078	7.099	0.745	0.0315	0.1233	-74.48
10A6	17.384	527.19	1474.68	0.0049	0.7368	0.0067	9.331	0.653	0.0307	0.1128	-72.82
10A6	18.777	527.19	1474.68	0.0091	1.4771	0.0061	11.759	0.576	0.0319	0.1046	-69.45
10A6	20.074	527.19	1474.68	0.0100	2.5137	0.0040	14.367	0.510	0.0235	0.0979	-75.98
10A6	21.291	527.19	1474.68	0.0032	0.9456	0.0034	17.143	0.452	0.0225	0.0926	-75.74
10A6	22.443	527.19	1474.68	0.0120	5.5234	0.0022	20.078	0.406	0.0160	0.0878	-81.73

TABLE A8-9. PULSATILE FLOW RESULTS FOR RUN #8, ELECTRODE B2.

ELECTRODE	DIMENSIONLESS FREQUENCY	REYNOLDS NUMBER	SCHMIDT NUMBER	MASS TRANSFER RATIO	PRESSURE RATIO	AMP	XAXIS	CORRECTION FACTOR	ASP	UCHIDA	PER CENT ERROR
B2	6.221	505.35	1611.97	0.0674	0.6319	0.1067	0.601	1.000	0.3202	0.3043	5.23
B2	8.798	505.35	1611.97	0.0032	0.1074	0.0302	1.700	0.954	0.0950	0.2184	-56.49
B2	10.775	505.35	1611.97	0.0106	0.2507	0.0421	3.123	0.890	0.1420	0.1797	-20.99
B2	12.442	505.35	1611.97	0.0012	0.0474	0.0250	4.808	0.831	0.0903	0.1563	-42.22
B2	13.911	505.35	1611.97	0.0027	0.0921	0.0296	6.720	0.759	0.1171	0.1402	-16.48
B2	15.238	505.35	1611.97	0.0029	0.1963	0.0149	8.834	0.673	0.0666	0.1283	-48.11
B2	16.459	505.35	1611.97	0.0055	0.3753	0.0148	11.132	0.593	0.0747	0.1190	-37.22
B2	17.596	505.35	1611.97	0.0060	0.5916	0.0101	13.600	0.528	0.0575	0.1115	-48.44
B2	18.663	505.35	1611.97	0.0035	0.5166	0.0067	16.229	0.469	0.0429	0.1052	-59.21
B2	19.673	505.35	1611.97	0.0130	1.8719	0.0069	19.007	0.422	0.0494	0.0999	-50.55

TABLE A8-10. PULSATILE FLOW RESULTS FOR RUN #9, ELECTRODE B2.

ELECTRODE	DIMENSIONLESS FREQUENCY	REYNOLDS NUMBER	SCHMIDT NUMBER	MASS TRANSFER RATIO	PRESSURE RATIO	AMP	XAXIS	CORRECTION FACTOR	ASP	UCHIDA	PER CENT ERROR
eB2	6.493	514.56	1551.49	0.0792	0.9311	0.0850	0.658	1.000	0.2551	0.2922	-12.69
eB2	9.182	514.56	1551.49	0.0035	0.0697	0.0509	1.862	0.945	0.1617	0.2096	-22.88
eB2	11.246	514.56	1551.49	0.0131	0.2851	0.0458	3.421	0.879	0.1565	0.1724	-9.22
eB2	12.985	514.56	1551.49	0.0028	0.1420	0.0200	5.267	0.817	0.0735	0.1499	-50.99
eB2	14.518	514.56	1551.49	0.0021	0.1262	0.0165	7.360	0.736	0.0671	0.1346	-50.15
eB2	15.904	514.56	1551.49	0.0027	0.1699	0.0160	9.675	0.640	0.0751	0.1230	-38.98
eB2	17.178	514.56	1551.49	0.0068	0.5805	0.0118	12.192	0.564	0.0627	0.1141	-45.04
eB2	18.364	514.56	1551.49	0.0060	0.7190	0.0083	14.896	0.498	0.0500	0.1069	-53.21
eB2	19.478	514.56	1551.49	0.0025	0.4623	0.0054	17.775	0.441	0.0368	0.1009	-63.51
eB2	20.531	514.56	1551.49	0.0154	3.0253	0.0051	20.818	0.396	0.0386	0.0959	-59.75

TABLE A8-11. PULSATILE FLOW RESULTS FOR RUN #10, ELECTRODE B2.

ELECTRODE	DIMENSIONLESS FREQUENCY	REYNOLDS NUMBER	SCHMIDT NUMBER	MASS TRANSFER RATIO	PRESSURE RATIO	AMP	XAXIS	CORRECTION FACTOR	ASP	UCHIDA	PER CENT ERROR
10B2	7.097	527.19	1474.68	0.0585	0.8711	0.0672	0.818	1.000	0.2015	0.2688	-25.05
10B2	10.037	527.19	1474.68	0.0052	0.1025	0.0506	2.314	0.923	0.1645	0.1924	-14.49
10B2	12.292	527.19	1474.68	0.0125	0.4063	0.0309	4.251	0.850	0.1089	0.1581	-31.11
10B2	14.194	527.19	1474.68	0.0014	0.1116	0.0125	6.546	0.765	0.0489	0.1375	-64.41
10B2	15.870	527.19	1474.68	0.0052	0.3018	0.0172	9.148	0.660	0.0780	0.1233	-36.70
10B2	17.384	527.19	1474.68	0.0052	0.7137	0.0073	12.025	0.568	0.0388	0.1128	-65.64
10B2	18.777	527.19	1474.68	0.0117	1.5360	0.0076	15.153	0.492	0.0466	0.1046	-55.45
10B2	20.074	527.19	1474.68	0.0129	2.6307	0.0049	18.514	0.429	0.0343	0.0979	-64.95
10B2	21.291	527.19	1474.68	0.0036	0.8844	0.0041	22.091	0.381	0.0321	0.0926	-65.27
10B2	22.443	527.19	1474.68	0.0155	5.6517	0.0027	25.874	0.344	0.0239	0.0878	-72.83

TABLE A8-12. PULSATILE FLOW RESULTS FOR RUN #8, ELECTRODE B4.

ELECTRODE	DIMENSIONLESS FREQUENCY	REYNOLDS NUMBER	SCHMIDT NUMBER	MASS TRANSFER RATIO	PRESSURE RATIO	AMP	XAXIS	CORRECTION FACTOR	ASP	UCHIDA	PER CENT ERROR
ØB4	6.221	505.35	1611.97	0.0638	0.6422	0.0994	0.601	1.000	0.2983	0.3043	-1.98
ØB4	8.798	505.35	1611.97	0.0040	0.1142	0.0346	1.700	0.954	0.1088	0.2184	-50.19
ØB4	10.775	505.35	1611.97	0.0106	0.2602	0.0408	3.123	0.890	0.1377	0.1797	-23.38
ØB4	12.442	505.35	1611.97	0.0015	0.0458	0.0328	4.808	0.831	0.1185	0.1563	-24.16
ØB4	13.911	505.35	1611.97	0.0030	0.0875	0.0343	6.720	0.759	0.1356	0.1402	-3.28
ØB4	15.238	505.35	1611.97	0.0025	0.2180	0.0113	8.834	0.673	0.0504	0.1283	-60.72
ØB4	16.459	505.35	1611.97	0.0049	0.3500	0.0139	11.132	0.593	0.0701	0.1190	-41.08
ØB4	17.596	505.35	1611.97	0.0067	0.6052	0.0111	13.600	0.528	0.0628	0.1115	-43.67
ØB4	18.663	505.35	1611.97	0.0036	0.5011	0.0073	16.229	0.469	0.0464	0.1052	-55.94
ØB4	19.673	505.35	1611.97	0.0123	1.8661	0.0066	19.007	0.422	0.0469	0.0999	-53.09

TABLE A8-13. PULSATILE FLOW RESULTS FOR RUN #9, ELECTRODE B4.

ELECTRODE	DIMENSIONLESS FREQUENCY	REYNOLDS NUMBER	SCHMIDT NUMBER	MASS TRANSFER RATIO	PRESSURE RATIO	AMP	XAXIS	CORRECTION FACTOR	ASP	UCHIDA	PER CENT ERROR
gB4	6.501	516.04	1542.96	0.0767	0.9800	0.0783	0.657	1.000	0.2349	0.2919	-19.53
gB4	9.194	516.04	1542.96	0.0038	0.0050	0.7555	1.859	0.945	2.3972	0.2093	045.13
gB4	11.260	516.04	1542.96	0.0130	0.2825	0.0462	3.415	0.879	0.1576	0.1722	-8.44
gB4	13.002	516.04	1542.96	0.0027	0.1917	0.0143	5.258	0.817	0.0526	0.1497	-64.84
gB4	14.537	516.04	1542.96	0.0030	0.2167	0.0140	7.348	0.737	0.0572	0.1344	-57.46
gB4	15.925	516.04	1542.96	0.0023	0.1115	0.0206	9.659	0.641	0.0964	0.1229	-21.53
gB4	17.200	516.04	1542.96	0.0069	0.6722	0.0103	12.172	0.564	0.0550	0.1140	-51.78
gB4	18.388	516.04	1542.96	0.0067	0.8229	0.0081	14.871	0.498	0.0488	0.1068	-54.26
gB4	19.503	516.04	1542.96	0.0035	0.6320	0.0055	17.745	0.442	0.0373	0.1008	-63.00
gB4	20.558	516.04	1542.96	0.0144	3.2546	0.0044	20.783	0.397	0.0335	0.0958	-65.01

TABLE A8-14. PULSATILE FLOW RESULTS FOR RUN #10, ELECTRODE B4.

ELECTRODE	DIMENSIONLESS FREQUENCY	REYNOLDS NUMBER	SCHMIDT NUMBER	MASS TRANSFER RATIO	PRESSURE RATIO	AMP	XAXIS	CORRECTION FACTOR	ASP	UCHIDA	PER CENT ERROR
10B4	7.107	528.75	1466.22	0.0556	0.9029	0.0616	0.817	1.000	0.1848	0.2684	-31.17
10B4	10.050	528.75	1466.22	0.0037	0.1298	0.0285	2.310	0.924	0.0926	0.1922	-51.79
10B4	12.309	528.75	1466.22	0.0117	0.4351	0.0268	4.244	0.850	0.0946	0.1579	-40.10
10B4	14.213	528.75	1466.22	0.0013	0.1325	0.0096	6.534	0.766	0.0375	0.1374	-72.71
10B4	15.891	528.75	1466.22	0.0045	0.3002	0.0150	9.132	0.661	0.0679	0.1231	-44.88
10B4	17.408	528.75	1466.22	0.0058	0.7099	0.0081	12.004	0.569	0.0428	0.1127	-62.02
10B4	18.803	528.75	1466.22	0.0101	1.6048	0.0063	15.127	0.493	0.0383	0.1044	-63.33
10B4	20.101	528.75	1466.22	0.0113	2.6478	0.0043	18.481	0.430	0.0298	0.0978	-69.52
10B4	21.320	528.75	1466.22	0.0025	0.8774	0.0028	22.053	0.381	0.0221	0.0924	-76.11
10B4	22.473	528.75	1466.22	0.0144	5.8997	0.0024	25.829	0.344	0.0212	0.0877	-75.78

TABLE A8-15. PULSATILE FLOW RESULTS FOR RUN #9, ELECTRODE B6.

ELECTRODE	DIMENSIONLESS FREQUENCY	REYNOLDS NUMBER	SCHMIDT NUMBER	MASS TRANSFER RATIO	PRESSURE RATIO	AMP	XAXIS	CORRECTION FACTOR	ASP	UCHIDA	PER CENT ERROR
9B6	6.501	516.04	1542.96	0.0762	0.9150	0.0833	0.657	1.000	0.2500	0.2919	-14.36
9B6	9.194	516.04	1542.96	0.0034	0.0214	0.1579	1.859	0.945	0.5009	0.2093	139.27
9B6	11.260	516.04	1542.96	0.0126	0.3109	0.0405	3.415	0.879	0.1383	0.1722	-19.67
9B6	13.002	516.04	1542.96	0.0029	0.1233	0.0232	5.258	0.817	0.0853	0.1497	-43.04
9B6	14.537	516.04	1542.96	0.0025	0.1652	0.0150	7.348	0.737	0.0609	0.1344	-54.70
9B6	15.925	516.04	1542.96	0.0026	0.2008	0.0129	9.659	0.641	0.0602	0.1229	-50.99
9B6	17.200	516.04	1542.96	0.0064	0.6401	0.0101	12.172	0.564	0.0535	0.1140	-53.02
9B6	18.388	516.04	1542.96	0.0061	0.8772	0.0070	14.871	0.498	0.0421	0.1068	-60.54
9B6	19.503	516.04	1542.96	0.0031	0.5892	0.0052	17.745	0.442	0.0353	0.1008	-64.95
9B6	20.558	516.04	1542.96	0.0146	3.1182	0.0047	20.783	0.397	0.0354	0.0958	-63.01

TABLE A8-16. PULSATILE FLOW RESULTS FOR RUN #10, ELECTRODE B6.

ELECTRODE	DIMENSIONLESS FREQUENCY	REYNOLDS NUMBER	SCHMIDT NUMBER	MASS TRANSFER RATIO	PRESSURE RATIO	AMP	XAXIS	CORRECTION FACTOR	ASP	UCHIDA	PER CENT ERROR
10B6	7.177	528.75	1466.22	0.0531	0.9012	0.0589	0.817	1.000	0.1768	0.2684	-34.15
10B6	10.050	528.75	1466.22	0.0045	0.1226	0.0368	2.310	0.924	0.1196	0.1922	-37.78
10B6	12.309	528.75	1466.22	0.0120	0.4627	0.0260	4.244	0.850	0.0917	0.1579	-41.92
10B6	14.213	528.75	1466.22	0.0027	0.1261	0.0216	6.534	0.766	0.0846	0.1374	-38.40
10B6	15.891	528.75	1466.22	0.0042	0.2536	0.0142	9.132	0.661	0.0646	0.1231	-47.51
10B6	17.478	528.75	1466.22	0.0055	0.7468	0.0074	12.004	0.569	0.0388	0.1127	-65.54
10B6	18.973	528.75	1466.22	0.0108	1.6161	0.0067	15.127	0.493	0.0406	0.1044	-61.09
10B6	20.411	528.75	1466.22	0.0123	2.8193	0.0044	18.481	0.430	0.0305	0.0978	-68.79
10B6	21.820	528.75	1466.22	0.0017	0.7589	0.0022	22.053	0.381	0.0173	0.0924	-81.33
10B6	22.473	528.75	1466.22	0.0141	5.9165	0.0024	25.829	0.344	0.0208	0.0877	-76.31

TABLE A8-17. PULSATILE FLOW RESULTS FOR RUN #8, ELECTRODE C2.

ELECTRODE	DIMENSIONLESS FREQUENCY	REYNOLDS NUMBER	SCHMIDT NUMBER	MASS TRANSFER RATIO	PRESSURE RATIO	AMP	XAXIS	CORRECTION FACTOR	ASP	UCHIDA	PER CENT ERROR
RC2	6.253	509.67	1577.25	0.0780	0.9040	0.0863	0.759	1.000	0.2588	0.3028	-14.54
RC2	8.844	509.67	1577.25	0.0024	0.2493	0.0095	2.146	0.931	0.0305	0.2173	-85.95
RC2	10.831	509.67	1577.25	0.0116	0.2240	0.0519	3.942	0.861	0.1808	0.1788	1.13
RC2	12.507	509.67	1577.25	0.0010	0.1015	0.0103	6.070	0.785	0.0395	0.1555	-74.60
RC2	13.983	509.67	1577.25	0.0020	0.0756	0.0264	8.483	0.688	0.1153	0.1395	-17.33
RC2	15.318	509.67	1577.25	0.0032	0.2773	0.0114	11.151	0.593	0.0577	0.1277	-54.79
RC2	16.545	509.67	1577.25	0.0052	0.4899	0.0106	14.052	0.517	0.0617	0.1184	-47.87
RC2	17.687	509.67	1577.25	0.0060	0.8172	0.0073	17.168	0.451	0.0485	0.1109	-56.31
RC2	18.760	509.67	1577.25	0.0037	0.6846	0.0054	20.486	0.401	0.0406	0.1047	-61.24
RC2	19.775	509.67	1577.25	0.0122	2.6573	0.0046	23.993	0.361	0.0382	0.0994	-61.52

TABLE A8-18. PULSATILE FLOW RESULTS FOR RUN #9, ELECTRODE C2.

ELECTRODE	DIMENSIONLESS FREQUENCY	REYNOLDS NUMBER	SCHMIDT NUMBER	MASS TRANSFER RATIO	PRESSURE RATIO	AMP	XAXIS	CORRECTION FACTOR	ASP	UCHIDA	PER CENT ERROR
eC2	6.501	516.04	1542.96	0.0856	1.0338	0.0828	0.833	1.000	0.2485	0.2919	-14.86
eC2	9.194	516.04	1542.96	0.0042	0.0777	0.0538	2.356	0.922	0.1752	0.2093	-16.29
eC2	11.260	516.04	1542.96	0.0140	0.3808	0.0367	4.327	0.847	0.1300	0.1722	-24.52
eC2	13.002	516.04	1542.96	0.0026	0.1430	0.0180	6.663	0.761	0.0709	0.1497	-52.63
eC2	14.537	516.04	1542.96	0.0021	0.1488	0.0141	9.311	0.654	0.0648	0.1344	-51.77
eC2	15.925	516.04	1542.96	0.0027	0.2218	0.0120	12.240	0.563	0.0640	0.1229	-47.92
eC2	17.200	516.04	1542.96	0.0061	0.7147	0.0085	15.424	0.486	0.0525	0.1140	-53.97
eC2	18.388	516.04	1542.96	0.0060	0.9706	0.0062	18.845	0.424	0.0438	0.1068	-59.02
eC2	19.503	516.04	1542.96	0.0032	0.7786	0.0040	22.486	0.376	0.0323	0.1008	-67.95
eC2	20.558	516.04	1542.96	0.0140	3.5054	0.0040	26.336	0.341	0.0353	0.0958	-63.17

TABLE A8-19. PULSATILE FLOW RESULTS FOR RUN #10, ELECTRODE C2.

ELECTRODE	DIMENSIONLESS FREQUENCY	REYNOLDS NUMBER	SCHMIDT NUMBER	MASS TRANSFER RATIO	PRESSURE RATIO	AMP	XAXIS	CORRECTION FACTOR	ASP	UCHIDA	PER CENT ERROR
10C2	7.107	528.75	1466.22	0.0610	0.9980	0.0611	1.035	0.999	0.1837	0.2684	-31.58
10C2	10.050	528.75	1466.22	0.0053	0.1420	0.0371	2.927	0.898	0.1239	0.1922	-35.53
10C2	12.309	528.75	1466.22	0.0118	0.4810	0.0244	5.378	0.813	0.0901	0.1579	-42.91
10C2	14.213	528.75	1466.22	0.0016	0.2140	0.0074	8.280	0.697	0.0319	0.1374	-76.79
10C2	15.891	528.75	1466.22	0.0039	0.3213	0.0121	11.572	0.581	0.0628	0.1231	-49.03
10C2	17.408	528.75	1466.22	0.0049	0.7876	0.0063	15.212	0.491	0.0383	0.1127	-65.97
10C2	18.803	528.75	1466.22	0.0100	1.7971	0.0055	19.169	0.419	0.0396	0.1044	-62.06
10C2	20.101	528.75	1466.22	0.0116	3.0817	0.0038	23.420	0.366	0.0307	0.0978	-68.56
10C2	21.320	528.75	1466.22	0.0015	0.7739	0.0020	27.945	0.329	0.0179	0.0924	-80.65

TABLE A8-20. PULSATILE FLOW RESULTS FOR RUN #8, ELECTRODE C4.

ELECTRODE	DIMENSIONLESS FREQUENCY	REYNOLDS NUMBER	SCHMIDT NUMBER	MASS TRANSFER RATIO	PRESSURE RATIO	AMP	XAXIS	CORRECTION FACTOR	ASP	UCHIDA	PER CENT ERROR
RC4	6.262	512.10	1568.64	0.0759	0.9445	0.0804	0.756	1.000	0.2411	0.3024	-20.29
RC4	8.855	512.10	1568.64	0.0021	0.0237	0.0871	2.138	0.931	0.2804	0.2171	29.19
RC4	10.845	512.10	1568.64	0.0107	0.3745	0.0286	3.928	0.861	0.0998	0.1786	-44.13
RC4	12.523	512.10	1568.64	0.0007	0.0920	0.0072	6.048	0.786	0.0276	0.1553	-82.22
RC4	14.001	512.10	1568.64	0.0023	0.1439	0.0161	8.452	0.689	0.0702	0.1393	-49.61
RC4	15.337	512.10	1568.64	0.0025	0.1935	0.0130	11.111	0.594	0.0656	0.1275	-48.59
RC4	16.566	512.10	1568.64	0.0049	0.5166	0.0096	14.001	0.518	0.0553	0.1183	-53.23
RC4	17.710	512.10	1568.64	0.0051	0.7205	0.0071	17.107	0.452	0.0469	0.1108	-57.63
RC4	18.785	512.10	1568.64	0.0032	0.5631	0.0056	20.412	0.402	0.0418	0.1045	-59.99
RC4	19.801	512.10	1568.64	0.0112	2.8906	0.0039	23.907	0.361	0.0321	0.0993	-67.67

TABLE A8-21. PULSATILE FLOW RESULTS FOR RUN #9, ELECTRODE C4.

ELECTRODE	DIMENSIONLESS FREQUENCY	REYNOLDS NUMBER	SCHMIDT NUMBER	MASS TRANSFER RATIO	PRESSURE RATIO	AMP	XAXIS	CORRECTION FACTOR	ASP	UCHIDA	PER CENT ERROR
9C4	6.501	516.04	1542.96	0.0782	0.9844	0.0795	0.833	1.000	0.2384	0.2919	-18.33
9C4	9.194	516.04	1542.96	0.0043	0.0672	0.0644	2.356	0.922	0.2098	0.2093	0.20
9C4	11.260	516.04	1542.96	0.0126	0.3706	0.0341	4.327	0.847	0.1208	0.1722	-29.82
9C4	13.002	516.04	1542.96	0.0021	0.1215	0.0169	6.663	0.761	0.0665	0.1497	-55.56
9C4	14.537	516.04	1542.96	0.0026	0.1485	0.0175	9.311	0.654	0.0804	0.1344	-40.22
9C4	15.925	516.04	1542.96	0.0026	0.2296	0.0112	12.240	0.563	0.0596	0.1229	-51.53
9C4	17.200	516.04	1542.96	0.0055	0.6846	0.0080	15.424	0.486	0.0493	0.1140	-56.71
9C4	18.388	516.04	1542.96	0.0059	0.9161	0.0064	18.845	0.424	0.0452	0.1068	-57.69
9C4	19.503	516.04	1542.96	0.0031	0.7096	0.0043	22.486	0.376	0.0344	0.1008	-65.83
9C4	20.558	516.04	1542.96	0.0123	3.2673	0.0038	26.336	0.341	0.0331	0.0958	-65.47

TABLE A8-22. PULSATILE FLOW RESULTS FOR RUN #10, ELECTRODE C4.

ELECTRODE	DIMENSIONLESS FREQUENCY	REYNOLDS NUMBER	SCHMIDT NUMBER	MASS TRANSFER RATIO	PRESSURE RATIO	AMP	XAXIS	CORRECTION FACTOR	ASP	UCHIDA	PER CENT ERROR
10C4	7.107	528.75	1466.22	0.0550	0.9330	0.0590	1.035	0.999	0.1772	0.2684	-33.99
10C4	10.050	528.75	1466.22	0.0052	0.1341	0.0388	2.927	0.898	0.1296	0.1922	-32.55
10C4	12.309	528.75	1466.22	0.0119	0.4716	0.0251	5.378	0.813	0.0927	0.1579	-41.29
10C4	14.213	528.75	1466.22	0.0024	0.2025	0.0117	8.280	0.697	0.0506	0.1374	-63.17
10C4	15.891	528.75	1466.22	0.0036	0.2963	0.0123	11.572	0.581	0.0635	0.1231	-48.42
10C4	17.408	528.75	1466.22	0.0044	0.7370	0.0060	15.212	0.491	0.0364	0.1127	-67.69
10C4	18.803	528.75	1466.22	0.0090	1.6500	0.0055	19.169	0.419	0.0391	0.1044	-62.53
10C4	20.101	528.75	1466.22	0.0103	2.8874	0.0036	23.420	0.366	0.0291	0.0978	-70.22
10C4	21.320	528.75	1466.22	0.0019	0.8040	0.0023	27.945	0.329	0.0212	0.0924	-77.04

TABLE A8-23. PULSATILE FLOW RESULTS FOR RUN #8, ELECTRODE C6.

ELECTRODE	DIMENSIONLESS FREQUENCY	REYNOLDS NUMBER	SCHMIDT NUMBER	MASS TRANSFER RATIO	PRESSURE RATIO	AMP	XAXIS	CORRECTION FACTOR	ASP	UCHIDA	PER CENT ERROR
#C6	6.242	512.10	1568.64	0.0748	0.8050	0.0929	0.756	1.000	0.2786	0.3024	-7.89
#C6	8.955	512.10	1568.64	0.0029	0.0282	0.1028	2.138	0.931	0.3311	0.2171	52.52
#C6	10.845	512.10	1568.64	0.0115	0.3532	0.0325	3.928	0.861	0.1131	0.1786	-36.66
#C6	12.523	512.10	1568.64	0.0009	0.0800	0.0108	6.048	0.786	0.0413	0.1553	-73.41
#C6	14.001	512.10	1568.64	0.0020	0.0670	0.0301	8.452	0.689	0.1310	0.1393	-5.94
#C6	15.337	512.10	1568.64	0.0022	0.1737	0.0129	11.111	0.594	0.0649	0.1275	-49.10
#C6	16.566	512.10	1568.64	0.0052	0.5615	0.0093	14.001	0.518	0.0541	0.1183	-54.29
#C6	17.710	512.10	1568.64	0.0052	0.6996	0.0075	17.107	0.452	0.0496	0.1108	-55.20
#C6	18.795	512.10	1568.64	0.0026	0.5702	0.0046	20.412	0.402	0.0347	0.1045	-66.81
#C6	19.801	512.10	1568.64	0.0112	2.5674	0.0044	23.907	0.361	0.0362	0.0993	-63.54

TABLE A8-24. PULSATILE FLOW RESULTS FOR RUN #10, ELECTRODE C6.

ELECTRODE	DIMENSIONLESS FREQUENCY	REYNOLDS NUMBER	SCHMIDT NUMBER	MASS TRANSFER RATIO	PRESSURE RATIO	AMP	XAXIS	CORRECTION FACTOR	ASP	UCHIDA	PER CENT ERROR
10C6	7.107	528.75	1466.22	0.0563	0.8706	0.0647	1.035	0.999	0.1943	0.2684	-27.60
10C6	10.050	528.75	1466.22	0.0042	0.1297	0.0322	2.927	0.898	0.1076	0.1922	-44.01
10C6	12.309	528.75	1466.22	0.0126	0.4773	0.0265	5.378	0.813	0.0976	0.1579	-38.16
10C6	14.213	528.75	1466.22	0.0021	0.1491	0.0144	8.280	0.697	0.0619	0.1374	-54.96
10C6	15.891	528.75	1466.22	0.0036	0.2658	0.0135	11.572	0.581	0.0697	0.1231	-43.38
10C6	17.408	528.75	1466.22	0.0049	0.6973	0.0070	15.212	0.491	0.0428	0.1127	-62.04
10C6	18.803	528.75	1466.22	0.0094	1.5484	0.0061	19.169	0.419	0.0435	0.1044	-58.38
10C6	20.101	528.75	1466.22	0.0109	2.8716	0.0038	23.420	0.366	0.0312	0.0978	-68.10
10C6	21.320	528.75	1466.22	0.0024	1.0661	0.0023	27.945	0.329	0.0206	0.0924	-77.73

APPENDIX 9

COMPUTER PROGRAM FOR ANALYSIS OF DIGITIZED PULSATILE FLOW DATA

```
      EXTERNAL FUN
      REAL MSTOR(50)
      INTEGER CYCLE
      DIMENSION A(50),B(50),C(50),PHI(50),PSTOR(50)
      IR1=5
      IW=6
C        FOURIER ANALYSIS AND SYNTHESIS
C        GIVEN TABULATED POINTS, SUBROUTINE FORRF CALCULATES
C        F(X)= A(0) +SUM(A(K)COS(KX) +B(K)SIN(KX)), K=1,...,M
C        THIS PROGRAM CONVERTS TO THE FORM
C        F(X)= A(0) +SUM(C(K)COS(KX +PHI(K))), K=1,...,M
C
C        N= NUMBER OF POINTS FOR FOURIER ANALYSIS SUCH THAT N .GE. 2*M+1
C        M= NUMBER OF HARMONICS DESIRED
C
C          PSTOR(I)= THE RATIO C(I+1)/C(1)  (PRESSURE DATA)
C          MSTOR(I)= THE RATIO C(I+1)/C(1) (MASS TRANSFER DATA)
      READ(IR1,100) N,M
  100 FORMAT (34X,I2,23X,I2)
      READ(IR1,102) CYCLE
  102 FORMAT (I1)
      DO 4 IDATA=1,2
C          IDATA=1 (PRESSURE), IDATA=2 (MASS TRANSFER COEFF.)
      IF (IDATA-1) 10,10,20
   10 WRITE(IW,500)
  500 FORMAT (1H1,14X,'PRESSURE DIFFERENTIAL DATA ANALYSIS')
      GO TO 30
   20 WRITE(IW,600)
  600 FORMAT (1H1,14X,'MASS TRANSFER COEFFICIENT DATA ANALYSIS')
   30 CONTINUE
      WRITE(IW,1000) N
 1000 FORMAT(1X ,14X,'NUMBER OF POINTS PER CYCLE IN THE FOURIER ANALYSIS
     1=',I3)
      WRITE(IW,101) CYCLE
  101 FORMAT (15X,'NUMBER OF CYCLES IN REAL TIME PER CYCLE IN THE FOURIE
     1R ANALYSIS=',I2)
C         NOTE-- THE DIGITIZED CURVE IS READ IN FUNCTION FUN
      CALL FORRF(FUN,N,M,A,B,IER,IDATA)
      IF(IER-1)2,1,1
1     WRITE(IW,200) IER
  200 FORMAT (20X,'*** ERROR ***   IER=',I4)
      CALL EXIT
    2 MI=M+1
      I1=0
      C(1)=A(1)
      WRITE(IW,300)
  300 FORMAT (1H0,14X,'HARMONIC',5X,'AMPLITUDE',3X,'PHASE(DEG)',/)
      WRITE(IW,400) I1,C(1)
  400 FORMAT (18X,I2,5XF12.4,4X,F6.1)
      DO 3 I=2,MI
      I1=I-1
      C(I)=SQRT(A(I)**2 +B(I)**2)
      PHI(I)=ATAN(-B(I)/A(I))
      PHI(I)=PHI(I)*360./(2.0*3.141593)
```

```
      WRITE(IW,400) I1,C(I),PHI(I)
    3 CONTINUE
      DO 40 I=1,M
      IF (IDATA-1) 31,31,35
   31 PSTOR(I)=C(I+1)/C(1)
      GO TO 40
   35 MSTOR(I)= C(I+1)/C(1)
   40 CONTINUE
    4 CONTINUE
C
C           WE NOW CORRECT THE MASS TRANSFER DATA USING FORTUNA'S
C           CORRECTION FACTOR AND COMPARE THE RESULT WITH UCHIDA'S THEORY
C
C           NOTE THAT PRIOR TO THIS POINT, NPT AND Y(I) HAVE BEEN READ
C           IN IN 'FUN'
C                READ IN THE PHYSICAL DATA FOR THIS RUN....
C           RNAME= RUN NUMBER--ELECTRODE NUMBER
C           DELEC= DIAMETER OF ELECTRODE (CM)
C           TEMP= TEMPERATURE (DEGC)
C           FREQ= FREQUENCY (RADIANS/SEC)
C           RE= REYNOLDS NUMBER
C           RMU= VISCOSITY (CENTIPOISE)
C           RHO= DENSITY (GRAMS/CC)
C           RNU= KINEMATIC VISCOSITY (CM**2/SEC)
C           DIFF= DIFFUSION COEFFICIENT (CM**2/SEC)
C           SC= SCHMIDT NUMBER
C           GZ= GRAETZ NUMBER
C           OMEGA= DIMENSIONLESS FUNDAMENTAL FREQUENCY
C
      READ(IR1,700) RNAME,DELEC,TEMP,FREQ,RE
  700 FORMAT (A4,6X,F7.4,3X,F5.1,5X,F6.3,4X,F8.2)
      WRITE(IW,740)
  740  FORMAT(1H1)
      WRITE(IW,750)
  750 FORMAT(//,T48,'MASS',/,T13,'DIMENSIONLESS',T28,'REYNOLDS',T37,'SCH
     2MIDT ',T47,'TRANSFER',T57,'PRESSURE',T81,'CORRECTION',T110,'PER CE
     3NT',/,T2,'ELECTRODE',T15,'FREQUENCY',T29,'NUMBER',T38,'NUMBER',T48
     4,'RATIO',T58,'RATIO',T67,'AMP',T74,'XAXIS',T83,'FACTOR',T93,'ASP',
     5T101,'UCHIDA',T111,'ERROR')
      DTUBE=1.631
      RNU= RMU(TEMP)/(100.*RHO(TEMP))
      DIFF= (TEMP+273.15)/RMU(TEMP)*2.5E-08
      SC= RNU/DIFF
      GZ= .82*DELEC/(DTUBE*RE*SC)
      OMEGA= DTUBE/2.*SQRT(FREQ/RNU)
      MBUG=M/CYCLE
      DO 50 J=1,MBUG
      I=J*CYCLE
      REALI=J
      DFREQ= SQRT(REALI)*OMEGA
      XAXIS= GZ*SC**(1.5)*DFREQ**3
      AFACT= FORTU(XAXIS)
      IF (AFACT) 50,50,45
   45 CONTINUE
```

```
      AMP= MSTOR(I)/PSTOR(I)
      ASP= AMP*3./AFACT
      THEOR= UCHID(DFREQ)
      ERR=(ASP-THEOR)/THEOR*100.
      WRITE(IW,800) RNAME,DFREQ,RE,SC,MSTOR(I),PSTOR(I),AMP,XAXIS,AFACT,
     1 ASP,THEOR,ERR
  800 FORMAT(//T4,A4,T16,F6.3,T28,F7.2,T37,F7.2,T48,F6.4,T57,F6.4,T65,F6
     2.4,T73,F6.3,T83,F5.3,T92,F6.4,T101,F6.4,T111,F6.2)
   50 CONTINUE
      WRITE(IW,183)
  183 FORMAT(1H1)
      CALL EXIT
      END
      SUBROUTINE FORRF(FUN,N,M,A,B,IER,IDATA)
      DIMENSION A(1),B(1)
C        THIS IS A SLIGHT REVISION OF THE IBM-SSP SUBROUTINE FORIF
C        CHECK FOR PARAMETER ERRORS
      IER=0
   20 IF(M) 30,40,40
   30 IER=2
      RETURN
   40 IF(M-N) 60,60,50
   50 IER=1
      RETURN
C        COMPUTE AND PRESET CONSTANTS
   60 AN=N
      COEF=2.0/(2.0*AN+1.0)
      CONST=3.141593*COEF
      S1=SIN(CONST)
      C1=COS(CONST)
      C=1.0
      S=0.0
      J=1
      FUNZ=FUN(0.0,-1,IDATA)
   70 U2=0.0
      U1=0.0
      AI=2*N
C        FORM FOURIER COEFFICIENTS RECURSIVELY
   75 X=AI*CONST
      F=FUN(X,1,IDATA)
      U0=F+2.0*C*U1-U2
      U2=U1
      U1=U0
      AI=AI-1.0
      IF(AI) 80,80,75
   80 A(J)=COEF*(FUNZ+C*U1-U2)
      P(J)=COEF*S*U1
      IF(J-(M+1)) 90,100,100
   90 Q=C1*C-S1*S
      S=C1*S+S1*C
      C=Q
      J=J+1
      GO TO 70
  100 A(1)=A(1)*0.5
```

```
      RETURN
      END
      FUNCTION FUN(X,N,IDATA)
      DIMENSION Y(1000)
      IR1=8
      IR2=9
C        READ Y(I), AND SET PARAMETERS
      IF(N) 10,10,20
C        READ NPT= POINTS PER CYCLE IN DIGITIZED CURVE
   10 IF(IDATA-1) 11,11,12
   11 READ(IR1,100) NPT
  100 FORMAT (55X,I4)
   12 CONTINUE
      XNPT=NPT
      PI=3.141593
      IF(IDATA-1) 110,110,120
  110 READ(IR2,200) (Y(I),I=1,NPT)
  200 FORMAT (1X,F10.5)
      GO TO 130
  120 READ(IR2,300) (Y(I),I=1,NPT)
  300 FORMAT (11X,F10.5)
  130 CONTINUE
      FUN=Y(1)
      RETURN
C        LOCATE X AND INTERPOLATE
   20 XMARK=X*XNPT/(2.0*PI)
      M=XMARK
      XM=M
      FUN=Y(M)+(XMARK-XM)*(Y(M+1)-Y(M))
      RETURN
      END
      FUNCTION RHO(T)
C        RHO=DENSITY IN GM/CC
      DIMENSION A(3)
      A(1)=1.0783
      A(2)=1.0804
      A(3)=1.0814
      IW=5
      IF(T-27.0) 1,3,2
    1 WRITE(IW,100) T
  100 FORMAT(10X,'**** TEMP OUTSIDE ALLOWABLE (27-33 DEG), T= ',F8.3)
      CALL EXIT
    2 IF (T-33.0)3,3,1
    3 I=0
      DO 6 J=1,7,3
      I=I+1
      XJ=J
      XT=T-(26.0+XJ)
      IF (XT) 5,4,6
    4 RHO=A(I)
      RETURN
    5 RHO=  (A(I)-A(I-1))*(T-23.0-XJ)/3. +A(I-1)
      RETURN
    6 CONTINUE
```

```
      CALL EXIT
      END
      FUNCTION FORTU(XAXIS)
      DIMENSION A(21),B(21)
C          FORTU= FORTUNA'S CORRECTION FACTOR, AFACT
      IW=5
      A(1)=1.00
      A(2)=1.05
      A(3)=1.10
      A(4)=1.20
      A(5)=1.30
      A(6)=1.50
      A(7)=2.7
      A(8)=4.0
      A(9)=4.9
      A(10)=5.6
      A(11)=6.4
      A(12)=7.4
      A(13)=8.0
      A(14)=10.0
      A(15)=13.0
      A(16)=17.0
      A(17)=20.0
      A(18)=23.0
      A(19)=26.0
      A(20)=28.0
      A(21)=32.312
      B(1)=1.00
      B(2)=.998
      B(3)=0.995
      B(4)=0.989
      B(5)=0.980
      B(6)=0.967
      B(7)=0.908
      B(8)=0.859
      B(9)=0.828
      B(10)=0.807
      B(11)=0.771
      B(12)=0.735
      B(13)=0.709
      B(14)=0.628
      B(15)=0.543
      B(16)=0.454
      B(17)=0.407
      B(18)=0.370
      B(19)=0.343
      B(20)=0.329
      B(21)=0.304
      IF (XAXIS-32.312)2,4,1
 1    FORTU=-1.0
      RETURN
 2    IF (XAXIS-1.0) 3,3,4
 3    FORTU=1.0
      RETURN
```

```
4       DO 7 I=1,21
        IF(XAXIS-A(I)) 6,5,7
5       FORTU=B(I)
        RETURN
 6      FORTU= (B(I)-B(I-1))*(ALOG(XAXIS)-ALOG(A(I-1)))/(ALOG(A(I))-ALOG(
       1 A(I-1))) +B(I-1)
        RETURN
7       CONTINUE
        CALL EXIT
        END
        FUNCTION RMU(T)
C          RMU=VISCOSITY IN CENTIPOISE
        DIMENSION A (7)
        IW=5
        A(1)=1.1924
        A(2)=1.1699
        A(3)=1.1466
        A(4)=1.1178
        A(5)=1.0882
        A(6)=1.0666
        A(7)=1.0433
        IF(T-27.0) 1,3,2
 1      WRITE(IW,100) T
 100    FORMAT(10X,'**** TEMP OUTSIDE ALLOWABLE (27-33 DEG), T= ',F8.3)
        CALL EXIT
 2      IF (T-33.0) 3,3,1
 3      DO 6 I=1,7
        XI=I
        XT=T-(26.0+XI)
        IF (XT) 5,4,6
 4      RMU=A(I)
        RETURN
 5      RMU=(A(I)-A(I-1))*(T-25.0-XI) + A(I-1)
        RETURN
 6      CONTINUE
        CALL EXIT
        END
        FUNCTION UCHID(X)
        P(X)=TWOPI*X
        BER(X)= 1.0-64.0*(X/8.0)**4 + 113.77778*(X/8.0)**8-32.36346*(X/8.0
       2)**12 + 2.64191*(X/8.0)**16-0.083496*(X/8.0)**20
        BEI(X)= 16.0*(X/8.0)**2-113.77778*(X/8.0)**6+72.81778*(X/8.0)**10-
       210.56766*(X/8.0)**14+0.52186*(X/8.0)**16-0.01104*(X/8.0)**22
        BERPR(X)= X*(-4.0*(X/8.0)**2+14.22222*(X/8.0)**6-6.06815*(X/8.0)**
       210+0.66048*(X/8.0)**14)
        BEIPR(X)= X*(0.5-10.66667*(X/8.0)**4+11.37778*(X/8.0)**8
       2-2.31168*(X/8.0)**12+0.14677*(X/8.0)**16)
        ABER(X)=(EXP(X/SQRT(2.0)))*(P(X)**(-0.5))*COS(X/SQRT(2.0)-DEL)
        ABEI(X)=(EXP(X/SQRT(2.0)))*(P(X)**(-0.5))*SIN(X/SQRT(2.0)-DEL)
        ABERP(X)=EXP(X/SQRT(2.0))*((P(X)**(-0.5))*(-SIN(X/SQRT(2.0)-DEL)*
       21.0/SQRT(2.0))+(-PI)*(P(X)**(-1.5))*COS(X/SQRT(2.0)-DEL)+
       31.0/SQRT(2.0)*(P(X)**(-0.5))*COS(X/SQRT(2.0)-DEL))
        ABEIP(X)=EXP(X/SQRT(2.0))*((P(X)**(-0.5))*( COS(X/SQRT(2.0)-DEL)*
       21.0/SQRT(2.0))+(-PI)*(P(X)**(-1.5))*SIN(X/SQRT(2.0)-DEL)+
```

```
     31.0/SQRT(2.0)*(P(X)**(-0.5))*SIN(X/SQRT(2.0)-DEL))
      BERSQ(X)=ABER(X)**2+ABEI(X)**2
      DEL=22.5/57.296
      PI=3.14159
      TWOPI=2.0*PI
      IF(X-8.0)12,12,11
11    C=(ABER(X)*ABEIP(X)-ABEI(X)*ABERP(X))/BERSQ(X)
      D=(ABER(X)*ABERP(X)+ABEI(X)*ABEIP(X))/BERSQ(X)
13    A=(2.0*C/X)**2
      B=(2.0*D/X)**2
      UCHID=SQRT(A+B)
      RETURN
12    C=(BER(X)*BEIPR(X)-BEI(X)*BERPR(X))/(BER(X)**2+BEI(X)**2)
      D=(BER(X)*BERPR(X)+BEI(X)*BEIPR(X))/(BER(X)**2+BEI(X)**2)
      A=(2.0*C/X)**2
      B=(2.0*D/X)**2
      UCHID=SQRT(A+B)
      RETURN
      END
```

Nomenclature

a	Constant of integration (equation 71)
a_n	Fourier coefficient of cosine
A	Defined in equation 28
A_e	Surface area of electrode
$\hat{A}$	Correction factor defined in equation 129
A_{mp}	Mass transfer to pressure amplitude ratio
A_{sp}	Shear rate to pressure amplitude ratio
B	Defined in equation 28
b_n	Fourier coefficient of sin
C	Concentration of ferricyanide ion (moles/liter)
$\overline{C}$	Time average concentration
c'	Fluctuating concentration
c_F	Amplitude of the fluctuating concentration
$\hat{c}$	Defined by equation 111
$\hat{c}_o$	Quasi-steady value of $\hat{c}$
C_B	Bulk concentration
C_W	Concentration at the wall
d	Electrode diameter (cm)
D	Pipe diameter; also defined in equation (A2-8)
$\mathcal{D}$	Diffusion coefficient (cm^2/sec)
E	Defined in equation (A2-8)
ΔE	Potential difference (volts)
F	Faroday's constant, 96,500 coulombs/eq. wt.

f_ϕ	Amplitude of first order fluctuation of ϕ Defined in equation 48
f_ϕ^0	First perturbation term of f_ϕ
f_ϕ^1	Second perturbation term of f_ϕ
f	Friction factor, equation (A4-1)
Gz	Graetz Number, equation 43
I	Instantaneous current
I_s	Steady flow current
$\overline{I}$	Time averaged cell current
I'	Fluctuating cell current = $I_F e^{i\omega t}$
I_F	Amplitude of fluctuating current
$J_n(x)$	Bessel function of the n^{th} order
K	Instantaneous mass transfer coefficient (cm/sec)
K_s	Steady state mass transfer coefficient
$<K_s>$	Spatial average of K_s
$\overline{K}$	Time averaged mass transfer coefficient
$<\overline{K}>$	Spatial average of $\overline{K}$
K'	Fluctuating mass transfer coefficient = $K_{F(n)} e^{in\omega t}$
$K_{F(n)}$	Amplitude of the n^{th} harmonic of the fluctuating mass transfer coefficient = $\lambda_{p(n)} K_{f(n)}$
$K_{f(n)}$	First order perturbation term for the n^{th} harmonic of the fluctuating mass transfer coefficient
$<K_f>$	Spatial average of K_f
K_{F_o}	Amplitude of quasi-steady fluctuating mass transfer coefficient
L	Equivalent electrode length, = .82 d
M{}	Modulus
M_1	Modulus of J_1

M_o	Modulus of J_o
N	Mass flux of ferricyanide ion
N_L	Defined by equation 105
Nu_F	Fluctuating Nusselt Number
n	Number of integral multiples of fundamental frequency
n_e	Number of electrons involved in electrolytic reaction
p	Pressure
P_s	Pressure gradient for steady flow, equation 14
Q	Non-defined quantity; also flow rate (cc/min)
Re	Reynold's Number
R	Pipe radius
R_{mp}	Mass transfer to pressure ratio (complex)
r	Radial position
Sc	Schmidt Number
S	Instantaneous shear rate
s'	Fluctuating shear rate
$\overline{S}$	Time averaged shear rate
$s_{F(n)}$	Amplitude of the fluctuating shear rate for n^{th} harmonic
T	Period of pulsation
u	Instantaneous axial velocity
u_s	Steady flow velocity
U_o	Area averaged mean velocity for steady flow
$\overline{U}$	Time averaged bulk velocity, = U_o
u'	Fluctuating component of velocity

u_n	Amplitude of fluctuating velocity, defined in equation 19
v	Velocity normal to wall, = 0
W	Refers to pipe wall
w_n	Defined by equation (A1-10)
W_K	Spectral density function for mass transfer coefficient
W_S	Spectral density function for shear rate
x	Axial position, position on electrode surface
y	Transformed radial position, = R - r
z	Correlation constant for equation 93
z_1, z_2, z_3	Expansion terms of z
α	$\Omega Sc^{1/2}$, equation 50
β	Defined in equation (A1-7)
$\Gamma( )$	Gamma Function
γ, or γ_n	Defined in equation 31
δ_n	n^{th} harmonic phase lag between shear rate and mass transfer coefficient
δ_T	Defined in equation (A4-6)
δ_C	Thickness of concentration boundary layer
δ_H	Hydrodynamic boundary layer
ζ	Defined by equation 40
η	Transformed y variable defined by equation 52; Also equal to $\frac{r}{R}$ in Appendix 1
Θ_n	Phase with respect to fundamental frequency of n^{th} harmonic of pressure gradient or mass transfer coefficient; also dimensionless variable of Appendix 3

Λ	Defined in equation 115
$\lambda_{p(n)}$	n^{th} harmonic pressure ratio amplitude
λ_s	Ratio of the amplitude of the oscillatory shear rate to the steady flow shear rate
λ_m	Ratio of the amplitude of the oscillatory mass transfer coefficient to the steady flow value
μ	Viscosity (g-cm/sec)
ν	Kinematic viscosity (cm^2/sec)
ξ	Transformed x variable defined in equation 51
ρ	Density (g/cc)
σ_T	Defined in equation (A4-6)
τ	Defined in equation 76; also instantaneous shear stress in Appendix 4
τ_s	Steady flow wall shear stress
ϕ	Dimensionless concentration defined by equation 34
ϕ_o	Steady state dimensionless concentration Solution given by equation 42
ϕ_1	First order fluctuation of ϕ
ψ	Defined in equation 56
ω	Fundamental frequency of pulsation (radians/sec)
Ω	Dimensionless frequency parameter, $= R\sqrt{\frac{n\omega}{\nu}}$

Bibliography

Abromowitz, M., and I. A. Stegun, Handbook of Mathematical Functions, 2nd Printing, Dover Pub. (1965).

Adams, C. W. M., "Arteriosclerosis in man, other mammals, and birds". Biological Revue 39: 372, (1964).

Anitschkow, N., in Arteriosclerosis (E. V. Cowdry, ed.), p. 271, New York, MacMillan (1933).

Atabek, H. B., and C. C. Chang, "Oscillatory Flow Near the Entry of a Circular Tube", Z.A.M.P. 12, p. 185, (1961).

Atabek, H. B., C. C. Chang, and L. M. Fingerson, "Measurement of Laminar Oscillatory Flow in the Inlet Length of a Circular Tube", Phys. Med. Biol. 9, 2, 219-227, (1964).

Baumgartner, H. R., and A. Studer, Path. Microbiol. 26: 129, (1963).

Bjorkerud, S., J. Atheroscler. Res. 9: 209, (1969).

Bjorkerud, S., Virchows Arch. Abt. A Path. Anat. 347: 197, (1969).

Bjorkerud, S., and G. Bondjers, Atherosclerosis 15: 285 (1972).

Bondjers, G., "Endothelial Integrity and Cholesterol Transfer in the Aorta of the Rabbit", Departments of Histology and Medicine, University of Goteborg, Goteborg, Sweden. (1972).

Bratzler, R. L., C. K. Colton, K. A. Smith, and R. S. Lees, paper No. 81a, AIChE Meeting, New York, Nov. 1972.

Carew, T. E., "Mechano-Chemical Response of Canine Aortic Endothelium to Elevated Shear Stress in Vitro", PhD Dissertation, The Catholic University of America, (1971).

Caro, C. G., J. M. Fitz-Gerald, and R. C. Schroter, "Atheroma and Arterial Wall Shear: Observation, Correlation and Proposal of a Shear Dependent Mass Transfer Mechanism for Atherogenesis", Proc. Roy. Soc. Lond. B.177, 109-159 (1971).

Constanides, P., "Lipid Deposition in Injured Arteries", Arch. Path. 85: 280, (1968).

Constanides, P., and M. Robinson, "Ultrastructural Injury of Arterial Endothelium", Arch. Path. 88: 99, (1969).

Denison, E. B., W. H. Stevenson, and R. W. Fox, "Pulsating Laminar Flow Measurements with a Directionally Sensitive Laser Velocimeter", AIChE Journal 17: 781, (1971).

Duguid, G. B., Postgrad. Med. J. 36: 226, (1960).

Duncan, L. E. Jr., K. Buck, and A. Lynch, "The Effect of Pressure and Stretching on the Passage of Labelled Albumin into the Canine Aortic Wall", J. Atheroscler. Res. 5: 69, (1965).

Eisenberg, M., C. W. Tobias, and C. R. Wilke, "Selected Physical Properties of Ternary Electrolytes Employed in Ionic Mass Transfer Studies", J. Electrochem. Soc. 103: 7, (1956).

Fagela-Alabastro, E., "Diffusion in Pulsating Flow in a Conduit", PhD. Dissertation, Rice University (1967).

Fagella-Alabastro, E., and J. D. Hellums, "A Theoretical Study on Diffusion in Pulsating Flow", AIChE J., 15: 2, 164 (1969).

Florio, P. J. Jr., and W. K. Mueller, "Development of a Periodic Flow in a Rigid Tube", Symposium on Unsteady Flow, ASME Fluids Engineering Division Conference, May 6-8, 1968, Philadelphia, Pennsylvania, Paper No. 68-FE-8, American Society of Mechanical Engineers, New York (1968).

Fortuna, G., "Effect of Drag Reducing Polymers on Flow Near a Wall", PhD. Dissertation, Univ. of Illinois, Urbana, (1971).

Fortuna, G., and T. J. Hanratty, "Frequency Response of the Boundary Layer on Wall Transfer Probes", Int. J. Heat Mass Trans. 14: pp. 1499-1507, (1971).

Fox, J. A., and A. E. Hugh, "Localization of Atheroma: A Theory Based on Boundary Layer Separation", Brit. Heart J., 28: 388, (1966).

French, J. E., Int. Rev. Exp. Path., 5: 253, (1966).

Fry, D. L., "Acute Vascular Endothelial Changes Associated with Increased Blood Velocity Gradients", Circulation Res., 22: 165, (1968).

Fry, D. L., "Certain Histologic and Chemical Responses of the Vascular Interface to Acutely Induced Mechanical Stress in the Aorta of the Dog", Circulation Res., 24: 93, (1969a).

Fry, D. L., "Certain Chemorheologic Considerations Regarding the Blood Vascular Interface with Particular Reference to Coronary Artery Disease", Circulation, suppl. IV to Vols. 39 and 40: 38, (1969b).

Getz, Godgrey S., D. Vesselinovitch, and R. W. Wissler, "A Dynamic Pathology of Atherosclerosis", Am. Jour. Med. 46: 657, (1969).

Gutstein, W. H., A. Lazzarini-Robertson, and J. N. LaTrillade, "The Role of Local Arterial Irritability in the Development of Arterio-Atherosclerosis", Am. Jour. Path. 42: 61, (1963).

Gutstein, W. H., G. A. Farrell, and D. J. Schneck, "In Vivo Demonstration of Junctional Blood Flow Disturbance by Hot Wire Anemometry", Atherosclerosis, 11: 485, (1970).

Hershey, D., and G. Song, "Friction Factors and Pressure Drop for Sinusoidal Laminar Flow of Water and Blood in Rigid Tubes", AIChE J. 13: 3, 491, (1967).

Knudsen, J. G., and D. L. Katz, Fluid Dynamics and Heat Transfer, McGraw Hill, (1968).

Krasuk, J. H., and J. M. Smith, "Mass Transfer in a Pulsed Column", Chem. Eng. Sci., 18: 591, (1963).

Lazzarini-Robertson, A., "Respiration of Human Arterial Intima and Atherogenesis", (Abstract), Fed. Proc. 21: (Part 2), 101, (1962).

Lazzarini-Robertson, A., Progr. Biochem. Pharmacol. 4: 305, (1968).

Leveque, M. A., "Les Lois de la Transmission de Chaleur par Convection", Annales des Mines, Memoires, Series 12, 13: (1928).

Lighthill, M. J., Proc. Roy. Soc. A, 224: 1, (1954).

Linford, R. G., and N. W. Ryan, "Pulsatile Flow in Rigid Tubes", J. Appl. Physiol., 20: 1078, (1965).

Ling, S. C., "Heat Transfer from a Small Isothermal Spanwise Strip on an Insulated Boundary", Trans. ASME, Journal of Heat Transfer, 85: 230, (1963).

Ling, S. C., H. B. Atabek, D. L. Fry, D. J. Patel, and J. S. Janicki, "Application of Heated-Film Velocity and Shear Probes to Hemodynamic Studies", Circ. Res., 23: 789, (1968).

Ling, S. C., and H. B. Atabek, "A Nonlinear Analysis of Pulsatile Flow in Arteries", J. Fluid Mech. 55: part 3, 493, (1972).

McDonald, D. A., Blood Flow in Arteries, Edward Arnold Publishers, (1960).

McFeeley, J. J., "The Response of a Diffusion-Controlled Electrode to Pulsed Laminar Flow", PhD. Dissertation, Polytechnic Institute of Brooklyn, (1972).

McLachlin, N. W., Bessel Functions for Engineers, Oxford University Press, London, (1941), (Reprint of 2nd edition), (1961).

McMichael, M., Private Communication, Chem. Eng. Dept., Rice University, Houston, Texas (1973).

Mitchell, J. E., "Investigation of Wall Turbulence Using a Diffusion Controlled Electrode", PhD. Dissertation, University of Illinois, Urbana, (1965).

Mitchell, J. E., and T. J. Hanratty, "A Study of Turbulence at a Wall Using an Electrochemical Wall Shear-Stress Meter", J. Flvid. Mech. 26: part 1, 199, (1966).

Mitchell, J. R. H., and C. J. Schwartz, Arterial Disease, Blackwell Scientific Publications, Oxford, (1965).

Müeller, A., Helvetica Physiologica Acta 12: 98, (1954).

Murphy, E. A., H. C. Rowsell, H. G. Downie, G. A. Robinson, and J. F. Mustard, "Encrustration and Atherosclerosis: The Analogy Between Early in vivo Lesions and Deposits which Occur in Extracorporeal Circulation", Caned. Med. Assoc. Jour., 87: No. 6, 259, (1962).

Mustard, J. F., E. A. Murphy, H. C. Rowsell, and H. G. Downie, "Platelets and Atherosclerosis", Jour. Atheroscler. Res., 4: 1, (1964).

Packham, M. A., H. C. Rowsell, L. Jorgenson, and J. F. Mustard, "Localized Protein Accumulation in the Wall of the Aorta", Exp. Mol. Path., 7: 214, (1967).

Reiss, L. P., "Investigation of Turbulence Near a Pipe Wall Using a Diffusion Controlled Electrolyte Reaction on a Circular Electrode", PhD. Dissertation, University of Illinois, Urbana, (1962).

Reiss, L. P., and T. J. Hanratty, "Measurements of Instantaneous Rates of Mass Transfer to a Small Sink on a Wall", AIChE J., 8, 2, 245, (1962).

Reiss, L. P., and T. J. Hanratty, "An Experimental Study of the Unsteady Nature of the Viscous Sublayer", AIChE J., 9, 2, 154, (1963).

Sako, Y., "Effects of Turbulent Blood Flow and Hypertension on Experimental Atherosclerosis", JAMA, pp. 134-138, Jan. 6, (1962).

Sandler, M., and G. H. Bourne, Atherosclerosis and its Origin, Academic Press, New York, (1963).

Sarpkaya, T., "Experimental Determination of the Critical Reynolds Number for Pulsating Poiseuille Flow", J. Basic Engineering 88(3), 589, (1966).

Siegel, R., and M. Perlmutter, "Heat Transfer for Pulsating Laminar Duct Flow", J. Heat Trans., 83, 1, (1961).

Stiles, R. K., and K. B. Bischoff, "An Investigation of the Wall Shear Stress in a Canine Aortic Model Using an Electrochemical Technique", paper No. 81e, AIChE Meeting, New York, Nov. 1972.

Texon, M., "A Hemodynamic Concept of Atherosclerosis, with Particular Reference to Coronary Occlusion", A.M.A. Arch. Int. Med., 99: 418, (1957).

Texon, M., A. M. Imparato, and J. W. Lord, "The Hemodynamic Concept of Atherosclerosis", A.M.A. Arch. Surg., 80: 55, (1960).

Texon, M., "The Role of Vascular Dynamics in the Development of Atherosclerosis", In: Atherosclerosis and its Origin, Sandler and Mourve (eds.), Academic Press, New York, (1963).

Tjotta, E., "The Distribution of Atheromatosis in the Coronary Artheries", J. Atheroscler. Res., 3: 253, (1963).

Uchida, S., "The Pulsating Viscous Flow Superimposed on the Steady Laminar Motion of Incompressible Fluid in a Circular Pipe", ZAMP, 7: 403, (1956).

Van Shaw, P., "A Study of the Fluctuations and the Time Average of the Rate of Turbulent Mass Transfer to a Pipe Wall", PhD. Dissertation, Univ. of Illinois, Urbana (1963).

Van Shaw, P., and T. J. Hanratty, "Fluctuations in the Local Rate of Turbulent Mass Transfer to a Pipe Wall", AIChE J., 10: 4, 475, (1964).

Wesolowski, S. A., C. C. Fries, A. M. Sabini, and P. N. Sawyer, "The Significance of Turbulence in Hemic Systems and in the Distribution of the Atherosclerotic Lesion", Surgery, 57: 155, (1965).

Womersley, J. R., "An Elastic Tube Theory of Pulse Transmission and Oscillating Flow in Mammalian Arteries", WADC Technical Report TR 56-614, Wright Air Development Center, (1957).

Zilversmit, D. B., and H. A. I. Newman, J. Atheroscler. Res., 4: 261, (1964).

Zilversmit, D. B., and H. A. I. Newman, Circulation, 33: 7, (1966).

Zilversmit, D. B., Ann. N. Y. Acad. Sci. 149: 710, (1968).